

Interaction Notes

Note 527

May 1997

**ETE III : APPLICATION OF THE ELECTROMAGNETIC TOPOLOGY
THEORY ON THE EMPTAC**

(ETE III - July 1996)

**J.P. Parmantier, V. Gobin,
F. Issac, L. Paletta ***

I. Junqua, Y. Daudy, J.M. Lagarde

**Office National d'Etudes et de
Recherches Aérospatiales
8, rue des Vertugadins
92290 Meudon, France
Tel: 33 1 46 23 50 64
Fax: 33 1 46 23 50 61**

**Centre d'Etudes de Gramat
46500 Gramat, France
Tel: 33 5 65 10 53 34
Fax: 33 5 65 10 54 09**

*** *Doctorant CIFRE Renault***

Abstract

This note presents an experiment carried out in July 1996 on the electromagnetic test bed aircraft (EMPTAC) at the Kirtland Air force Base (Albuquerque, New-Mexico). This experiment, which followed previous tests, carried out in 1993 and 1995, intended to use the topological concepts to analyze electromagnetic interference on a large structure in a wide frequency range. The cable network under study was running inside the whole aircraft and was fully modeled in the CRIPTE[®] code. Computational and experimental data are compared in the case of local current injections. Measurements under the ELLIPTICUS antenna are analyzed.

Intentionally blank

CONTENTS

1. INTRODUCTION	7
1.1 Context	7
1.2 Recalls on Electromagnetic Topology	7
1.3 Chronological experimentation	8
1.4 Objectives of ETE III experiment	8
2. DESCRIPTION OF THE WIRING UNDER STUDY	11
2.1 Overview of the EMPTAC aircraft description	11
2.2 Recall of main results obtained during previous experiments (1993/1995)	12
2.3 Description of the wiring under study in the 1996 study	15
3. NUMERICAL MODELING PRINCIPLES	19
3.1 The tube modeling	19
3.1.1 General principles	19
3.1.2 Generation of the geometry of tubes	20
3.1.3 CRIPTE code calculation on tubes	23
3.1.4 Interest of the random generation of the geometry of tube sections	25
3.1.5 Influence of the connector	28
3.2 Modeling of the cable network under study in the topological code CRIPTE	30
3.2.1 Introduction	30
3.2.2 Principle of sub-network decomposition	31
3.2.3 Topological model of the cable network under study	32
3.3 Performances of calculations	35
4. MEASUREMENTS	39
4.1 Generalities on local injections	39
4.2 Calibration of the probes	41
4.2.1 Injection calibration	41
4.2.2 Measurement calibration	42

Intentionally blank

5. ANALYSIS OF EXPERIMENTAL DATA & NUMERICAL SIMULATIONS	45
5.1 Comparison between measurements and calculations on the forward shielded volume	45
5.1.1 Objectives	45
5.1.2 Local bulk current injection	45
5.1.3 Current injection on one wire	51
5.2 Measurements and CRIPTE code calculation on the whole network	53
5.2.1 LD7 current injection	53
5.2.2 Influence of the connection of the whole network	58
5.2.3 LD6 current injection	59
5.3 Analysis of measurements under ELLIPTICUS	64
5.3.1 Introduction	64
5.3.2 Analysis of the electromagnetic environment inside the lower shielded volume	65
5.3.3 Analysis of bulk currents measurements	66
5.4 Principles of 3D mapping of bulk currents	67
5.5 Application of 3D planar visualization	69
CONCLUSION	71
APPENDIX A : DESCRIPTION OF THE B1B VOLUME	73
A-1 Description of the geometry of the B1B volume	73
A-2 Description of the connections on the LD11 and LD12 boxes	79
APPENDIX B : CALCULATION OF THE ATTENUATION OF SIGNAL ALL ALONG AN OVER SHIELDED BUNDLE	81
APPENDIX C : DESCRIPTION OF TOPOLOGICAL NETWORKS	83
REFERENCES	93

Intentionally blank

1. INTRODUCTION

1.1 Context

This report reviews a common experiment between the OFFICE NATIONAL D'ETUDES ET DE RECHERCHES AEROSPATIALES (ONERA), the CENTRE D'ETUDES DE GRAMAT (CEG) and the PHILLIPS LABORATORY (PL). This experiment (ETE III) has been performed in July 1996 as part of the DEA, MWDDEA 7336 on the atmospheric environment, as a third phase of a program starting three years ago. The final objective of this program intends to apply the Electromagnetic Topology approach to qualify and quantify coupling phenomena of an electromagnetic threat with a real cable network running inside the EMPTAC, available at the Kirtland Air Force Base (Albuquerque, New-Mexico).

The authors wanted this document to be a description of the experimental and computational work they performed during the test. But, they also wanted it to be a technical tool for the future works they intend to carry out on this subject. The first draft of this paper has been written during the experiment, as the numerical simulations. Back in France, a few additional calculations were carried out to provide more accurate results.

1.2 Recalls on Electromagnetic Topology

The Electromagnetic Topology (EMT) is a method to analyze complex electromagnetic coupling problems, originally developed during the 70's ([1]). The objective of this theory is to break down a complex system into elementary subsystems, in order to find proper rules for the design of hardened structures.

Since 1987, ONERA has decided to complete studies on EMC using this theory, from experimental and theoretical points of view ([2], [3]). The final purpose is to improve the potentiality of this method in order to be able to understand electromagnetic interactions on complex structures, such as an aircraft submitted to various kinds of threats. An important point is to be able to predict both qualitatively and quantitatively final interference on equipment.

A numerical code, named CRIPTE[®] and based on the BLT equation ([4]), has been developed by ONERA to achieve this purpose. After various validations on canonical structures and cable networks, ONERA and CEG decided to evaluate how Electromagnetic Topology could be used and applied to a real cable network running inside a structure such as the EMPTAC, initially designed with topological rules.

1.3 Chronological experimentation

As a first attempt to achieve this final purpose, in a first experiment (ETE I), carried out in October 1993 at the PHILLIPS LAB, a simplified cable network was installed in the cockpit and in the lower shielded volume ([6], [7]). This particular cable network was made of simple bundles constituted of two or three elementary conductors, but was running along this existing EMPTAC cable network. This simple network had been wholly characterized, in terms of inductance, capacitance parameters, in France, before installation in the aircraft.

As local electromagnetic threats, current injections were performed on this simplified cable network, in order to validate its experimental characterization. Numerical simulations and preparatory experiments had previously been achieved in France.

The agreement between computations and measurements of voltages and currents resulting from the current injection being satisfactory, the EMPTAC aircraft was placed under the ELLIPTICUS antenna (in the frequency range from 300 KHz to 100 MHz), available at the KIRTLAND AIR FORCE BASE, on LESLI facility. The objective was to see if the Electromagnetic Topology approach could be applied to evaluate voltages and currents induced on the simplified network by this global irradiation.

Furthermore, the Electromagnetic Topology approach applied to the existing network located in the cockpit and the lower shielded volume enabled a qualitative analysis concerning the main points of entry of the electromagnetic interference inside the aircraft.

The second experimentation on this aircraft (ETE II), carried out in June 1995, intended to focus on the analysis of coupling phenomena inside the EMPTAC when this one was irradiated under the ELLIPTICUS antenna in the frequency range from 100 MHz to 1 GHz. ETE II test was specially devoted to measurement. The main objective was to point out if interference could propagate on cables at the frequencies under study. No definitive conclusion could be obtained. But the experiment was merely useful to prepare the experiment described in this document.

1.4 Objectives of ETE III experiment

As respect to both previous experiments, the main specific objectives of the ETE III experiment can be summarized in the following points :

1 - a wide frequency band analysis, from 300 KHz to 1 GHz. In fact the analysis of measurements during the ETE II experiment pointed out how the understanding of the physics of EM coupling on cables could be hard if the low frequency EM responses were not previously performed.

2 - analysis of the coupling on a large cable network. During the ETE I and ETE II experiments, the problem was restricted to the analysis of the coupling on one cable in the cockpit volume and the wiring inside the forward shielding volume. In the ETE III experiment, the

objective is to simulate a large network running everywhere inside the aircraft, from the cockpit volume up to the aft shielded volume.

3 - a full modeling of the cable wiring, that is to say numerical simulations with no introduction of any measured data in the models. Such numerical simulations, carried out with the CRIPTE code, had been undertaken during ETE I, but networks under study were very simple ones. Some numerical simulations on EMPTAC harness had been undertaken but tools and numerical simulation methods were not mature enough to achieve the meshing of a large cable network. The lack of maturity of the CRIPTE tools (for instance, absence of graphical interface) was also the reason why no numerical simulations could be undertaken during this phase.

4 - low levels measurements. The ETE III experiment, entirely devoted to the actual EMPTAC wiring, whereas the ETE I experiment was dealing with a simplified network built in France and installed into the aircraft, pointed out the requirement of low level measurements. The low level measurements are due to the hardened topology of the aircraft. Generally, bulk current measurements on wires or even on cable bundles may require major precautions inside the aircraft. Two kinds of excitations have been carried out : local injections with current injectors and global illumination under the ELLIPTICUS antenna.

The technical objectives laid on scientific questions we wanted to answer. These scientific objectives can be summarized in three questions :

1 - do cables still continue to propagate for frequencies higher than 100 MHz ? Generally, it is said that cables cannot propagate in high frequency. In fact we tried to show that signal at the extremity of a cable could be due to a propagation on the wiring. Of course, the signal is generally attenuated. Nevertheless, does this attenuation exclusively come from losses (resistive or radiating losses) or is this attenuation due to multiple variations of cable propagation characteristics (propagation and characteristic impedance matrices) all along their length (specially because of twisting or simply because of the unknown position of wires inside the bundles) ?

2 - does local coupling dominate and for which frequencies ? The answer to this question is important and closely related to the existence of significant propagation at high frequency. In the affirmative, the response in one test point of a cable could be obtained by the single knowledge of sources in the vicinity of the test point. In this case, further questions should be relevant such as :

- what part of the entire network has to be modeled ?
- what kinds of terminal loads have to be introduced at the termination of the selected network ?

3 - what are the limitations of the CRIPTE code. In fact, the CRIPTE code is based on Electromagnetic Topology principles, but its specificity lays on the tube modeling. Tubes represent parts of cable bundles, described in the code with the transmission line theory. To what frequency range can this approximation still be applied ? Of course, this question is related to the first one. The second question dealt with the capability of the CRIPTE code to treat a large network. Can we numerically determine cable characteristics, even if their geometry is not precisely known ? Applying Electromagnetic Topology breakdown concepts, are we able to describe such a large network on computers with limited performance (workstations) ?

Intentionally blank

2. DESCRIPTION OF THE WIRING UNDER STUDY

2.1 Overview of the EMPTAC aircraft description

The EMPTAC aircraft has been designed using topological rules, in order to achieve a balanced quality of the shielding effectiveness in its different parts. It is possible to identify various areas which can be considered as independent of each other, provided that we except the wiring running in every part of the EMPTAC.

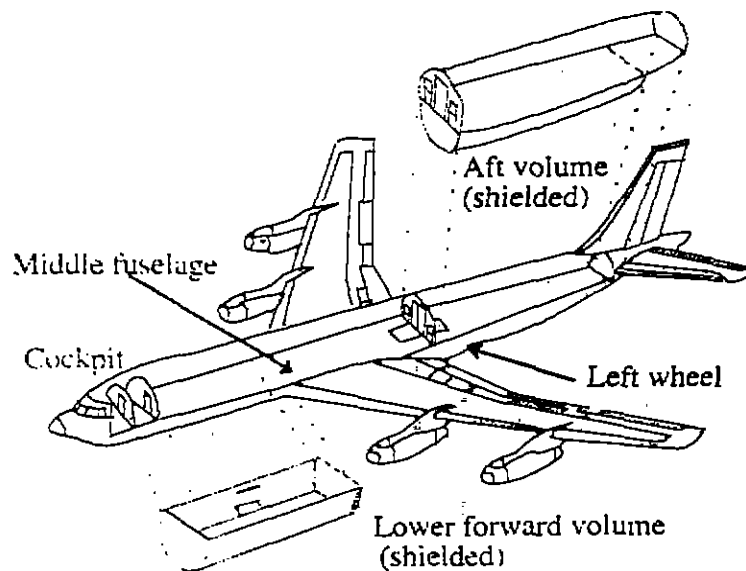


Fig. 2-1 : General Description of the EMPTAC

On Figure 2-1 and Figure 2-2, we can see the various parts of the EMPTAC among which :

- the Lower Forward Shielded Volume
- the Forward Fuselage
- the Left Wheel
- the Cockpit
- the Aft Shielded Volume

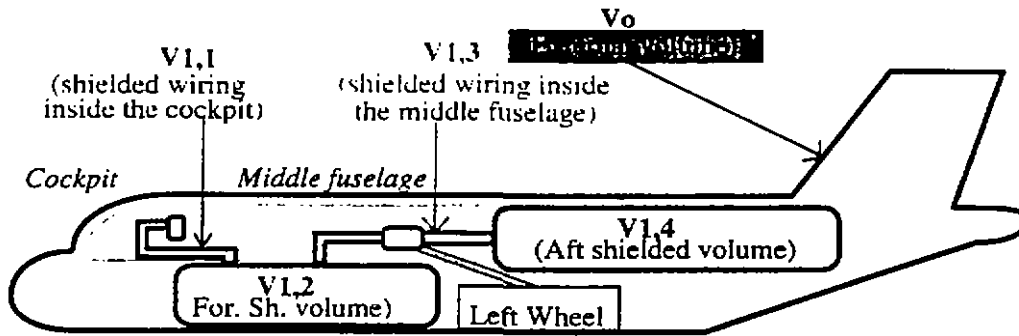


Fig. 2-2 : Schematic topological breakdown of the EMPTAC

2.2 Recall of main results obtained during previous experiments (1993/1995)

During the last experiments, our efforts were devoted to the study of a small part of the total wiring of the EMPTAC : the bundle under study was running from the cockpit to the lower volume.

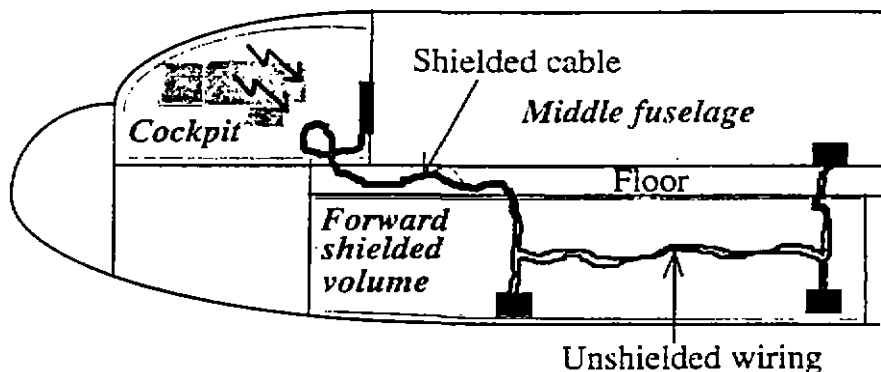


Fig. 2-3 : Detail of the wiring studied during the 1993 ETE-I and 1995 ETE-II experiments

Only the Cockpit and the Lower Forward Shielded Volume (LFSV) had been studied. A shielded cable (21 conductors) running in the cockpit was connected to the unshielded wiring of the LFSV (Figure 2-3). A simplified network, composed of just a few wires but with the same lengths as the original one, had been previously built in France and experimentally characterized. Once at Albuquerque (New Mexico), it had been installed parallel to the previous one, already present in the EMPTAC. After complementary verification of the properties of this new wiring into the aircraft, modeling calculations with the CRIPTE code had been carried out. Figure 2-4 represents a topological network used by CRIPTE. The EMPTAC had been illuminated by the ELLIPTICUS Antenna (Figure 2-5) available at the Philips Laboratory (sweeping in a large frequency range). Various theoretical and experimental studies were carried out and we can recall one of the best results obtained.

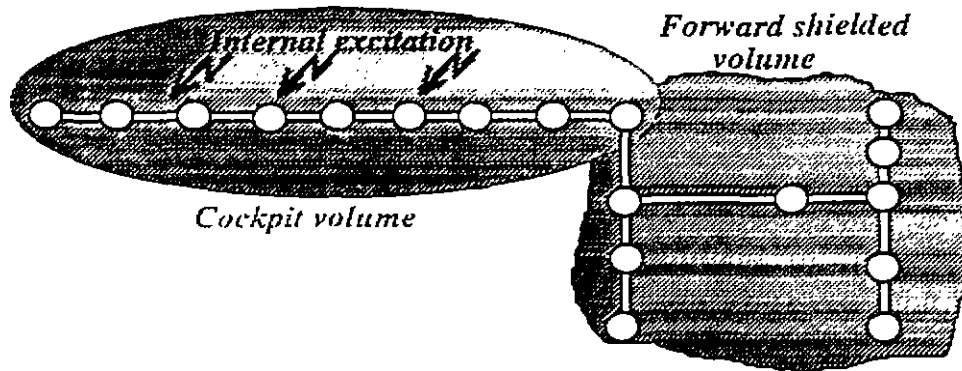


Fig. 2-4 : Network used by the CRIPTE numerical code to analyze the response of the front part of the EMPTAC

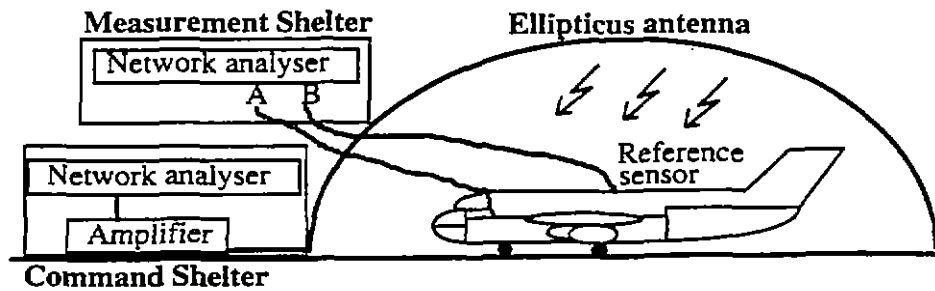


Fig. 2-5 : EMPTAC illuminated with the ELLIPTICUS Antenna (PHILLIPS LABORATORY, LESLI Facility)

After having experimentally characterized the equivalent generator (representing the ELLIPTICUS illumination on the shielded cable of the cockpit), two sets of responses of the structure had been recorded. In a first phase, the shielded cable in the cockpit was correctly grounded at both ends. In a second step, this shield was intentionally disconnected at one end. In that case a single resistance value was changed in the topological network used in CRIPTE.

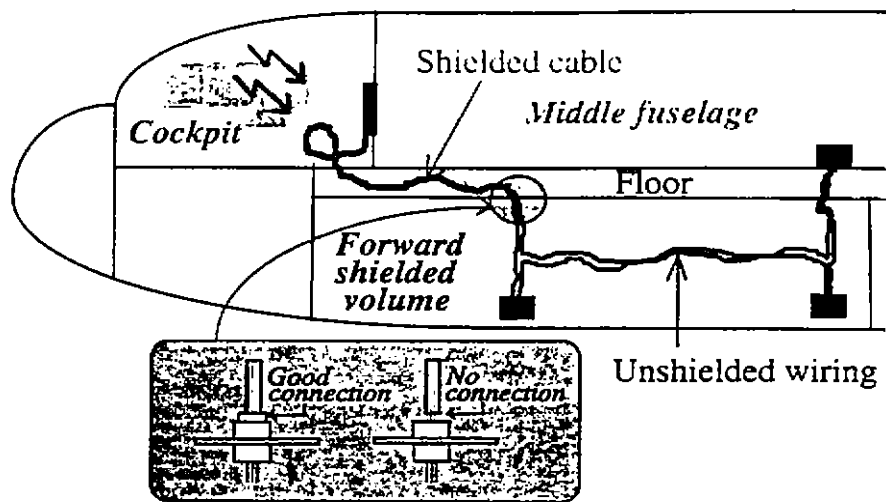


Fig. 2-6 : Study of the wiring connection
(with the shield in the cockpit volume grounded and disconnected)

A comparison between a numerical result and an experimental measurement is plotted on Figure 2-7. It proves the advantage of a topological approach. A lot of complementary results of these experiments are available in a synthesis document.

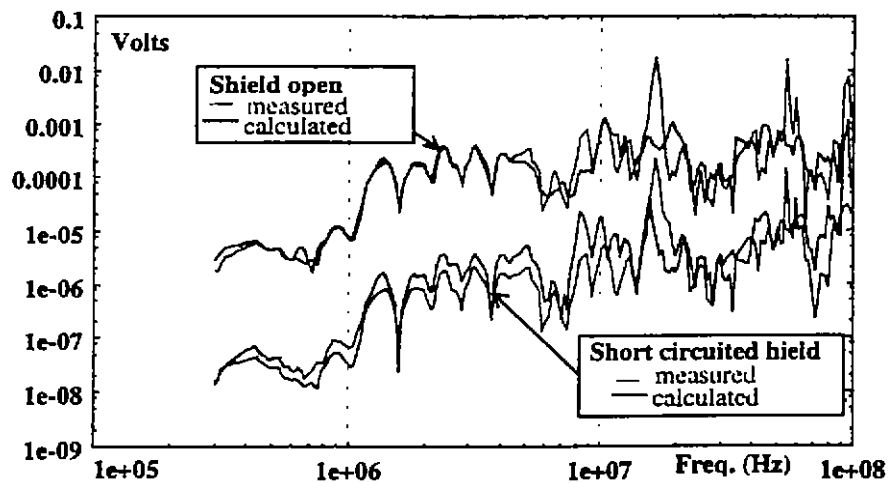


Fig. 2-7 : Comparison of the numerical results (CRIPTE) and the experimental measurements for the two different shield connections

2.3 Description of the wiring under study in the 1996 study

During the 1996 study, presented in this document, we decided to analyze the behavior of a much larger wiring running in every parts of the aircraft. Figure 2-8 represents the total network available in the EMPTAC. This so called "modified wiring" has been build following topological rules. For example, in each well shielded part of the aircraft, bundles are unshielded. On the contrary, in the naturally poorly shielded volumes (cockpit, fuselage), wires are protected by a shield grounded at both ends. The various bundles are connected to different boxes which simulate the electronic equipment on an aircraft. We can distinguish various kinds of boxes :

- the terminal boxes (generic name "Ldxx") are composed of the terminal loads of each individual wires (values from 0 Ω up to 100 k Ω).

- some junction boxes (generic name "Jbxx") allow a separation of the wires in various parts of the EMPTAC.

- at some locations, we can also find filtering boxes (generic name "Fbxx") composed of passive filters.

The bundles are composed of various kinds of individual cables (single conductors, unshielded or shielded twisted pair of cables, three wire cables,...). The total number of wires per bundle is varying between 1 and 38. At each interface (output of a box, the walls between two areas of the EMPTAC), the wires are connected to male and female connectors (up to 20 pins).

A real time study (experiment and modeling) was achieved during the three weeks 1996 experiment. For this, a simplified part of the total network was selected (Figure 2-9). It was a necessary condition to perform the calculations in real time on the workstation (HEWLETT PACKARD 712/60 with 32 Mega-bytes memory) available on the site of the experiment. The wiring runs in every part of the EMPTAC and each kind of component is represented (boxes, conductors, bundles, connectors). The complexity of this wiring remains representative of the general network, some bundles being composed of up to 22 conductors.

Even though a selected network was extracted from the total existing one, it remained impossible to give a detailed description of each conductors in this report (the definition document of the total EMPTAC network is composed of more than 300 pages !) ([8]). Therefore, as an example, we only present a small part of the whole network. The chosen part is the so-called "B1B box" because it is one of the most complex volume that we have encountered. A schematic description of the B1B volume is represented on Figure 2-10.

Each line on the figure (noted "Nbxxxx") represents a bundle composed of up to 8 conductors. The so-noted "Jxxx" and "Pxxx" are the locations of the connectors.

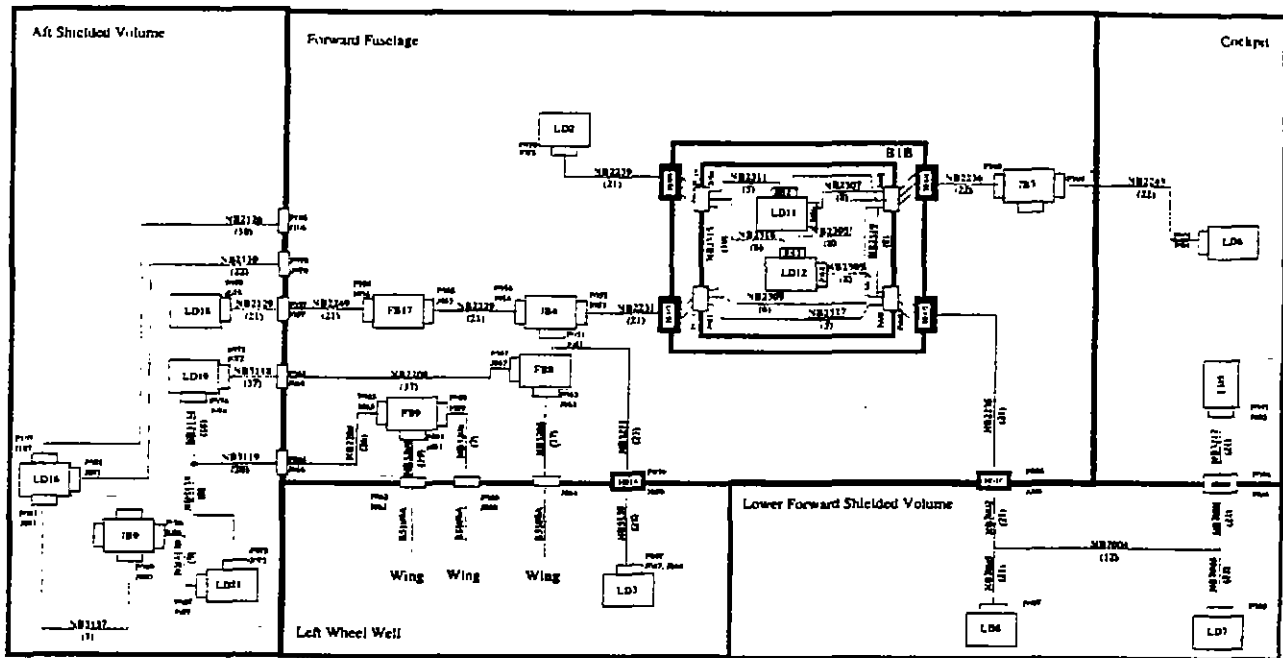


Fig. 2-8 : Total modified wiring of the EMPTAC

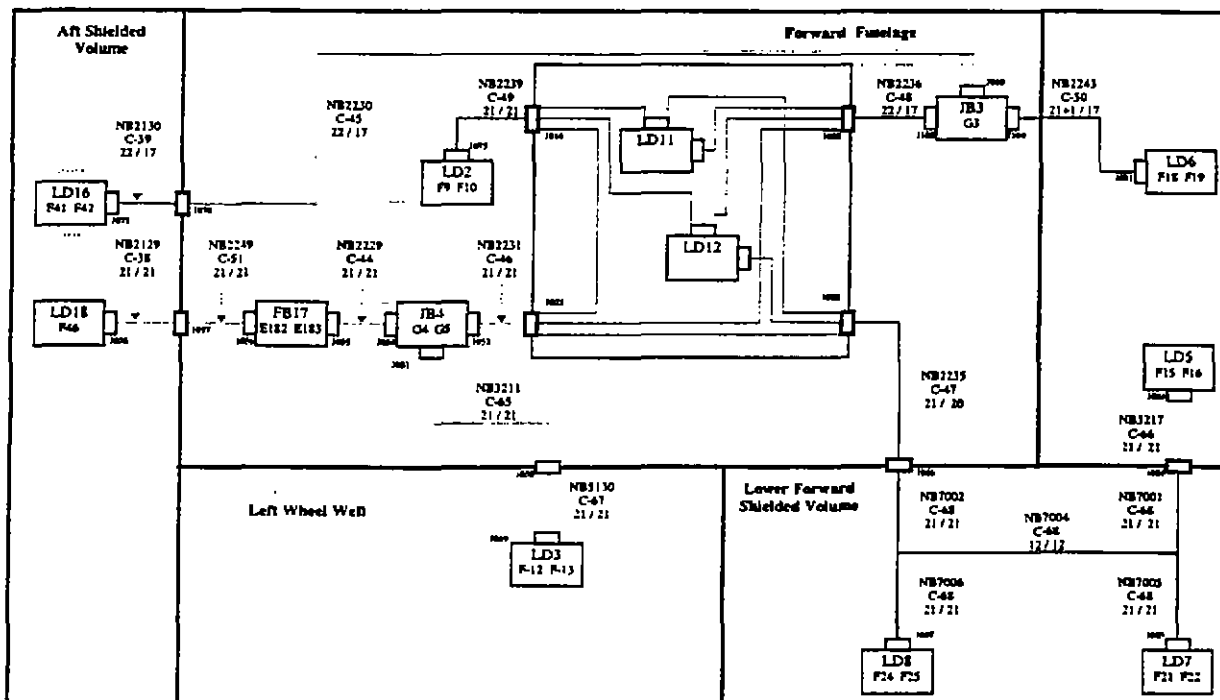


Fig. 2-9 : Selected modified network for the 1996 experiments

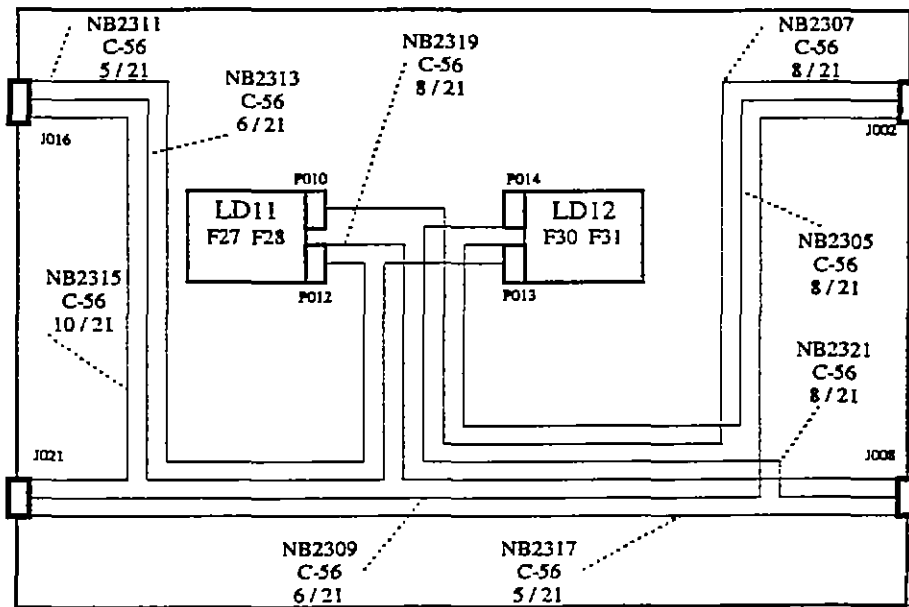


Fig. 2-10 : Schematic description of the BIB volume

Intentionally blank

3. NUMERICAL MODELING PRINCIPLES

3.1 The tube modeling

3.1.1 General principles

In the current version of the CRIPTE[®] code ([9]), only homogeneous sections of cable bundles are modeled. This means that the characteristic parameters of a tube are constant all along the tube length. This is the reason why, generally, the different parts of an entire cable wiring has to be decomposed in several tubes. Tube data files contain the per unit length resistance, inductance, conductance and capacitance (R, L, G, C) matrices. These values are used to generate the propagation and characteristic impedance matrices of the tubes. The propagation matrix is related to the different modes propagating inside the tube and the characteristic impedance matrix is related to the matching of the cable ([4]).

Two ways can be considered to characterize tubes : experimental and numerical approaches. From the beginning of ONERA's and CEG's work in EM Topology, a large effort has been undertaken to measure R, L, G, C parameters of cables ([10]). Direct methods based on the measurement of R, L, G, C parameters with an impedance meter or indirect methods based on scattering parameters (S-parameters) measurements have been carried out and validated in many experiments performed by ONERA and CEG. The second one is certainly the most promising because it is perfectly suited for an automation of the measurement process. Nevertheless, the simple way to measure S-parameters requires to load the input ports of the cable with 50 Ω loads (internal impedance of the network analyzer). The problem is that generally, terminal loads are not 50 Ω real equipment. During last ETE II experiment, a method has been applied to measure S-parameters on the actual loads of the cable (Topological S-parameter measurements). This method is based on the use of a current injector and a current probe ([11]).

All the measurement methods could reveal themselves hard and tedious when generalized on the overall wiring of an entire aircraft. This is the reason why one of the main objectives of ETE III was to compute R, L, G, C parameters thanks to a two dimension code named LAPLACE developed at ONERA and available with the CRIPTE code package. The code calculates the inductance and capacitance matrices of the tubes. If necessary, the existence of dielectric insulators can be introduced in the description of constitutive wires. The calculation of the LAPLACE code is based on the application of a method of moments on a meshing of a section of a multiconductor line ([12]). One specificity of this code lays on its original way to describe unknown on circular contours thanks to circular basis functions. By this way, elementary wire and shield sections can be modeled with accuracy in an efficient way. Non circular electric conductors can also be introduced. This is useful to describe the reference structure shape of any non shielded multiconductor cable.

The cables of the EMPTAC aircraft contain a large number of elementary wires (up to 39 wires in the BIB bay). Modifications have been undertaken on LAPLACE code to allow the calculation on such big multiconductor lines. Dynamic allocation has been systematically implemented on large size matrices of the code. The precision of the calculation depends on the number of basis functions applied on each contour (metallic or dielectric). Different trials performed in France before the experiment have pointed out the fact that the reference conductor had to be described with a significant number of basis functions, whereas elementary conductors can be described with less basis functions. Typically, in our calculations, the number of basis functions for the reference conductor has been fixed to 70 unknowns whereas the number for circular contours (electric and dielectric) has been fixed to 20 or 30 unknowns. For special requirements, these numbers have been modified.

Resistance values are not calculated but estimated as respect to previous measurements. For all wires, the static per unit length resistance has been chosen equal to 100 m Ω /m whereas the one for the reference conductor has been chosen equal to 2 m Ω /m. A frequency dependence of each tube has been imposed, applying a skin effect formulation on each wire. The parameters introduced in the formulae supposed the wires made of copper, with a radius equal to 0.4 mm. Of course, the resistance obtained is not exactly the one of the wires but it gives a significant variation of losses.

3.1.2 Generation of the geometry of tubes

The description of the geometry of the cable bundles presents two main difficulties :

1 - the first one deals with the fact that the knowledge of the position of elementary wires inside the bundle is not precisely known

2 - the second one deals with the fact that the meshing of sections of bundles which present a large number of wires may become rapidly very tedious.

In order to avoid these two drawbacks, ONERA developed a numerical software, named ALEATUB, which allows a random generation of the geometry of sections of cable bundles. In one calculation, several pieces of geometry of the same cable bundle may be generated and their R, L, C matrices can be calculated automatically. If a model of a tube has to be used several times in one or several networks, different samples of tube data files can be generated with the ALEATUB utility.

The following information may be entered in ALEATUB to generate random pieces of geometry of sections of tubes :

- the radius of wires and the radius of dielectric insulators. In EMPTAC, the most common wires have a 20 AWG gauge, but the ground wires generally present a 22 AWG gauge. Furthermore, we have introduced a special radius for the shielded twisted pairs. Only the shield has been modeled. The internal geometry of the twisted cable shield has been separately

calculated and the characteristic parameters have been used in specific networks. For the three kinds of wires, an equivalent radius has been considered. They are summarized in table 3-1.

Type of wire	Dielectric radius (mm)	Metallic radius (mm)	Resistance (Ω/m)
20 AWG	0.61	0.41	0.1
22 AWG	0.48	0.32	0.1
Shield of pairs	1.10	1.09	0.1

Table 3-1 : Equivalent radius used for the 3 different types of wires encountered on EMPTAC wiring

- the nature of the reference conductor (a metallic plane or a shield). If the reference is specified as a shield, the radius of the shield is automatically computed to contain all the internal wires. If the reference is specified as a metallic plane (for unshielded multiconductor cables), the average height of the cable has to be given. The average height is equal to the distance between the reference plane and the center of the bundle. If this distance is inferior to the equivalent radius of the set of wires, the set of wires is imposed to lay on the reference plane. In fact, this procedure is the one applied to describe a cable laying on the reference plane. For both kinds of references, the static resistance has been chosen equal to 1 m Ω/m ,

- the maximum distance between wires (randomly generated). By this way, wires are not constrained to be in contact.

- the existence of groups of wires which are always in contact inside a bundle. A group is specified by an identification number and a number of internal conductors. Each conductor has its geometry fixed with local coordinates. This has been applied for two kinds of groups: the unshielded twisted pairs and the unshielded three wires cables. The geometry of each cable is reported in the following table 3-2.

Type of cable	wire	x coordinate	y coordinate
Twisted pairs	Wire 1	-0.6097	0.
	Wire 2	+0.6097	0.
Three wire cables	Wire 1	0.	0.
	Wire 2	2.285	0.
	Wire 3	1.1425	1.979

Table 3-2 : Local geometry used for the two kinds of elementary groups encountered in EMPTAC wiring

Figure 3-1 gives an example of a tube section geometry generated with the ALEATUB software. It deals with the *nb7001* cable, laying on the metallic plane in the forward shielded volume. For this cable, all the elementary wires present a 20 AWG gauge.

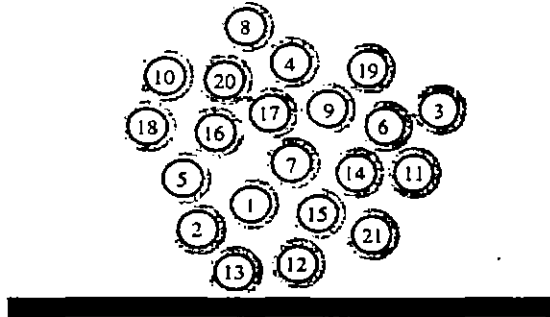


Fig. 3-1 : Example of the geometry of a tube section (the forward shielded volume nb7001 cable), generated with the ALEATUB software

Figure 3-2 gives an example of the *nb2249* cable, located in the fuselage volume at the aft volume separating panel. This cable presents a reference which is a shield. Wires with larger radius represent equivalent shielded pairs (for which only the shield has been modeled).

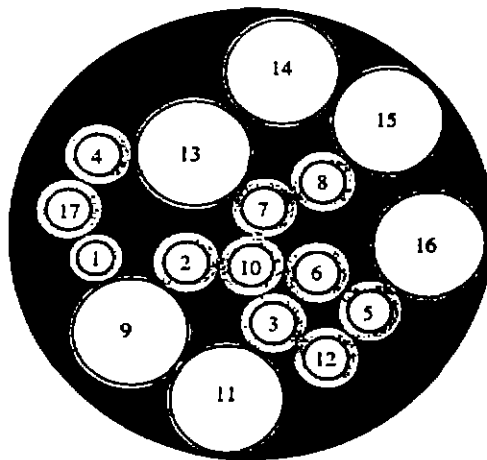


Fig. 3-2 : Example of a tube section of the nb2149 cable, generated with the ALEATUB software

The interest of groups also lays in the possibility it offers to generate bundles, themselves made of bundles. This case occurs in the B1B volume for which elementary bundles are gathered to constitute other bundles. Figure 3-3 gives an example of a bundle made of 6 elementary bundles. The description is given as follows (tube *b1b_1h0* of B1B topological sub-network) :

- nb2311 : from wire 01 to wire 05
- nb2319 : from wire 06 to wire 11
- nb2307 : from wire 12 to wire 18
- nb2305 : from wire 19 to wire 25
- nb2313 : from wire 26 to wire 32
- nb2321 : from wire 33 to wire 39

The geometry of each group associated to an elementary bundle has been itself generated randomly thanks to the ALEATUB computer code. Then, the total bundle has also been generated randomly thanks to the ALEATUB utility again. Of course, in this ultimate calculation, the geometry of each elementary group has been considered as fixed in a local reference.

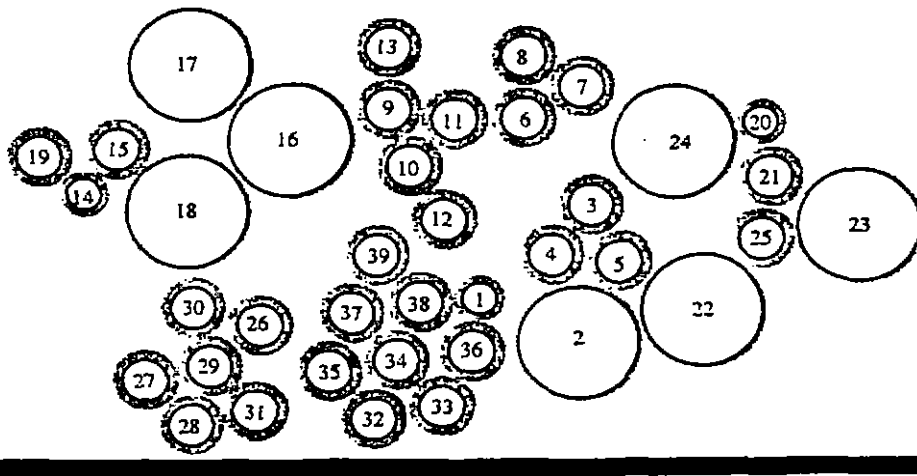


Fig. 3-3 : Example of a tube section of the BIB bay volume, generated with ALEATUB by associating elementary bundles

3.1.3 CRIPTE code calculation on tubes

On each tube, the CRIPTE code calculates the propagation characteristics (propagation matrix, characteristic impedance matrix). These results lay on a diagonalization of complex numbers (eigen values calculations). In the CRIPTE code, the algorithm lays on a numerical method. For tubes containing a big amount of elementary wires, the convergence may sometimes not be obtained. We tried to overcome this drawback by taking advantage of the random localization of wires inside the bundle : we introduced an analytical resolution for the gamma (γ) matrix diagonalization.

The analytical diagonalization of a matrix is possible in very special construction cases. This is particularly the case when all the diagonal terms are equal and when all the extra-diagonal terms are equal. This is exactly what our matrices look like if we consider that wires can be located anywhere inside the bundle. The diagonal and extra-diagonal terms can be respectively approximated by the average of all the diagonal and extra-diagonal terms.

The following question was to determine on which matrix we had to average terms. The diagonalization lays on the products of Z and Y matrices. Z and Y are respectively the per unit length impedance matrix the per unit length admittance matrix of the tube. It has been previously demonstrated in France that averaging Z and Y before the gamma calculation of big bundles gave bad results in a high frequency numerical process. Indeed, eigen values of the gamma diagonalized matrix are significantly different : it means that the common mode and the differential modes velocities are strong. The good solution deals with averaging the product of Z and Y.

Nevertheless, the bundle is not perfectly twisted, that is to say that all the diagonal and all the extra diagonal terms are not respectively exactly identical. For this, we applied a perturbation calculation which generates several differential propagation velocities on the bundle. Then, the characteristic impedance matrix is numerically calculated by multiplying the propagation matrix, coming from the analytical diagonalization described before, and the Z per length impedance matrix, with no average. The result is a Zc characteristic matrix depending closely on the geometry of the cable.

Such analytical calculations are available only for bundle harness type cable, for which the internal geometry is not controlled. It is not available anymore for cables such as shielded elementary cables because in this case the geometry of a section remains identical along the cable length. More, such a method is not available if one intends to process the internal domain of shielded cables located in a bundle with a single tube. In this case, the transfer impedance and admittance values appear theoretically as very small terms added or subtracted to the external domain terms ([13]). This is the reason why shielded twisted pair have been modeled separately in all the networks that we considered during the ETE III experiment.

Moreover, the computation time for calculating modes in an analytical way is widely improved compared to the numerical way. Nevertheless, the numerical mode calculation has been used in delayed calculations performed in France, after the experiment. The reason of this choice was that, we wanted the geometry of tubes in elementary section not to be averaged. In fact, we considered that the average could be supplied thanks to the link of a sufficient number of elementary tubes. The difference between both kinds of calculations revealed itself very small.

Anyway, using the analytical or the numerical method, we are able to model two important aspects of the propagation on a bundle :

1 - two propagation velocity values. One deals with the common mode, the others (n-1 modes for a n wire cable) deal with the differential velocities. These velocities are quite similar. Theoretically they should be exactly identical if the cable was perfectly twisted,

2 - due to the variation of the location of wires inside a bundle, the equivalent transmission line presents a set of mismatching along its length.

3.1.4 Interest of the random generation of the geometry of tube sections

The random generation of the geometry of tube sections presents two main advantages :

- the meshing of the multiconductor cable geometry is straightforward and very rapid. By this way, several geometry sections can be calculated for the same wire constitution of a tube,
- the random generation allows us to take into account the unknown position of all the wires inside the bundle. Indeed, the position of a wire in the bundle changes all along the running of the cable.

The second point reveals itself very interesting from a physical point of view. We asked ourselves if the multiple mismatching of the cable could not be at the origin of the attenuation of the signal between the two extremities of the cable. The multiple mismatching are due to the variation of the position of the wires inside the bundle along the running of the cable. For this, we tried to model the scattering parameters of a 6 meters length cable composed of a 21 elementary wires cable (*nb2235* from the Lower Shielded Volume to the BIB bay volume), breaking it down in 60 tubes. For this, 6 elementary sub-networks made up with 10 tubes have been calculated, constituting a piece of a 1 meter long cable (Figure 3-4). All the tubes used in the sub-network model present different characteristic parameters calculated with the ALEATUB utility. The tube length is equal to 10 cm and contains 21 elementary wires.

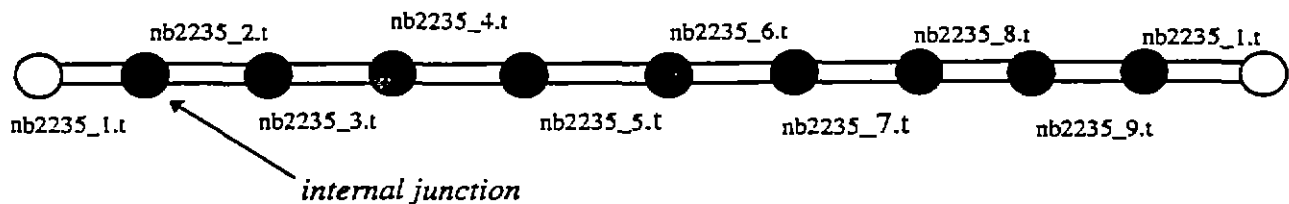


Fig. 3-4 : Elementary network used to generate the one meter long piece of the *nb2235* cable

Then, the equivalent junctions coming from the previous sub-network calculation have been connected in order to constitute the 6 meters long cable (Figure 3-5). The interconnection tubes have a zero cm length. The direction of the connection between equivalent junctions has been alternated to increase the mismatching between the 1 meter long pieces of cables.

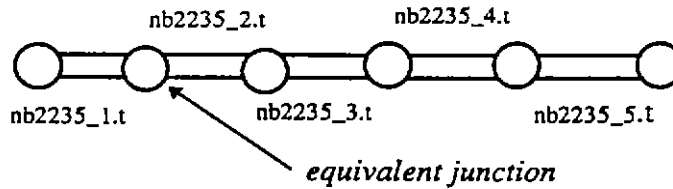


Fig. 3-5 : Global network modeling of a 6 meters length of the nb2235 cable connecting six equivalent junctions (described on figure 3-4)

Figure 3-6 presents a transmission coefficients and a mutual coupling between two wires, obtained with two methods:

- a calculation with only one tube of 6 meters,
- the calculation with 60 tubes of 10 centimeter each.

The attenuation of the transmission S-parameters (S_{21}) appears obviously on the curves. This result is very important because it goes against the common idea that, because of the transmission line model, the attenuation on a tube is only provided by introducing losses in their models (many times the question of the existence of radiation losses is quoted). The figure also represents a mutual coupling S-parameter between wire 1 and wire 4 (S_{41}). In fact, these curves demonstrate :

- first, that an attenuation is obtained when the position of elementary wires change all along its length,
- secondly, that this attenuation may be reproduced by a transmission line network model, connecting several tubes generated randomly, each with constant characteristic parameters

Figure 3-7 presents the voltage obtained at one extremity of an internal wire when a 1 volt generator is applied on all the wires at the other extremity. It represents the effect of a bulk current injection (BCI). One may notice the significant attenuation on both transmission response and mutual response.

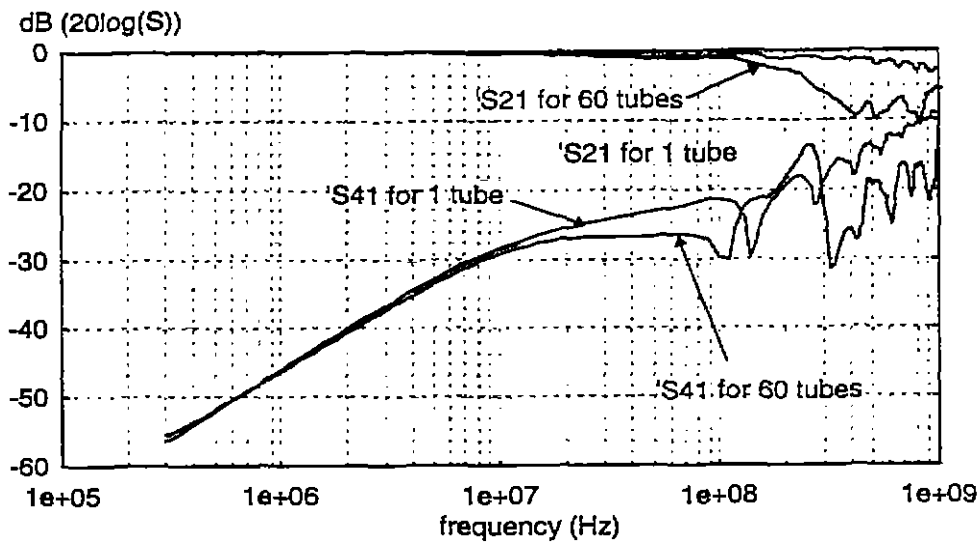


*Fig. 3-6 : S-parameters of a 6 meter long nb2235 cable,
Results obtained with two topological networks :
- made up with only one tube
- made up with 60 elementary tubes*

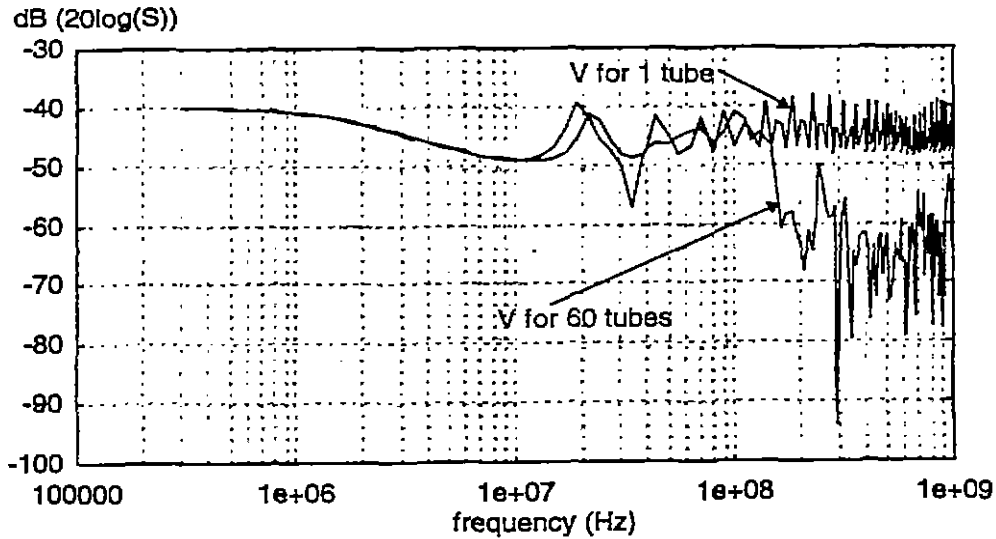


*Fig. 3-7 : Voltage at one extremity of a 6 meters long nb2235 cable,
stressed at the other extremity by a 1 volt generator on all the wires.
Results obtained with two topological networks :
- made up with only one tube
- made up with 60 elementary tubes*

Figure 3-8 presents the voltage obtained at the other extremity of the cable when the first wire is the only one to be stressed with a 1 volt generator. The interesting result is that both direct coupling on the excited wire (V_1) and mutual coupling on another wire (V_2) have quite the same level and the same behavior above 100 MHz. Such a result has been noticed many times in measurements.

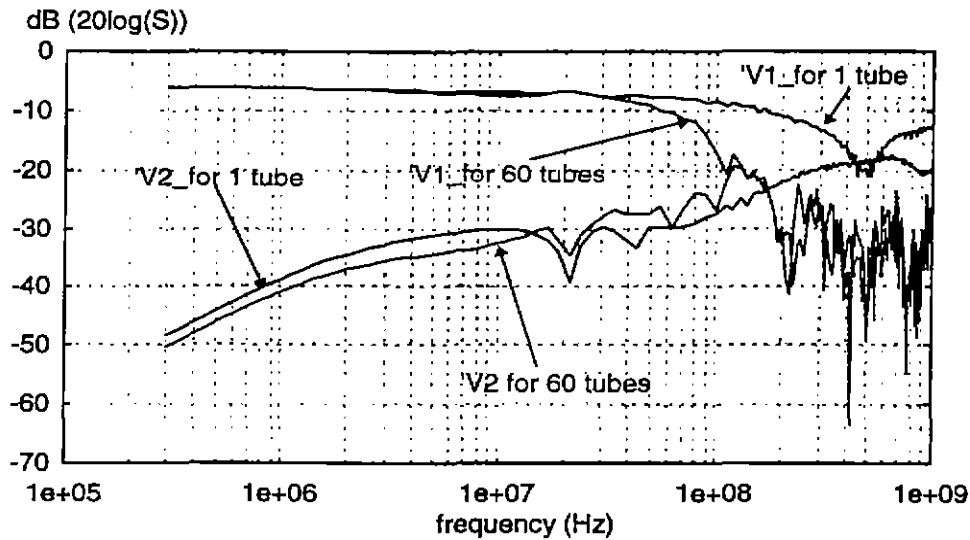


Fig. 3-8 : Voltage at one extremity of a 6 meter long nb2235 cable, excited at the other extremity by 1 volt on wire number 1.

Results obtained with two topological networks :
 - only one tube
 - 60 elementary tubes

3.1.5 Influence of the connector

In order to simplify numerical models, connectors are not taken into account in the topological models. However, in high frequency, the effects of the connector may play a significant role in the wiring response.

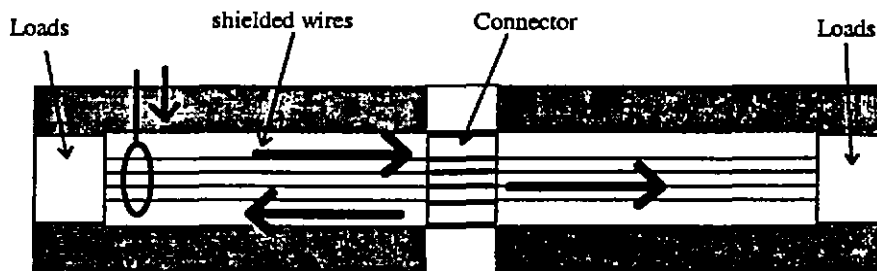


Fig. 3-9 : Scheme applied to analyze the influence of the connector

In order to check this assumption, we defined two models (figure 3-9) :

- first, a shielded transmission line, 2 meters long, with 21 individual wires, between two load boxes. In the middle of the line, a connector, 10 centimeters long, was introduced.

- secondly, the same line as in the first case, but 1 meter long, with no wire and loads after the connector. The source is a 1 Volt generator distributed on all the 21 wires and located at the beginning of tube number one.

The first problem can be modeled by the network drawn on figure 3-10. The characteristic impedance of the shielded wires is noticed Z_{c1} while the characteristic impedance of the connector is noticed Z_{c2} . The second problem is simply modeled by two tubes with open circuits on the right of the connector (fig 3-11).

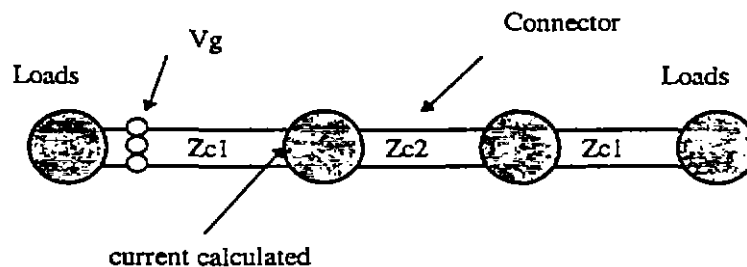


Fig. 3-10 : Model of a connector between two cables linking load boxes

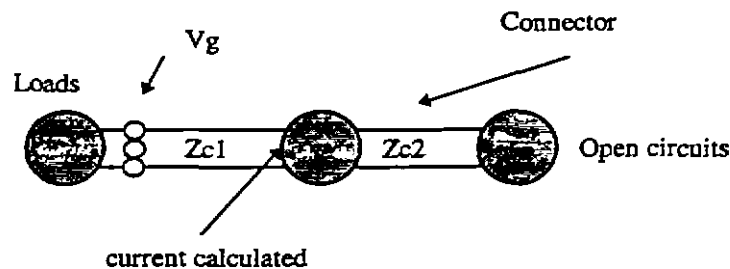


Fig. 3-11 : Model of a connector at one extremity of a cable

In both cases, the bulk current is calculated just before the connector (figure 3-12). In low frequencies, it is obvious that the bulk current in the first configuration is higher than the second one. With loads on the right and the left, the low frequency current is quite constant. On the contrary, in the second configuration, the bulk current increases by 20 dB per decade. But, above 50 MHz, current levels are similar. Such phenomenon is in agreement with measurements. It confirms the fact that the signals we measured at few centimeters of an open circuit loads was really a physical current, and not noise.

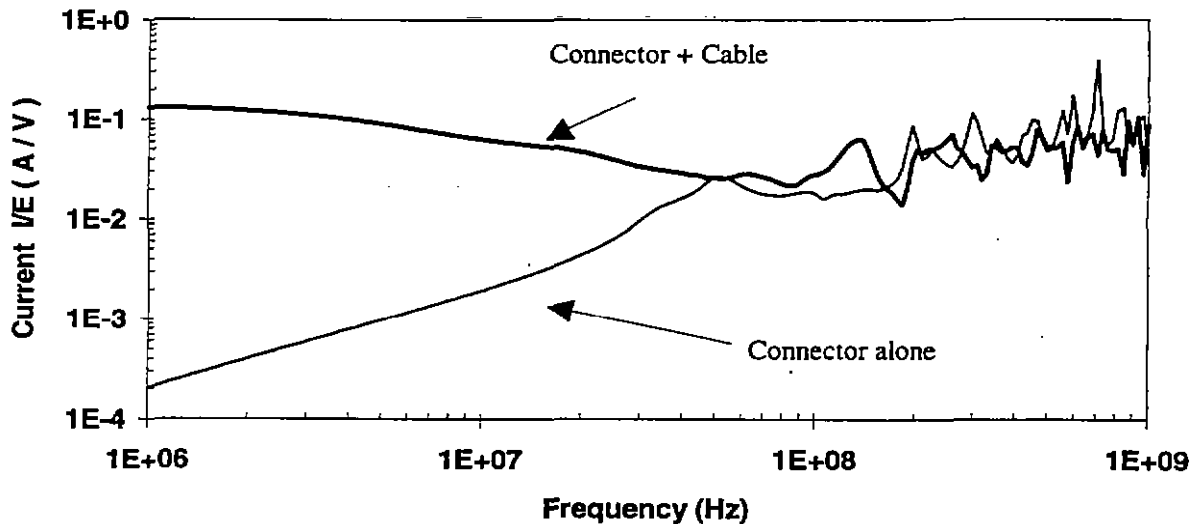


Fig. 3-12 : Comparison between two bulk currents before the connector (see figure 3-10 and figure 3-11)

3.2 Modeling of the cable network under study in the topological code CRIPTE

3.2.1 Introduction

The cable network under study was constituted of many bundles from 12 individual conductors up to more than 30 individual conductors. The direct calculation in the topological CRIPTE code of the whole network was clearly impossible in real time, considering our poor performance workstation. That is the reason why we chose to take profit from :

- the ability of the CRIPTE code to compute sub-networks equivalent models. The scattering parameters of a limited part (sub-network) of a network can be computed individually in order to be processed as any other junctions in the whole network,
- the topological volumes constituting the EMPTAC aircraft in which is running the cable network under study.

By using these properties, the total modeling of the cable under study was sufficiently reduced to run during the experimentation, enabling real time analysis of coupling phenomena.

3.2.2 Principle of sub-network decomposition

Let us recall that the topological modeling of a cable network is constituted of :

- "tubes", representing the homogeneous sections of harness described as respect to the Multiconductor Transmission Line theory. The traveling waves at each extremities of these tubes are related to each other thanks to a propagation matrix.
- "junctions", representing loads or branching of cables in other directions. The input and output waves are related to each other thanks to a scattering matrix.

But, one can imagine that since junctions are considered as black boxes, a reduced part of a whole network could be represented as a junction, what we call sub-network, under the restriction that one do not want to process voltage and currents inside this sub-network ([14]).

Let us take the example of an unshielded cable bundle constituted of N individual wires, running inside a structure and loaded with various terminal loads (see figure 3-13). In order to model correctly this problem, one must split up this bundle into various tubes of homogeneous sections depending on the bundle running and on the bundle varying average height over the reference plane. Let us assume, for example, that several current injections are applied at one of its extremity. Generally, one is interested only in the current and voltage induced at the other extremity (because this bundle at terminal loads may represent different sensitive equipment).

In a complex structure, this direct topological modeling could be quite big. The numerical size of the matrix to be inverted in that problem is around $2 \times N \times M \times I$, where M is the total number of tubes required for a precise characterization of the bundle running inside the structure and where I is the number of studied injection configurations ("source terms").

But if one only needs currents and voltages resulting of several injections at both extremities, one can reduced this numerical size by computing just once, the junction, or scattering parameters, of a sub-network which is equivalent to the tubes, except the tubes at both extremities, of the cable bundle (see figure 3-15). Once this equivalent junction has been processed, one has to link this equivalent junction to the terminal loads via the extremity tubes and to apply the several injections on this extremity tube ([9]). In that configuration, the total size of this problem is $2 \times N \times M$ (size of the sub-network computation) added to $2 \times N \times I$ (size of I resolutions of BLT equation on the reduced network).

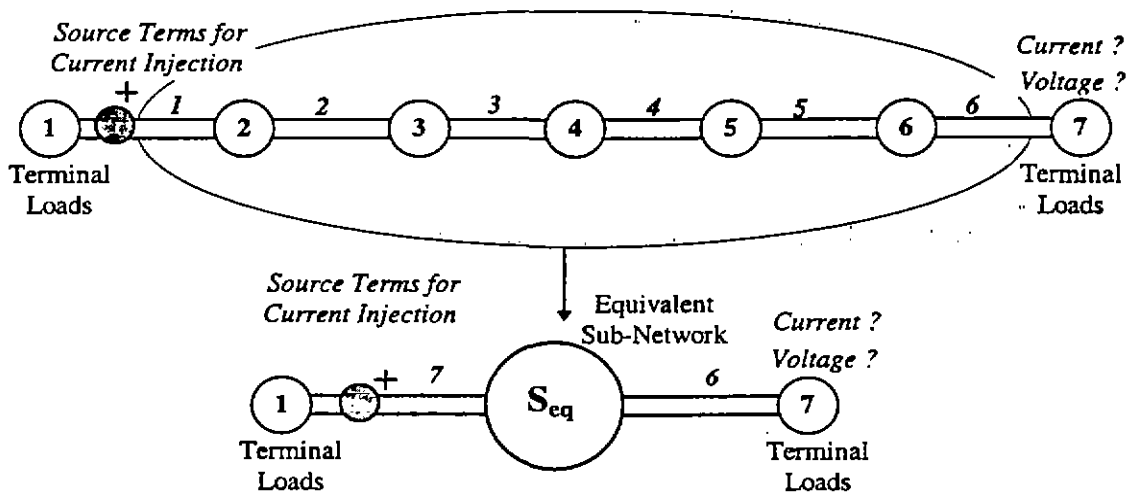


Fig. 3-13 : Principle of sub-network decomposition

Moreover, this procedure enables to change the terminal loads without processing the whole topological network. One can easily realize how these sub-network computation may efficiently enlighten the topological modeling of a complex cable network.

3.2.3 Topological model of the cable network under study

In EMPTAC wiring, some of the cables are constituted of twisted shielded pair ; their shield can be considered as another shielding level. As a first approximation, we assumed that this shield was good enough, that is to say that the current on the shield did not induce any interference on the inner twisted pair. Consequently, the inner twisted pair running inside the aircraft could be considered as a network independent of the other cables. Of course, the shields of these twisted pairs have been introduced in the modeling of bundles as any other unshielded wire short circuited to the reference ground at each terminal junction, in order to represent the physical connection at the connector level.

From these remarks, one can distinguish two classes of independent networks running inside the EMPTAC:

- networks gathering unshielded elementary cables, and shields of twisted shielded pairs. Their electrical parameters are calculated by means of the LAPLACE code (see 3.1), where the reference conductor is the ground plane for non shielded bundles or the bundle overshield,
- networks gathering inner pair, where the electrical parameters are computed with the LAPLACE code. Then, the reference conductor is the shield.

Therefore, this principle of sub-network compaction has been applied to the cable network under study. Each cable network of the first class of networks previously described, running inside a physical topological volume (cockpit, forward shielded volume, fuselage, aft shielded volume, B1B volume) has been modeled and computed individually as a sub-network. The second class of network, concerning the inner twisted pair has been modeled without taking into account the topological volumes since their reference was the shield.

Then, the processed sub-networks were connected together in order to compute the whole cable network by applying a source terms. At this point, the source could be whatever incident electromagnetic interference or bulk current injection.

As an example, let us take the shielded bundle, named NB2239, which is connecting the B1B through connector J016 to LD2 box through connector J075. This bundle is running inside the aircraft along a semi circle around the aircraft section. But, in this bundle, there are other cables involving connections to other connectors (J021 at LD11 and LD12).

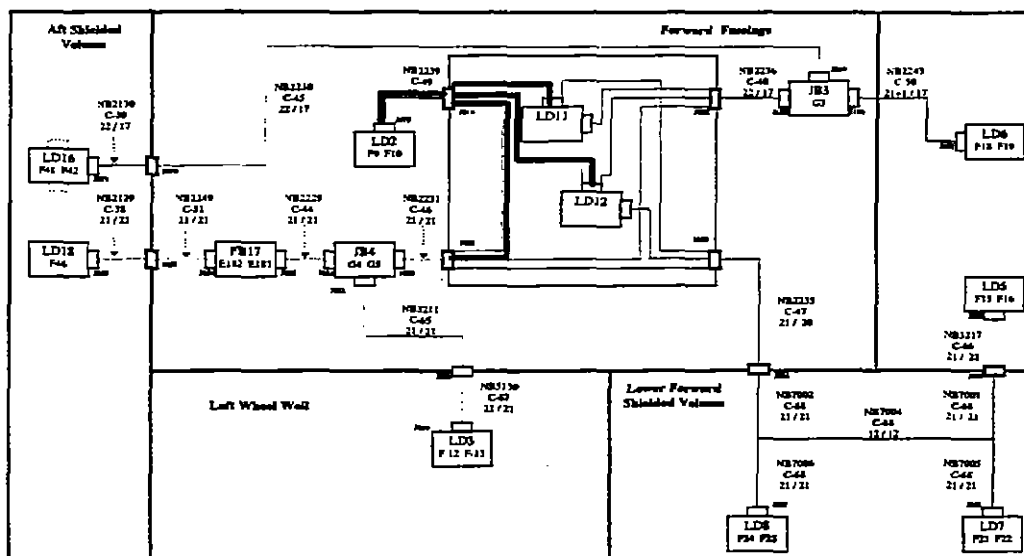


Fig. 3-14 : Running of bundle NB2239 inside the aircraft

Bundle NB2239 being shielded is considered as a topological volume and can be modeled as a sub network, named LD2 (figure 3-14). This bundle is constituted of one shielded twisted pair, one twisted three wire cable and 17 single wires. Therefore the topological model of this bundle is composed of two topological sub-networks :

- the first one is related to the modeling of the equivalent bundle constituted by the twisted three wire cable, the 17 single wires and the shield of the twisted shield pair, running from junction box LD2 to junction connector J016.

- the second one is related to the inner wires of the twisted shielded pair running from junction box LD2 to junction connector J012, LD11.

The resulting topological sub-networks are described on figure 3-15.

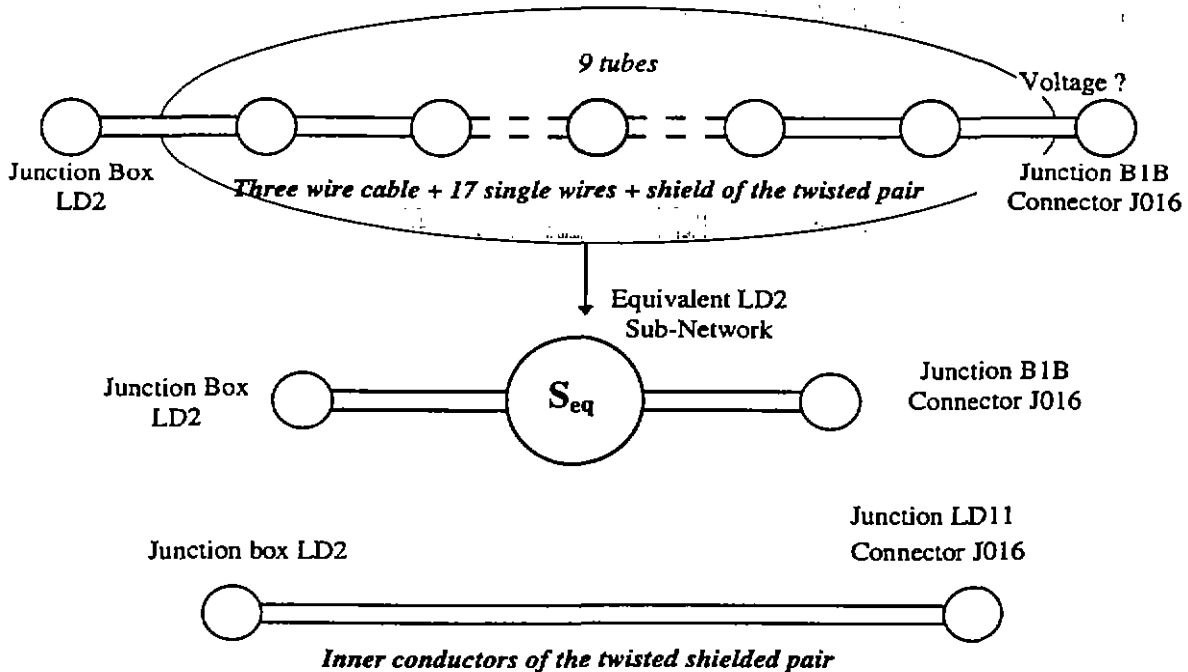


Fig. 3-15 : Sub-networks relative to bundle NB2239 (Three wire cable + 17 one wire cables + shield of the twisted shielded pair and shield of the twisted pair)

This principle has been applied to the whole cable network. Figure 3-16 represents the topological model of the cable under study in the whole aircraft using the previous principles. The tubes and junctions in dotted lines represent the inner two conductors of the twisted shielded pair. The entire set of sub-networks is reported in Appendix 1.

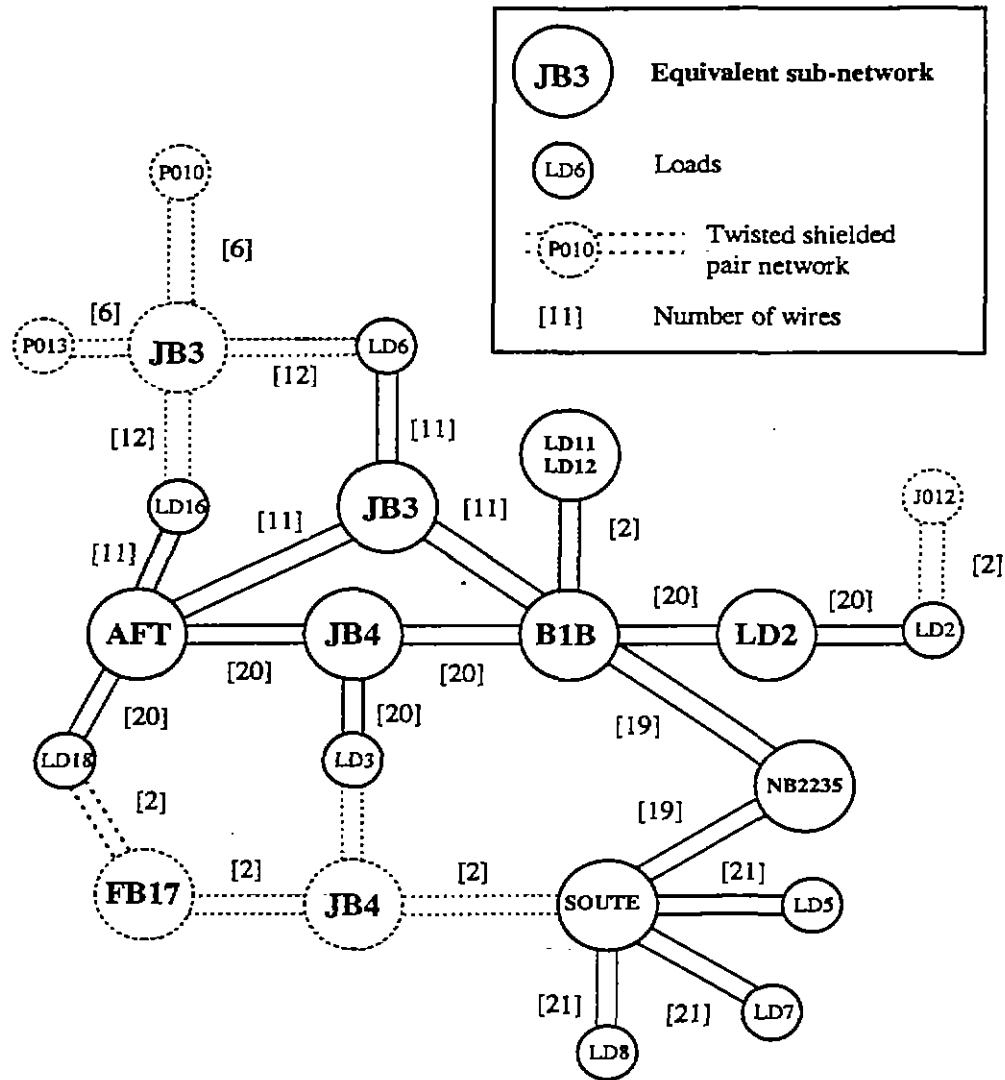


Fig. 3-16 : Topological modeling of the whole cable network under study

3.3 Performances of calculations

All the calculations made during this experiment have been carried out, in real time, on two small workstations with limited computing performance :

- a HEWLETT PACKARD 712/60 with 32 Mega Bytes of memory,
- a HEWLETT PACKARD 715/64 with 28 Mega Bytes of memory.

Of course, it was not possible to process the entire network of EMPTAC with a single computer. This is the reason why the global network under study has been broken down in elementary sub-networks. More, some of the sub-networks have been themselves broken down in elementary volumes to optimize computation time. Thanks to the topological decomposition, each computer has been used to calculate the elementary sub-networks.

Table 3-3 gives an overview of the performance of the calculations performed on these two computers. All the calculations were made on 150 points, between 300 kHz and 1 GHz. The global network of the EMPTAC was decomposed in 7 networks. This problem represents more than 1300 meters of wire, which are modeled by 3036 wires in the CRIPTE code. The results represent more than 400 Megabytes of data for 116 hours of computational calculation. However, computation time could be easily reduced using judicious compactions of sub-networks.

The most complex networks were B1B, JB3 and JB4. Their sizes were quite similar. Unfortunately, table figure 3-17 shows that the JB3 network needed more than 40 hours of computer calculation whereas the others need about 10 hours. The difference in computation time is due to the type of decomposition of the networks in small sub-networks. JB3 is cut in two sub-networks which are calculated at the same time (what is possible with the CRIPTE code). It requires the full memory of the computer during the calculation, which explains the loss of time. On the other hand, B1B and JB4 were cut in three sub-networks which each needs about 3 hours of computational calculation. Then equivalent S-parameters of B1B and JB4 networks are performed in few hours. This example justifies the use of equivalent S-parameters on networks and sub-networks in optimizing time of computational calculation. This example also demonstrates that such a process is perfectly suited for a paralleled algorithm for which each compaction of a sub-network could be computed with a specific processor.

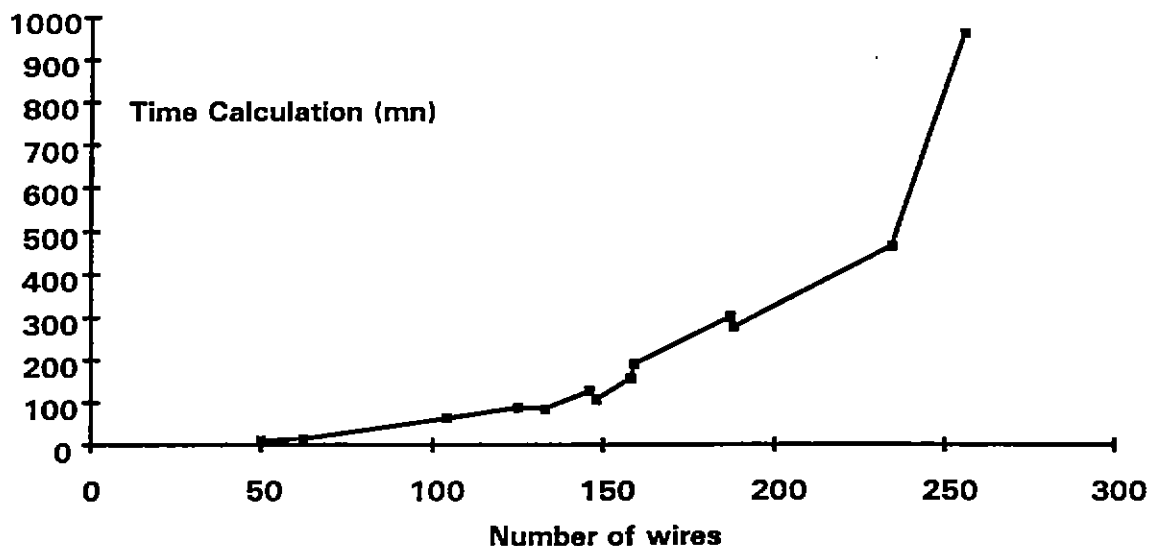


Fig. 3-17 : Number of wires and time calculation on HP 715/64

Network RUN - SEQ	Number of wires	Length of wires (m)	CPU Time (h:mn)	Size of resulting files (MBytes)
AFT_sre1 + AFT_sre2	229 + 158	169.80 + 71.70	10:27	15 + 4
AFT_tot	62	0.00	0:16	37
AFT	449	241.50	10:43	57
B1B_sre1	159	63.80	3:11	38
B1B_sre2	148	21.34	1:58	45
B1B_sre3	104	10.60	1:04	37
B1B_tot	133	0.00	1:26	50
B1B	544	95.74	7:39	170
JB3_sre1 + JB3_sre2	283 + 294	81.90 + 57.22	45:48	7 + 15
JB3_tot	50	0.00	0:12	11
JB3	627	139.12	46:00	33
JB4_sre1	146	58.53	2:08	16
JB4_sre2	125	57.44	1:29	16
JB4_sre3	188	173.88	4:37	16
JB4_tot	123	0.00	1:12	35
JB4	582	289.85	9:26	83
LD2	187	116.02	5:02	16
nb2235	158	120.62	2:38	16
soute (BLT)	234	288.77	10:59	1.2
soute (SEQ)	234	288.77	7:44	68
ETE III (BLT)	255	55.92	16:00	3.9
EMPTAC96	3036	1347.54	116:11	428

Table 3-3 : Time calculation during ETE III experiment

The objective of the sub-networks calculations is to obtain the equivalent S-parameter matrix and the equivalent voltage THEVENIN generator. The computational time depends on the number of elementary wires inside the sub-network. The size of equivalent S-parameter files depends on the number of wires of the external tubes ([3]). By this way, one may still obtain a small size of resulting S-parameter files with a long time calculation on a sub-network containing a big amount of tubes. Provided that the number of external tubes remains low. But, the size of S-parameter files may still appear very large. The main reason is that they are direct access files written on a 64 bytes record length. In the future, the size of these files could be easily optimized by coding data in binary mode.

The calculation of the equivalent THEVENIN generator comes from a BLT resolution involving all the wires of the sub-network. The resulting file contains the open circuit voltages on the wires of the external tubes. Data are coded in sequential ASCII mode. For this reason, for the same number of wires, the size of the resulting file is smaller than the S-parameter file.

In the next future, the computation time could be largely reduced using a specific linear system resolution algorithm managing with sparse matrices ([15]).

If one looks at the final network, one must keep in mind that the problem which has been studied presents the following characteristics :

- number of unknowns = 6072
- number of tubes = 131
- number of junctions = 138

4. MEASUREMENTS

Two kinds of measurements have been carried out with different goals :

- local injection with a current injector
- illumination under the ELLIPTICUS Antenna

In this section we will describe only the injection setups. The setups for the ELLIPTICUS measurements are similar to the one given in the Interaction Notes, Note 306.

4.1 Generalities on local injections

Before studying the whole aircraft submitted to a global illumination supplied by the ELLIPTICUS Antenna, it was necessary to analyze the propagation of electromagnetic energy in the electrical network. The purpose was to get a better understanding of the different interference paths for the currents at various frequencies. A lot of questions had to be answered such as :

- is there an upper frequency limit for the propagation of current ?
- what is the effect of the cavities on the coupling to and between bundles ?

Another point was to carry out a source injection which allowed us to split up the problem of the electrical characterization ([R], [L], [C] parameters of the network itself) and the problem of the sources terms applied on it. A local injection with a current injector presents has the advantage to help to the validation of the network modeling.

The injector was located in the LD7 box, inside the Lower Forward Volume or in LD6 box, inside the cockpit volume (see figure 4-1). The measurement probe was inserted on every test-point of interest in each volume of the EMPTAC.

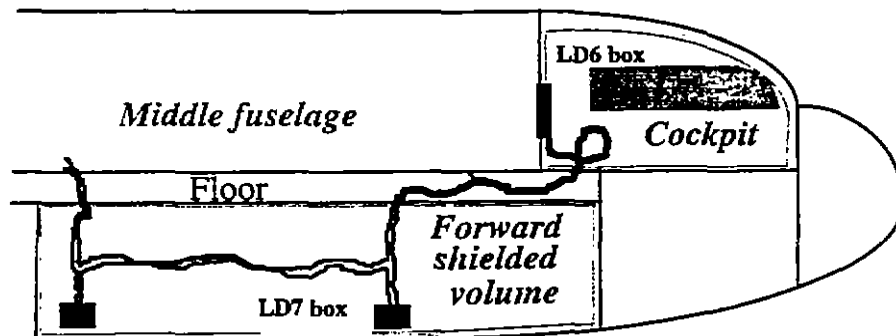


Fig. 4-1 : Location of LD7 box and LD6 box injection points

The typical experimental set-up was composed of :

- a network analyzer,
- amplifiers and attenuators,
- optic fiber links,
- a current injector,
- a measurement current probe.

During a first phase of the experiment, all the experimental set-up laid on the floor of the Lower Forward Volume (LFV), close to the LD7 box. The current injection probe was located outside the box. The goal was to achieve a correct ground reference for most of the equipment. Unfortunately, a first set of measurements showed that high frequency results were sensitive to the presence of the set-up. Some interpretations of this observation can be proposed.

In fact, the LFV can be seen as an empty cavity. At high frequency, the energy injected into LD7 box could not only be driven by the network (propagation taken into account by the CRIPTE code) but also partially transferred to some resonant modes of the LFV. If this assumption is true, the presence of the experimental set-up clearly affects the results. Note that the exact behavior of the fields in the cavity is of a great interest.

A second point is due to the possible leakage of the experimental set-up (common mode currents on the cable connected to the injection probe, fields radiated out of the amplifier...). These fields are also supposed to be converted into cavity modes, coupled to the cables and thus measured with the currents of interest.

In order to avoid the second problem, the whole set-up was finally removed from the LFV and installed into the fuselage. The current injection probe was also installed into the LD7 box. Then a new problem happened. It was the lack of ground reference for the injection probe. We checked that a current could be measured on the cable connected to the current injection probe. To minimize it, we placed the cable as close as possible to the wall of the LFV and we added a few number of ferrite devices on it.

Nevertheless, the sensibility of the current measurement probe to something that was not the injected current was a first alert showing that the high frequency measurements in a complex environment such as the EMPTAC had to be studied with care. We will discuss later other observations concerning the high frequency measurements.

The assumption of the resonant properties of the cavity was proved in another indirect way. The measurement of a current in one of the box of the LFV was reproduced in two conditions (with the door of the volume open and closed). As seen on figure 4-2 (representing the transfer function between the measured current and the injector equivalent generator E), the coupling level is a little bit smaller when the door is opened. It means the open door does not affect the propagation (first order analysis) but reduces the Q of the cavity. The decrease of the measured current suggests that there is a contribution of the resonant fields to the coupling.

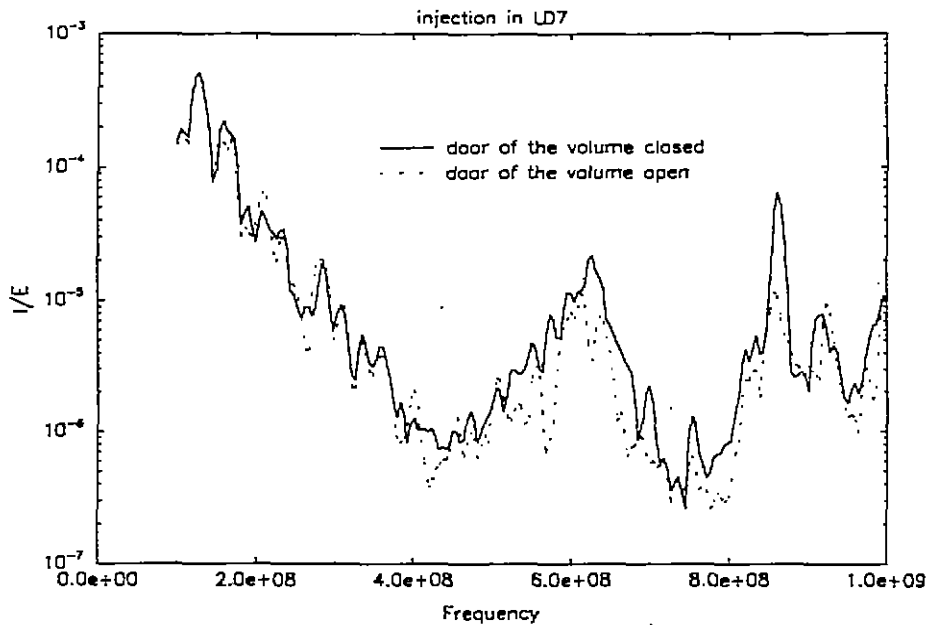


Fig. 4-2 : Influence of the opening of the Lower Forward Volume on the coupling

4.2 Calibration of the probes

4.2.1 Injection calibration

In most of the measurements, we used the 91550-1 probe to inject energy on the wiring located in the LD7 box, inside the Lower Forward Volume, or in the LD6 box, inside the cockpit volume. In order to get the best accuracy in measurements, the calibration was done in the same conditions as during a regular measurement in laboratory.

We calibrate the probe on a short line (10 cm long) with 50Ω (at one end the load is due to the input impedance of the Optic Link Transmitter). The experimental set-up is represented on figure 4-3 and on figure 4-4.

The gain of the optic link was different in each frequency range. The average value of the gain was about 33 dB.

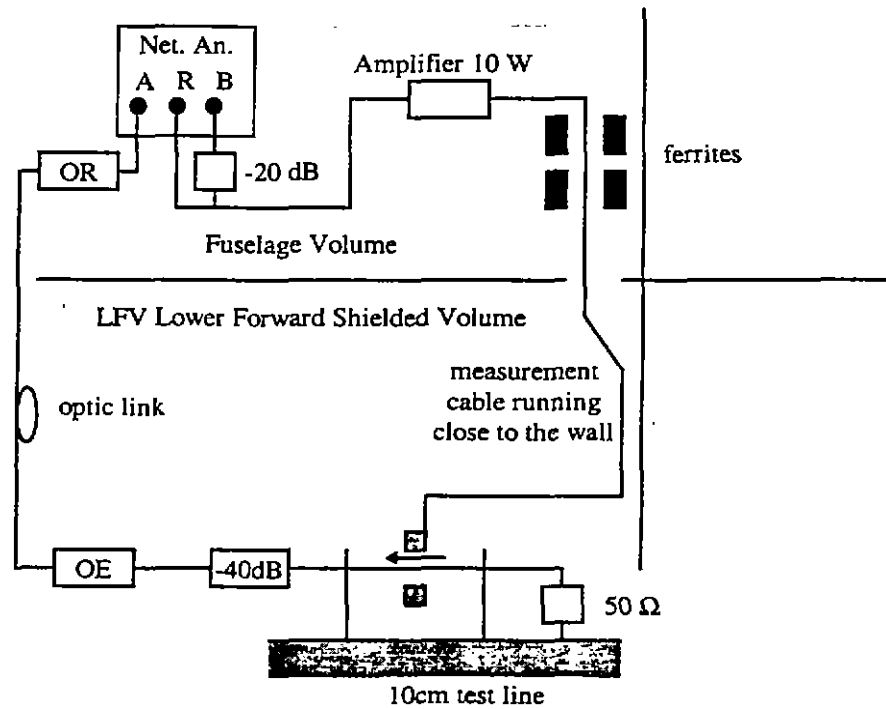


Fig. 4-3 : Calibration of the 91550 injection probe

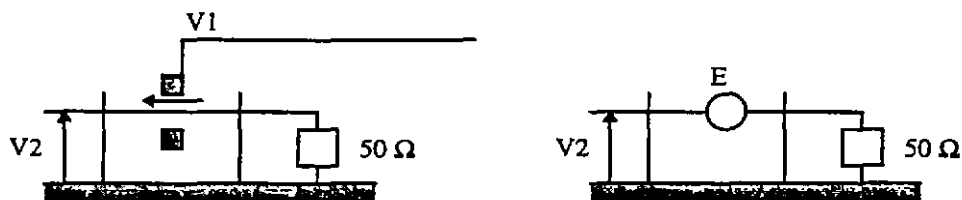


Fig. 4-4 : Equivalent model of the "current" injection on the test line

As respect to figure 4-4, we can say that the measured transfer function is equal to $V2$ over $V1$. This transfer function can also be expressed in terms of E , the equivalent voltage generator produced by the injector :

$$FT_{inj} = \frac{V2}{V1} = \frac{E}{2 \cdot V1}$$

4.2.2 Measurement calibration

In most cases, the currents on the bundles were measured with a 94111 probe. Two kinds of calibration procedure have been tested. The first one is a transfer function calibration, close to the

91550 calibration, using a small test line. The second one is based on S-parameters measurements following the principle described on the figures 4-5 and 4-6.

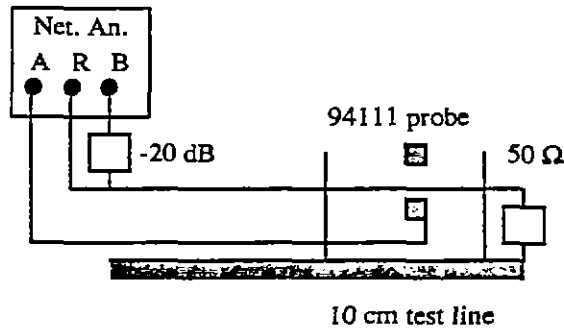


Fig. 4-5 : Calibration of the 94111 measurement probe

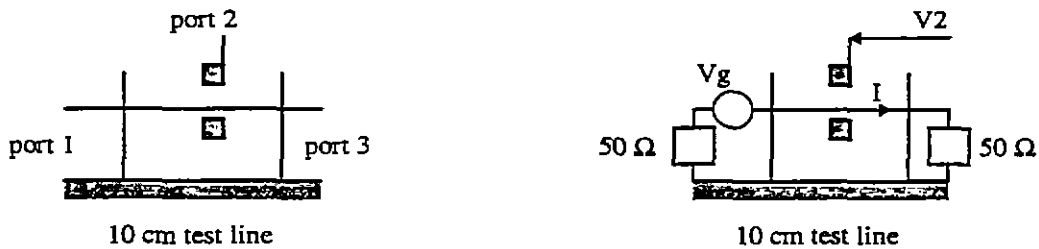


Fig. 4-6 : Equivalent model of the test line seen as a multiport and equivalent model of its transmission S_{21} S-parameter measurement

We can write that the current measured on the test line is equal to I. And consequently, we may express the S_{21} transfer S-parameter function as a function of I. We have :

$$I = V_g / 100$$

$$\Rightarrow S_{21} = \frac{2 \cdot V_2}{V_g} = \frac{V_2}{50 \cdot I}$$

So, the transfer impedance Z_t of the probe is directly related to the S_{21} measurement :

$$Z_t = \frac{V_2}{I} = 50 \cdot S_{21}$$

The general scheme for a transfer function measurement between a terminal box (LD7 for instance) and any of the other boxes is depicted on figure 4-7 :

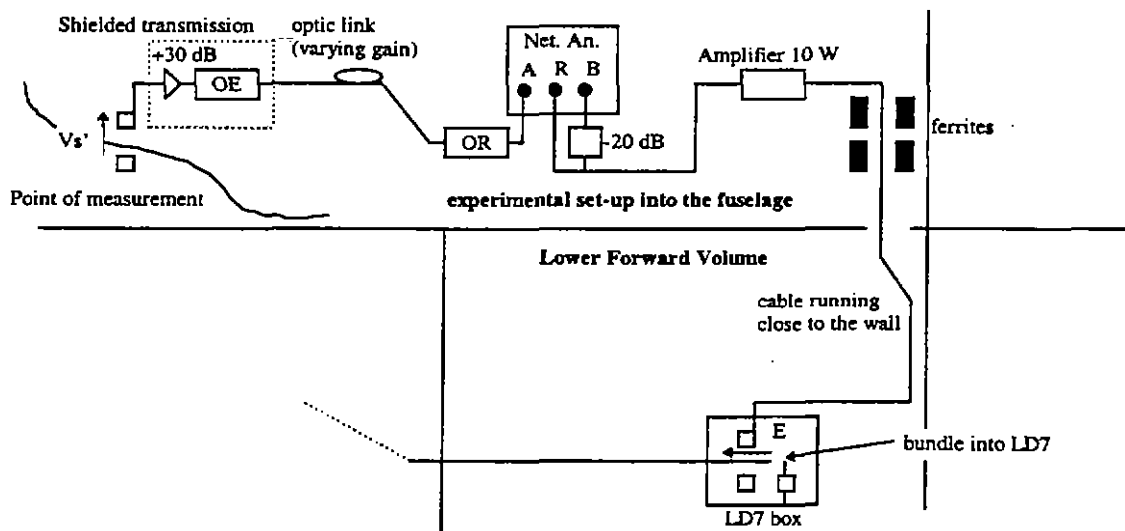


Fig. 4-7: General scheme for the measurements

In order to increase the signal/noise ratio, the total frequency range (300 KHz to 1 GHz) was cut into 3 parts. The gain of the optic link was modified in each frequency range.

Finally, the data processing applied to any measured current I in the EMPTAC was always normalized to the electrical generator E injected on the cable. This choice allowed us to make direct comparisons of the experimental results with the CRIPTE code. In all the models, a 1 Volt generator was applied on all the wires of the chosen bundle (the source tube).

The direct measurement is A/R . We can then deduce the following expressions:

$$\frac{I_s}{E} = \frac{V_s'}{50 S_{21} E} = \frac{V_s'}{50 S_{21} 2 FTinj R} = \frac{I}{100 S_{21} FTinj Gain R} \frac{A}{R}$$

where *gain* is 30 dB (when present) plus the varying gain of the optic link.

Applying this process, we assumed that the transfer function generator E was the same during the calibration and any measurement. However, this is not exactly true because the input impedance of the injector depends on its load (the probe can be seen as the primary of a transformer). During the calibration, the load was 50Ω . During any measurement, it depended on the global impedance of the total wiring of the EMPTAC. Therefore, R and E were not rigorously identical during the two phases. This problem would have disappeared if S_{21} measurement had been carried out. Unfortunately, this was not an easy calibration to perform, because of the presence of the amplifier. In practice, we have neglected this problem : it was considered as a second order discrepancy.

5. ANALYSIS OF EXPERIMENTAL DATA & NUMERICAL SIMULATIONS

5.1 Comparison between measurements and calculations on the forward shielded volume

5.1.1 Objectives

At the first step of the calculation, the elementary equivalent sub-network models had to be validated. For all of them, the scattering parameters between ports connected by a same wire have been tested in low frequency, and it has been checked that this parameter was equal to 1. Of course, the forward shielded volume had been exhaustively studied during the previous two experiments. Nevertheless, let us insist on the fact that the numerical simulations performed during ETE III were full simulations, that is to say that all the parameters introduced were modeled (the source, the wiring, the junctions). During ETE I and ETE II, some tube characteristics had to be measured because, at this time, the LAPLACE code was not ready to perform big calculations. Moreover, only a few number of numerical simulations had been performed on network A (the real wiring, as installed inside the airplane). Most of the measurements and calculations were performed on network B (the test wiring ([6]) installed by ONERA and CEG) : the study was conducted in the same way as for network A, but network B was made of very simple cables.

The sub-network dealing with the coupling in the forward volume and the cockpit is easily obtained by disconnecting the wiring at J006, and by connecting a short circuit connector at this point. In this configuration, the cockpit shielded cable, terminated on LD5 box, still remains connected to the shielded volume wiring, at J004 level.

5.1.2 Local bulk current injection

The first test performed dealt with a bulk current injection inside the LD7 box. Total current has been measured at J006, J007 (inside LD8 box), J005 (inside LD7 box) and J003 (inside the LD5 box).

As a first calculation, the network used by the CRIPTE code for the calculation is similar to the one depicted on figure 2-4. One can notice that the tube breakdown has been made roughly. Particularly, the shielded cable, inside the cockpit volume, has been decomposed in only 3 tubes, what we suspected not to be sufficient to obtain a significant attenuation. In ETE I experiment, the cockpit shielded volume had been split up into 10 tubes. In ETE III experiment, only the internal problem of the shielded cable was considered, whereas in ETE I, both external (the

shield) and internal coupling had been taken into account. Because of the numerical method used in our diagonalization, such a process could not be applied easily on shielded cables (see 3-1-3) ([13]). All these calculations were performed in real time, during the experiment.

As a second calculation, performed afterwards in France, we tried to see the influence of taking into account a random twisting on the cables. For this, the previous tubes, have been decomposed in small tubes. For each decomposition, an equivalent junction has been calculated. The decomposition has been made every 10 cm. The other characteristic of these calculations is that the modes on the tubes have been computed with a numerical algorithm, not in an analytical way, as for the real time calculation, during the experiment.

For each of these test points, figures 5-1 to 5-4 present the overlay of the results obtained with CRIPTE code and the measurements. Each of these plots are decomposed in two sets of curves :

- figure of type a, dealing with the real time calculation (with a rough tube decomposition),
- figure of type b, dealing with the delayed calculation, (with a decomposition every 10 cm).

On all these curves of type a, a common observation may be carried out. The calculation gives good results in a low frequency domain (up to 100 MHz) but is not in accordance at higher frequencies (from 100 MHz to 1 GHz). The agreement in low frequency shows that the random decomposition of tubes is sufficient to describe the coupling on the network at this frequency range. Generally, the average value of computed and measured results are similar except for figure 5-1 (current obtained at J003). The CRIPTE code calculation presents an attenuation but it is not comparable to the one of the measurement. Two main causes may be suspected :

- in high frequency, the circuit equivalent to the injector may be different whereas the generator used in the calculation has a magnitude which remains constant.

- the number of elementary tubes used to describe the shielded cable is certainly not sufficient to produce a significant attenuation on the internal wires.

Figures of type b, seem to give more accurate results under 100 MHz. The reason is due to the decomposition of cables in a sufficient number of elementary tubes. The average of the coupling on the whole wiring is then made naturally by the number of elementary tubes.

In high frequency, from 100 MHz, the tube decomposition seems to give a good representation of the tube mismatching. This seems to verify the hypothesis we suggested for which the attenuation on the wiring is mainly due to the fact that there is no propagation on the wiring. By this way, the main hypothesis of a radiation due to the wiring should be excluded. One will notice that a 10 cm decomposition would give a good representation of the cable up to 200 MHz (if we adopt a criterion for the sampling equal to $\lambda/5$, where λ is the wave length under study). Effectively, after 200 MHz, the modeling becomes higher than the measurement.

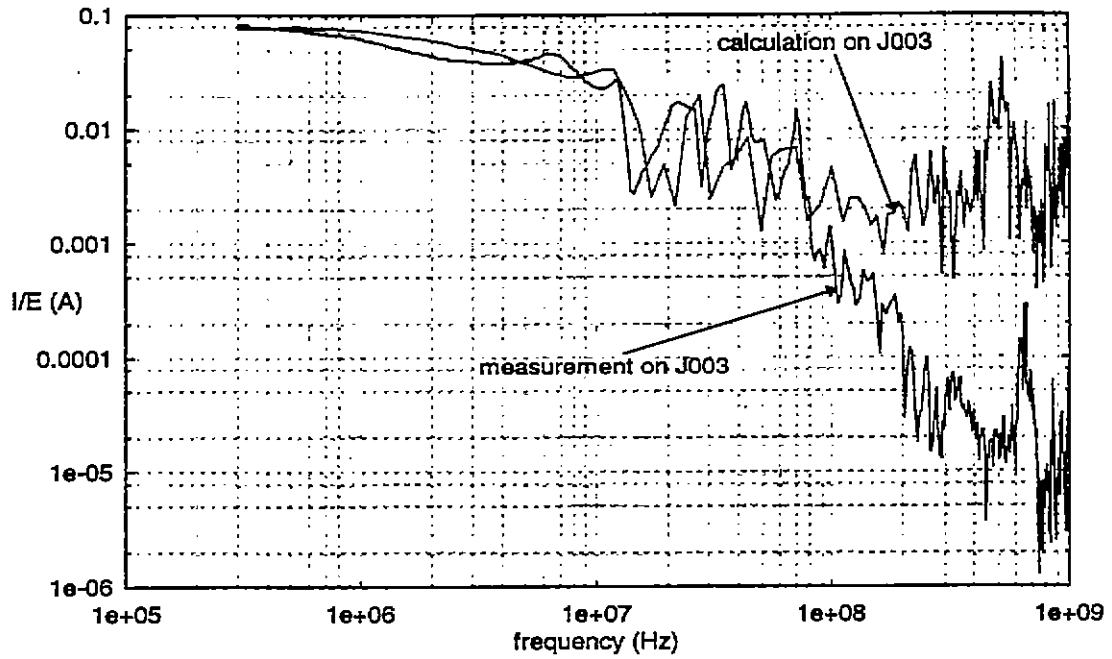


Fig. 5-1-a : Rough tube decomposition

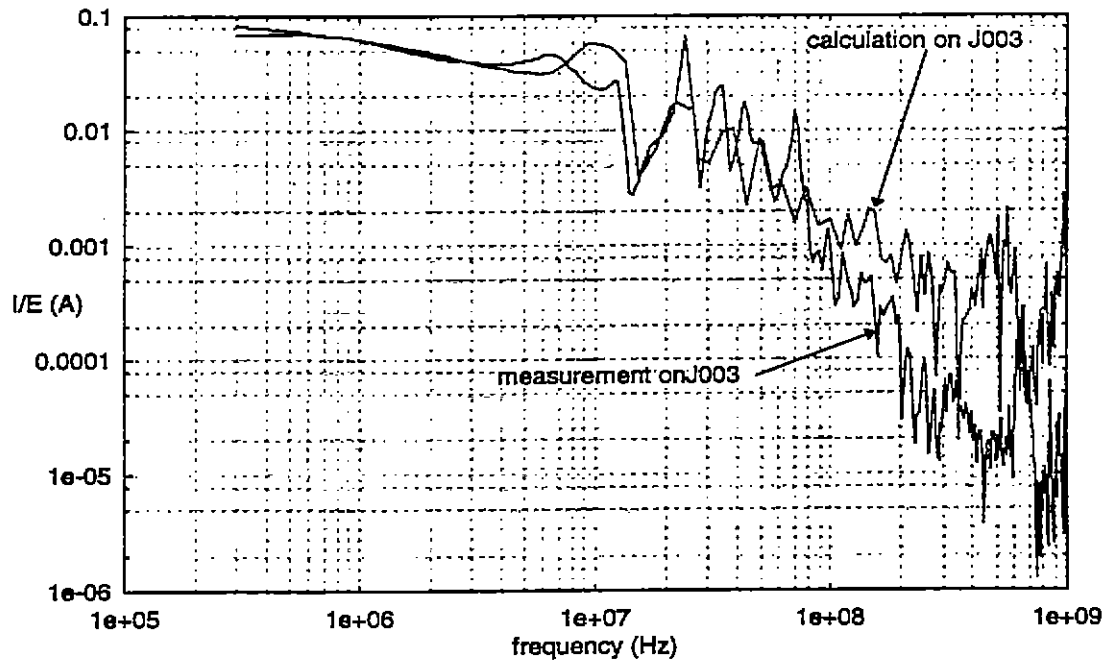


Fig. 5-1-b : 10 cm tube decomposition

*Fig. 5-1 : Comparison of bulk current obtained at J003
for a bulk current injection at J005 (inside LD7)*

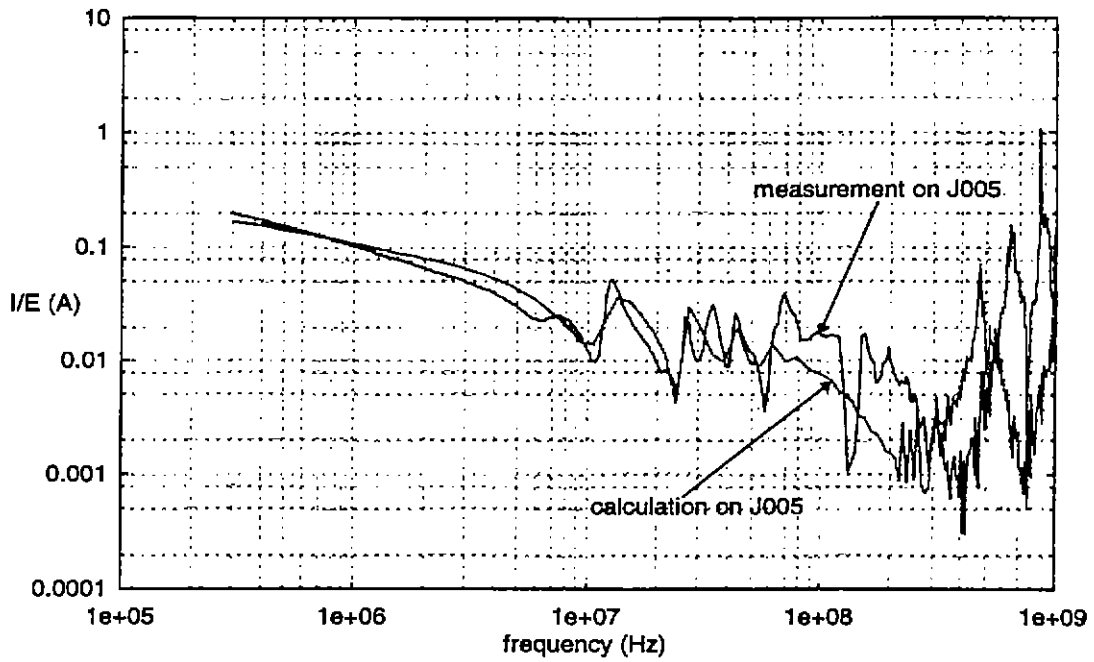


Fig. 5-2-a : Rough tube decomposition

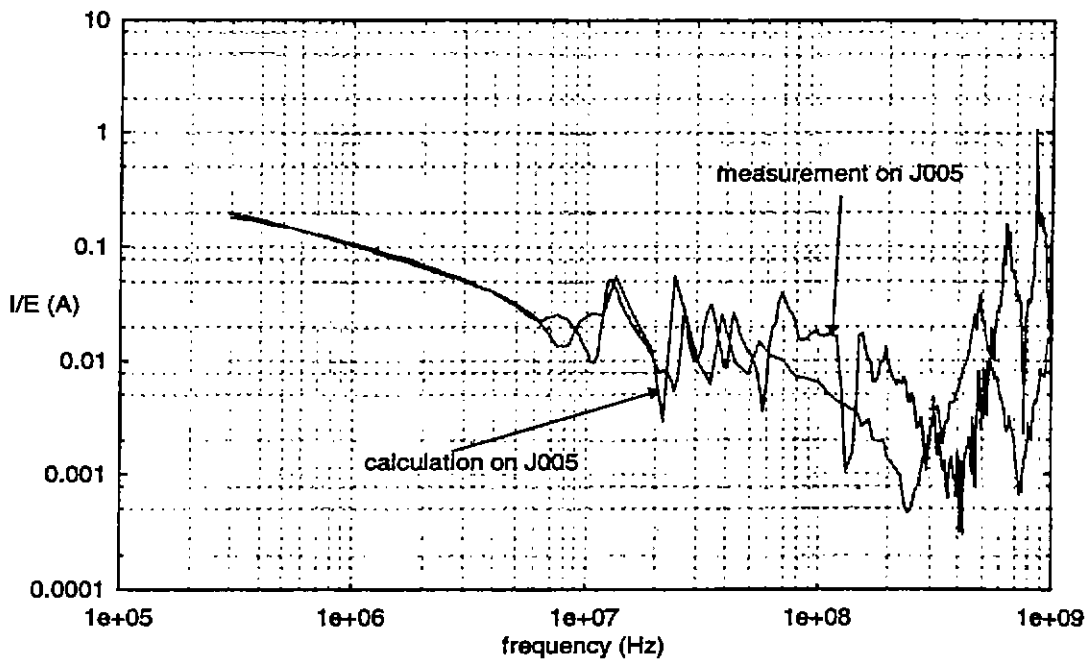


Fig. 5-2-b : 10 cm tube decomposition

Fig. 5-2 : Comparison of bulk current obtained at J005 for a bulk current injection at J005 (inside LD7)

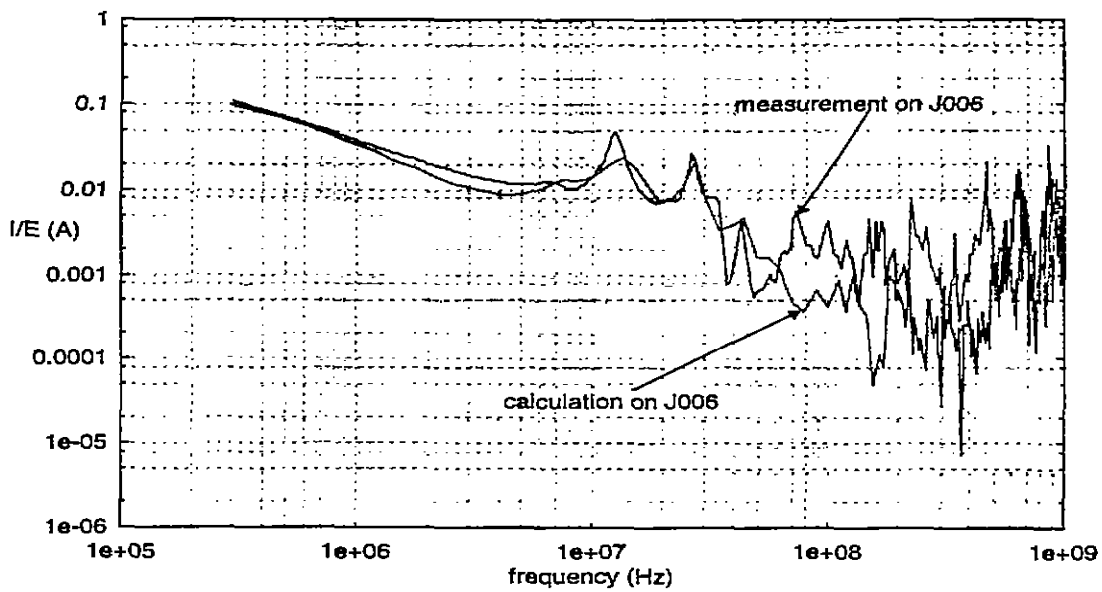


Fig. 5-3-a : Rough tube decomposition

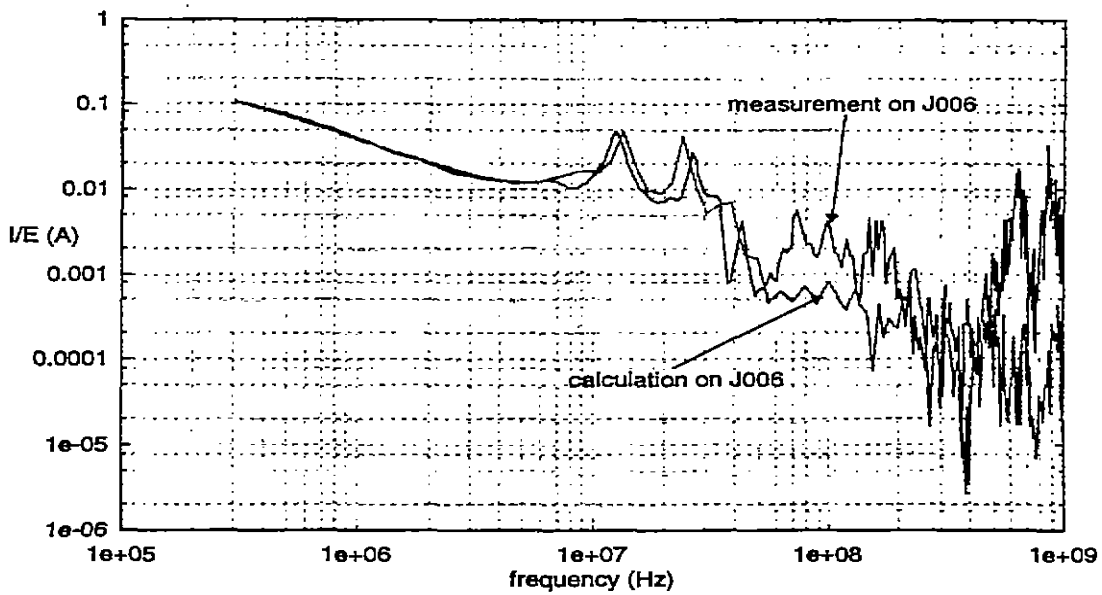


Fig. 5-3-b : 10 cm tube decomposition

Fig. 5-3 : Comparison of bulk current obtained at J006 for a bulk current injection at J005 (inside LD7)

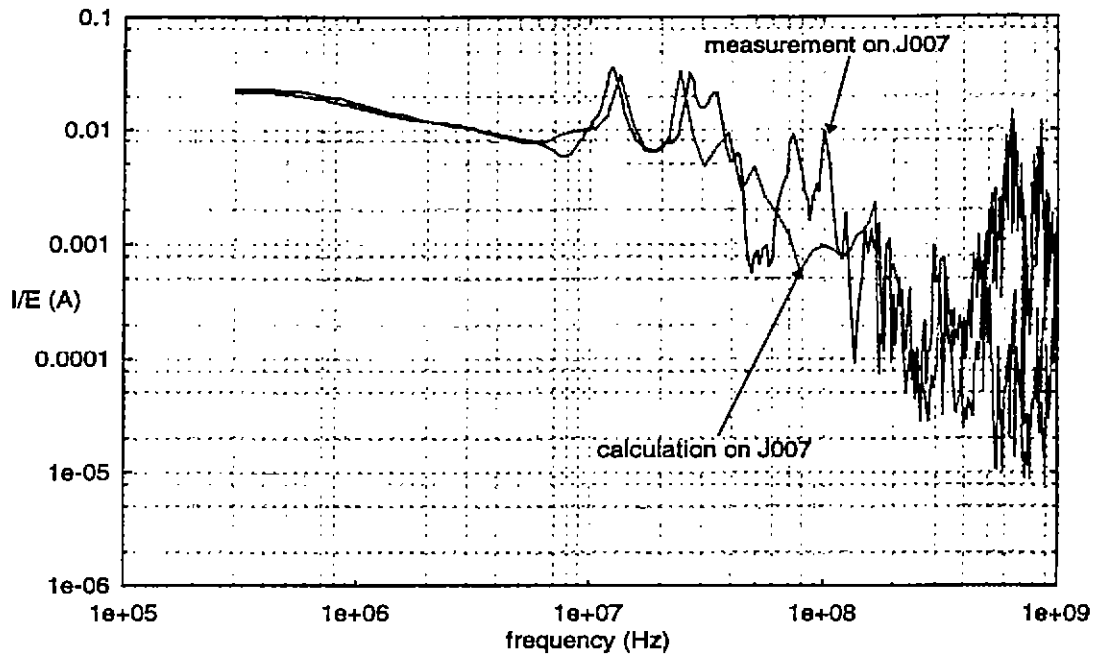


Fig. 5-4-a : Rough tube decomposition

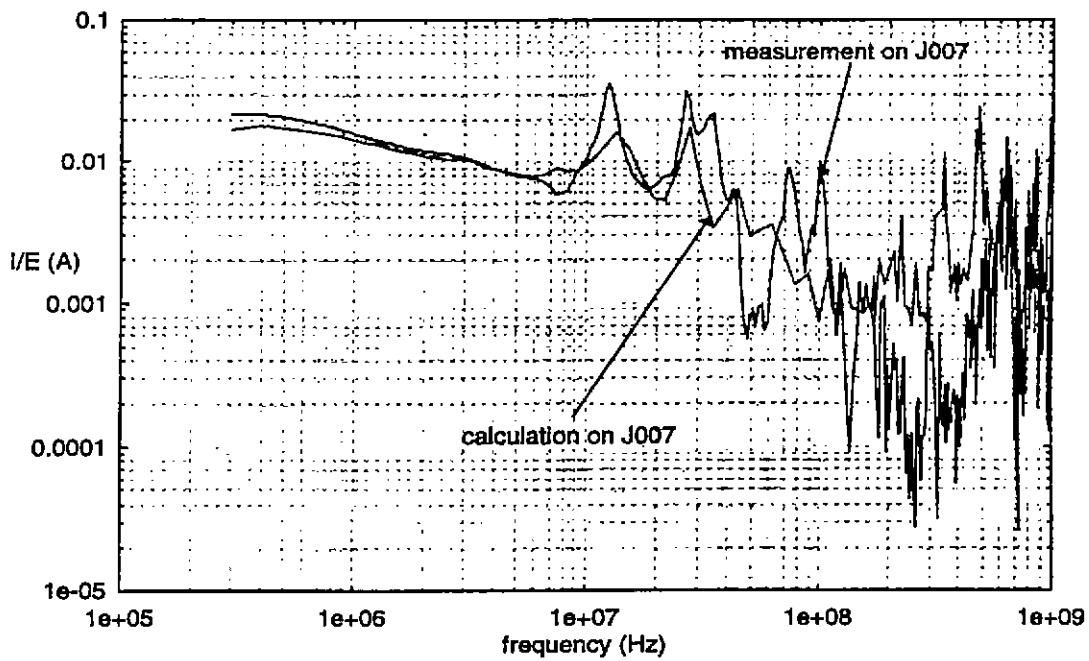


Fig. 5-4-b : 10 cm tube decomposition

*Fig. 5-4 : Comparison of bulk current obtained at J007
for a bulk current injection at J005 (inside LD7)*

The other interesting point lays in the fact that, when we analyze closely the calculated and measured results, we observe the same behavior depending on the location of the test point as respect to the location of the source. The current injector is placed on LD7, that is to say on J005 connector. At low frequency, results at J007 (on LD8) and J006 have quite the same magnitude as J005 result. But in high frequency, this amplitude becomes smaller because of the distance from the source. Moreover, in low frequency, the calculations obtained with a 10 cm tube decomposition are more precise but the decomposition does not improve the modeling in high frequency. This is due to the fact that taking into account the distance from the measurement points and the source point does not require a precise decomposition. On the contrary, at J003 (at LD5 level, in the cockpit), the results obtained with the 10 cm decomposition are more precise. This is due to the fact that LD5 is far from the source (about 10 meters). Consequently, the mismatching is more important than for the previous cases. To visualize the mismatching, one could say that the number of mismatching transitions is equal to the number of 10 cm elementary tubes encountered. Of course, this number becomes greater, when the distance increases.

5.1.3 Current injection on one wire

The second type of calculations dealt with a voltage injection on the first wire of the bundle at LD7. Figure 5-5 shows two signals obtained by CRIPTE and by measurement at J006. J006 is connected to a short circuit connector, as in the previous case. Once more, calculations were performed at different time, during the experiment (figure 5-5-a) and afterwards, in France (figure 5-5-b). The difference between type a and type b figures is the same as the one described in the previous section.

On figure 5-5-a, the agreement between measurement and the CRIPTE code simulation is good in low frequency, up to 100 MHz. The agreement is not as good as in the case of a bulk current injection : the reason is that the calculation depends strongly on the geometric meshing used for the tubes. In our case, let us recall that all the geometry sections of tubes have been calculated randomly. In high frequency we may carry out the same conclusions as in the previous example : the modeling used in CRIPTE code is not accurate enough to reproduce the attenuation of signal (from 100 MHz to 1 GHz).

In fact, this is what was made on type b calculations. In low frequency, results are quite similar as type a calculations, except the differential coupling on wire AA which is better reproduced (maybe due to the calculation of propagation modes on tube with a numerical method). From 1 MHz, we clearly observe the effect of the mismatching due to the tube decomposition. Of course, because of the 10 cm decomposition, the 20 dB attenuation slope is limited to 200 MHz. Nevertheless, the securing point of the calculations is that computed results behave as the measurements in high frequency. Particularly, one must notice that the response on the excited wire, and the differential response on an other wire have the same attenuated magnitude in high frequency (up to 200 MHz).

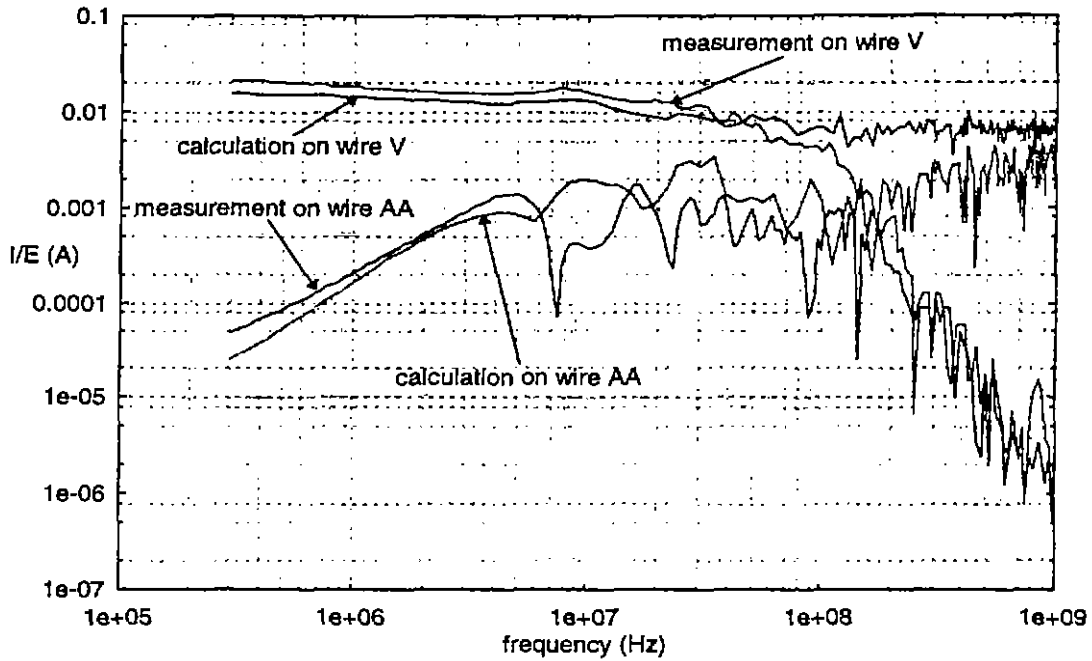


Fig. 5-5-a : Rough tube decomposition

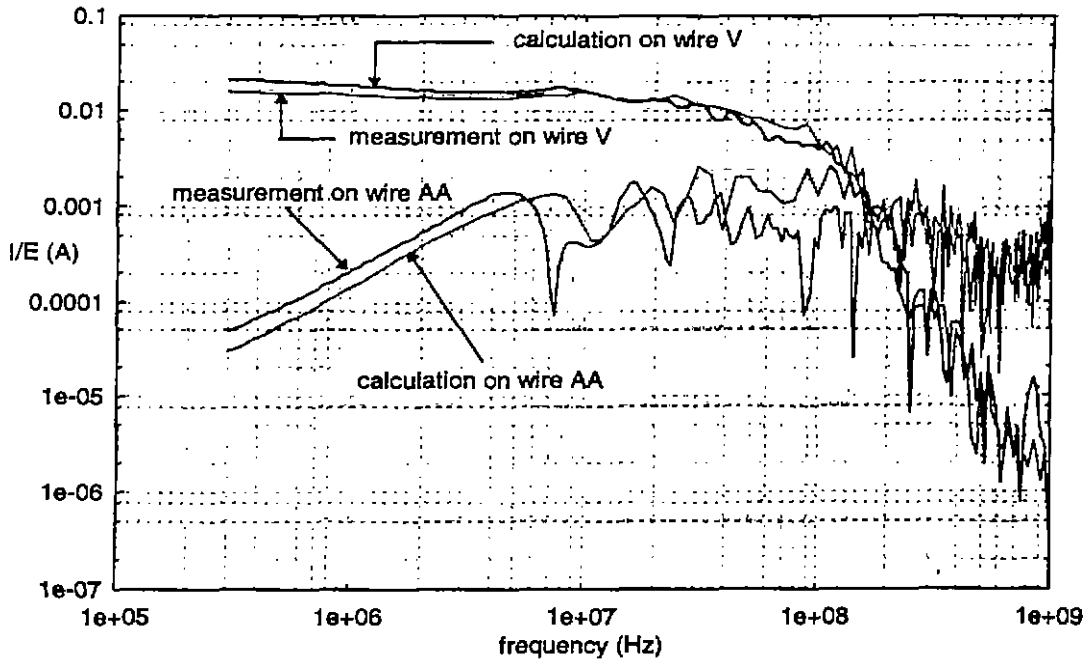


Fig. 5-5-b : 10 cm tube decomposition

Fig. 5-5 : Comparison of bulk current obtained at J006 for an injection at J005 (inside LD7) on wire 1.

5.2 Measurements and CRIPTE code calculation on the whole network

In this section, we will present bulk current results for local current injections. The difference with the previous section is that now, the entire network is connected to the forward shielded volume.

5.2.1 LD7 current injection

The first set of comparisons deals with a bulk current injection on all the wires inside LD7. All the results reported on figure 5-6 to 5-8 deal with global current measurements at different test points of the electrical network. The numerical calculation has been achieved by applying a 1 volt generator on all the wires at J005. All the currents presented on the curves are normalized to the injected voltage generator.

In the following plots, the difference between the type a, b, c curves is the following :

- type a : measurements
- type b : real time calculation (with a rough tube decomposition)
- type c : delayed calculations (with a 10 cm tube decomposition)

For all results, one may notice once more that the agreement between measurement and calculation is good under 100 MHz, and less precise in high frequency, depending on the tube decomposition.

The agreement is good up to 100 MHz, for both type b and c calculations. Specially, the common mode coupling on J003, J005 and J006 and the differential coupling on J007 are well reproduced. In high frequency, once more, type c calculation is more accurate. Specially, the attenuation on J003, J007 and J006, which are far from the injection point LD7 is modeled, and the signal on J005, close to LD7 is well estimated. Such an observation could make us think that, far from the source, the signal does not depend on the load connected at the termination. This point will be confirmed in section 5.2.2.

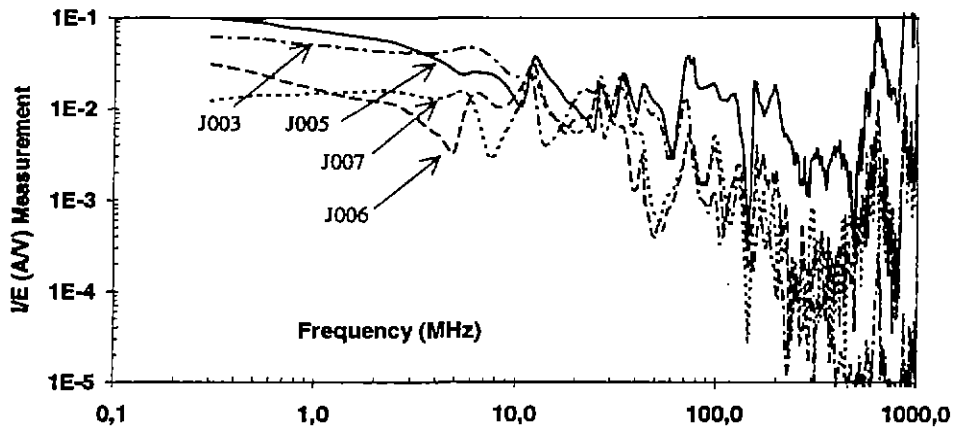


Fig. 5-6-a : Measured currents on J003, J005, J06 and J007 for an injection on LD7

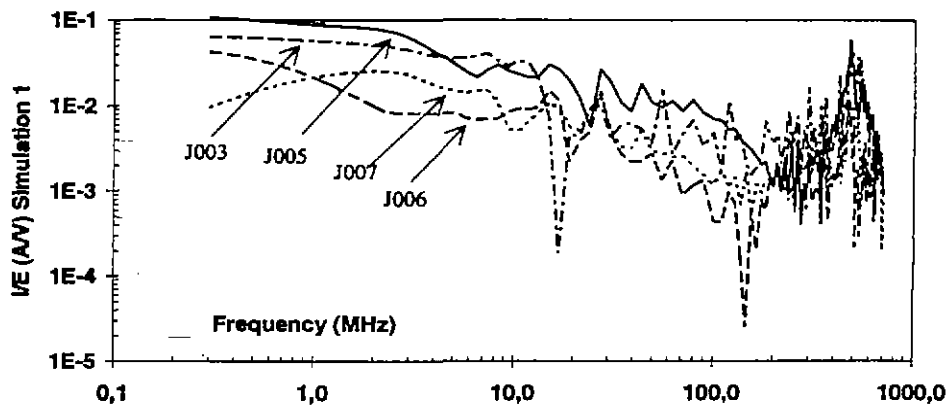


Fig. 5-6-b : Calculated currents on J003, J005, J06 and J007 for an injection on LD7 with a rough tube decomposition

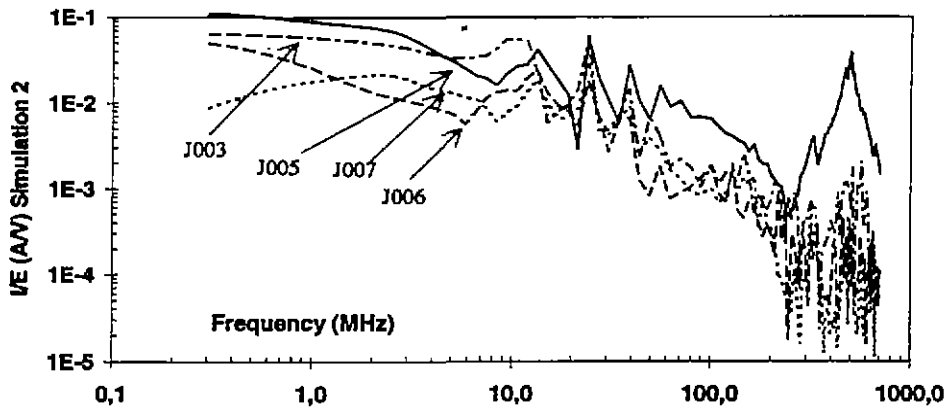


Fig. 5-6-c : Calculated currents on J003, J005, J06 and J007 for an injection on LD7 with a 10 cm tube decomposition

Fig. 5-6 : Comparison of currents measured and computed on J003, J005, J06 and J007 for an injection on LD7

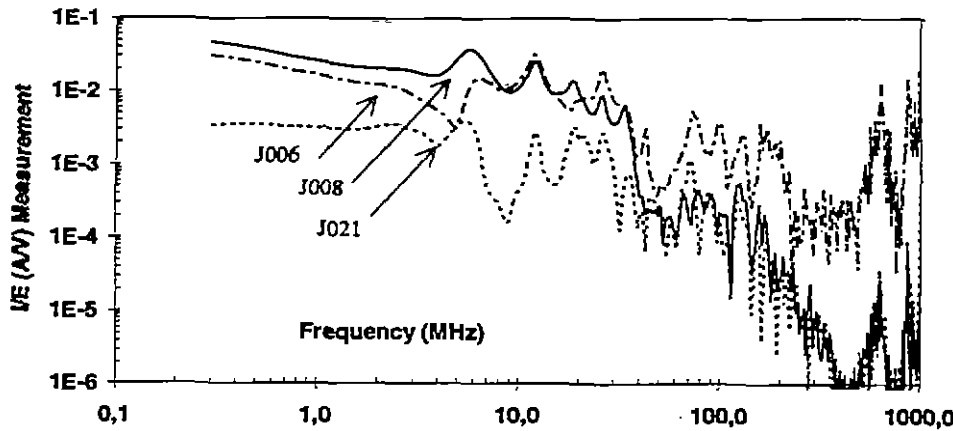


Fig. 5-7-a : Measured currents on J006, J008, J021 for an injection on LD7

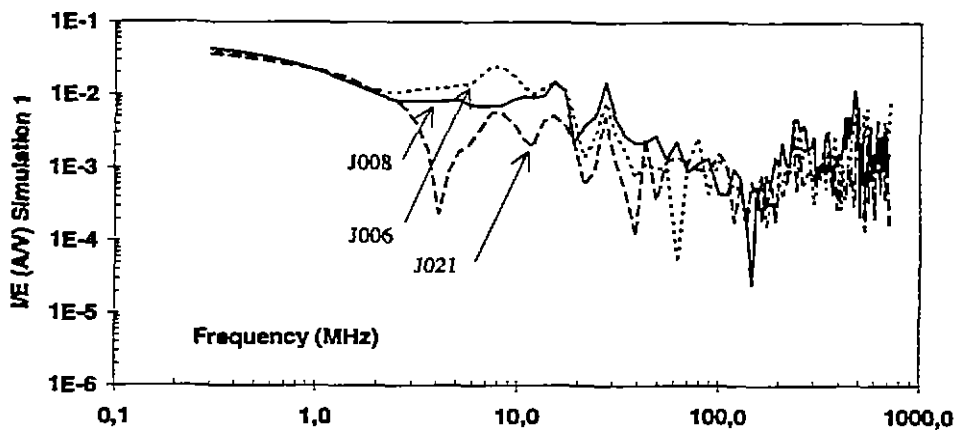


Fig. 5-7- b : Calculated currents on J006, J008, J021 for an injection on LD7 with a rough tube decomposition

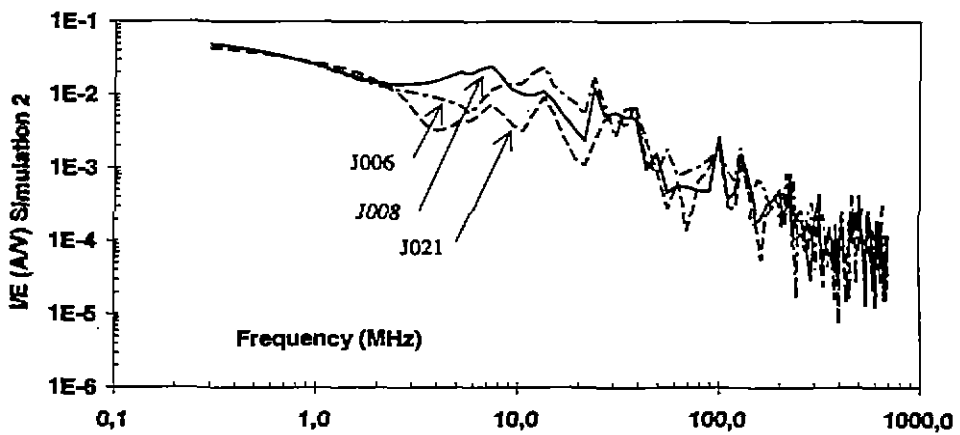


Fig. 5-7-c : Calculated currents on J006, J008, J021 for an injection on LD7 with a 10 cm tube decomposition in the cockpit and forward volumes

Fig. 5-7 : Comparison of currents measured and computed on J005, J006, J071 for an injection on LD7

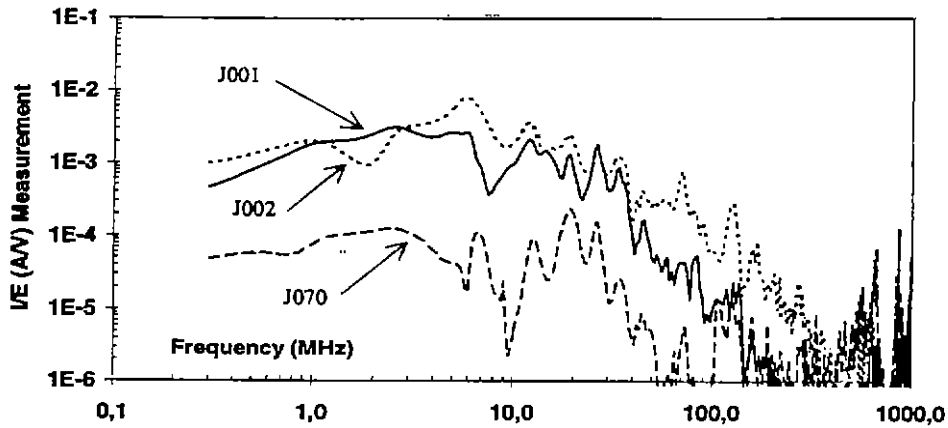


Fig. 5-8-a : Measured currents on J001, J002, J070 for an injection on LD7

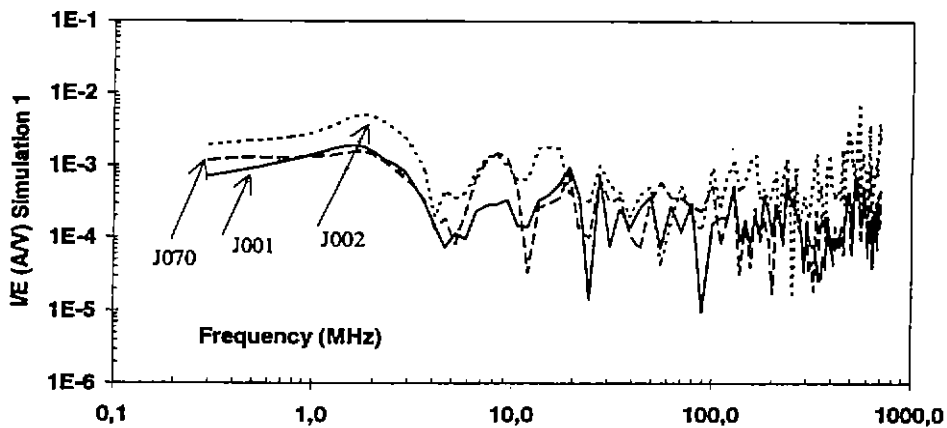


Fig. 5-8-b : Calculated currents on J001, J002, J070 for an injection on LD7 with a rough tube decomposition

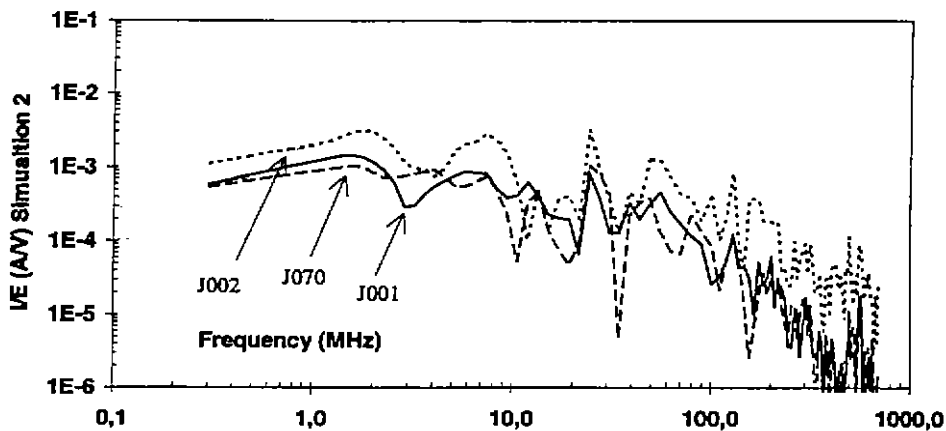


Fig. 5-8-c : Calculated currents on J001, J002, J070 for an injection on LD7 with a 10 cm tube decomposition

Fig. 5-8 : Comparison of currents measured and computed on J001, J002, J070 for an injection on LD7

Figure 5-7 presents the coupling on the shielded bundle nb2235, in the fuselage volume (at J006 interface with the forward shielded volume, and J008, inside B1B box), and at J021, behind the B1B box. The interesting point in the measurement is that, up to 100 MHz, the signal on the shielded cable is similar at both extremities. But in high frequency, the measured signal at J008, farther from the injection point than J006, presents a greater attenuation. This phenomenon is not taken into account in the CRIPTE code numerical simulation. At J021, we can see the effect of a direct transmission of signal from J008.

As described in [8] a three wires cable should connect these two test points. The CRIPTE code simulation finds a signal at J021 a little lower than the input current at J008 but in the measurement, the same signal is much more smaller. No real explanation could be carried out at this time : we can suspect a rough meshing of B1B volume in the CRIPTE code but the bad low frequency calculation results would rather make us think of a bad modeling of terminal loads inside the B1B volume. Moreover, bad data in the reference wiring description book ([8]) may not be excluded, as it has been noticed several times during ETE-L. A more accurate meshing, with a number of tubes generated randomly, might certainly have given a significant attenuated signal.

Figure 5-8 depicts the signal at three other test points where wiring is connected to JB3 junction box : J001, at the level of LD6, inside the cockpit, J002, point of entry of B1B volume, and J070, at the interface between the fuselage and the aft volumes (see figure 2-9). In low frequency, we can verify that in the computed results, the input current at J002 is equal to the sum of the current at J001 and J0070. In high frequency, the three signals have an equivalent level whereas the measured signal does not follow these rules. At this time, the validity of measurement at J070 is suspected.

Finally, as a conclusion of the analysis of the LD7 injection (J005 test point), we may give the following conclusions :

- in low frequency, up to 100 MHz, the signal is constrained to enter B1B bay through J008, and the signal coming out of this box comes from differential coupling with stressed wires. The modeling of such coupling strongly depends on the accuracy of the terminal loads, on the accuracy of the tube decomposition and on the accuracy of the tube section geometry,

- in high frequency (from 100 MHz to 1 GHz), an obvious attenuation, increasing with the linear distance from the injection point is demonstrated, whereas it is not with calculations. May be, once more, a strongest tube decomposition could help to obtain more significant attenuation. Nevertheless, one must remember that all measurements are made inside the boxes. The attenuation may also be due to an average field generated inside the boxes by the input current, this field being able to interfere with the wires inside the boxes.

5.2.2 Influence of the connection of the whole network

As referred to sections 5.1.2. and 5.2.1., the fact that we measure and calculate bulk currents at different points in the forward volume with an injection localized in LD7 allows us to observe the influence of the whole network (considered as an equivalent complex load applied at J006) and a short circuit at J006 (the rest of the network is totally disconnected from the forward volume). Comparisons between the whole network connected and disconnected to the forward volume are plotted for bulk currents measured at J003, J005, J006 and J007 (figures 5-9 and 5-10).

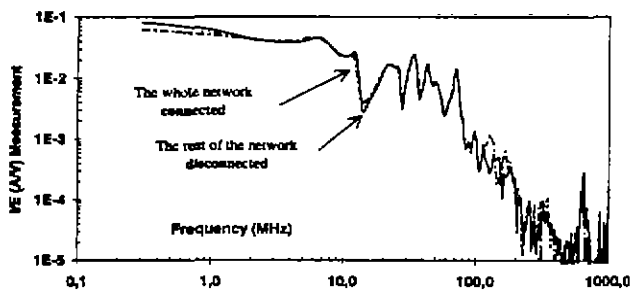


Fig. 5-9-a : Currents measured on J003

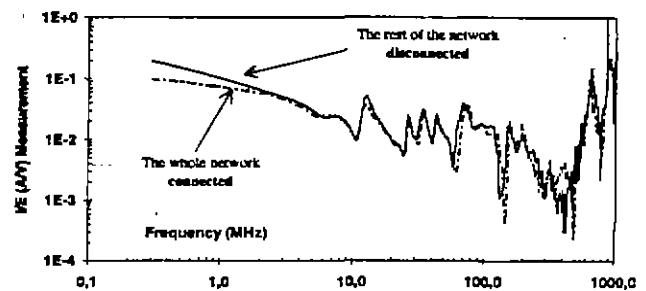


Fig. 5-9-b : Currents measured on J005

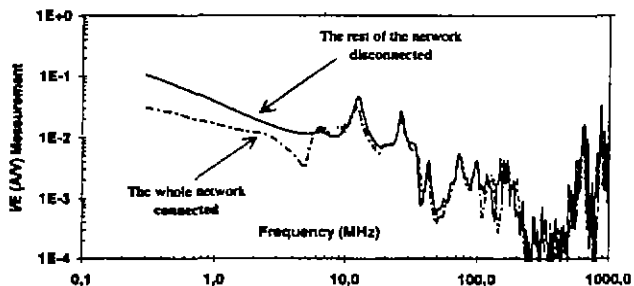


Fig. 5-9-c : Currents measured on J006

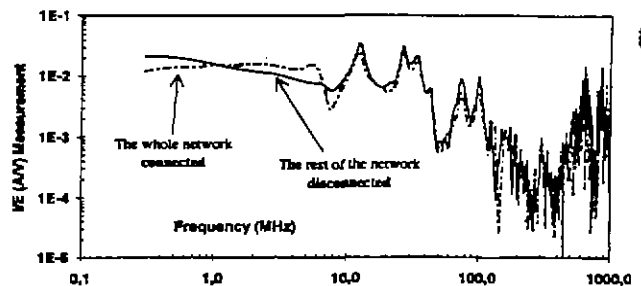


Fig. 5-9-d : Currents measured on J007

Fig. 5-9 : Comparison of currents measured, for an injection on LD7, with the rest of the network connected or not connected to the forward volume

We can observe that the connection or disconnection of the whole network to the forward volume has no influence on bulk currents measured not far from the injection point. Of course, at low frequencies, we may observe some differences on the amplitudes. It is mainly due to the fact that we replaced some resistive loads from the forward fuselage and from the B1B volume by short circuits. However, results become similar from 10 MHz to 1 GHz.

This general result is obtained with measurements and numerical calculations. It means that this physical phenomenon is clearly reproduced by CRIPTE code. In the future, it might be interesting to define rules that would simplify any complex problem in a smaller one. The

description of the network could be limited in the vicinity of the injection point. If the threat is distributed all over the network, simplification rules would be quite similar.

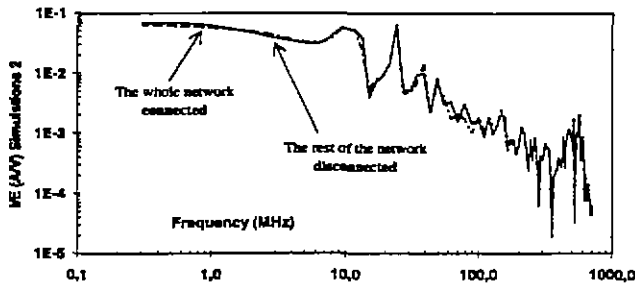


Fig. 5-10-a : Currents calculated on J003

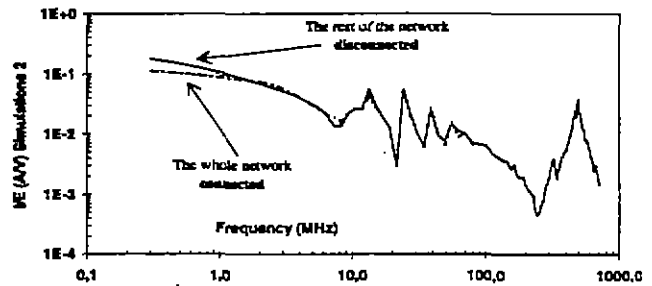


Fig. 5-10-b : Currents calculated on J005

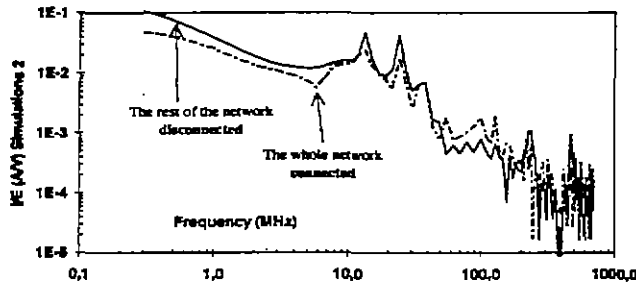


Fig. 5-10-c : Currents calculated on J006

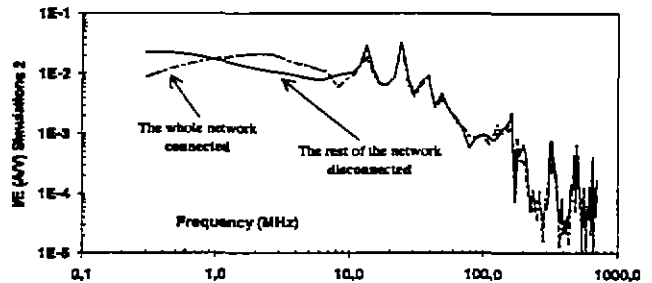


Fig. 5-10-d : Currents calculated on J007

Fig. 5-10 : Comparison of currents calculated, for an injection on LD7, with the rest of the network connected or not connected to the forward volume

5.2.3 LD6 current injection

The other injection point considered in the comparisons between the CRIPTE code and measurements was in LD6. It offered the advantage that the number of existing wires running in the whole aircraft structure is much more numerous than in the example with LD7 injection.

Same conclusions as for LD7 injection may be given, that is to say :

- computed results present an average level similar to the measurements,
- the agreement up to 100 MHz is satisfactory,
- from 100 MHz an attenuation still appears in all the measured results but not in the computed results, even with a precise tube decomposition in the cockpit volume and forward volume. the same reasons as for LD7 injection may be mentioned. But in this case, LD6 is not directly connected to the cockpit volume and forward volume bundles. consequently, the effect of a precise tube decomposition is much more less significant than LD7 injection case.

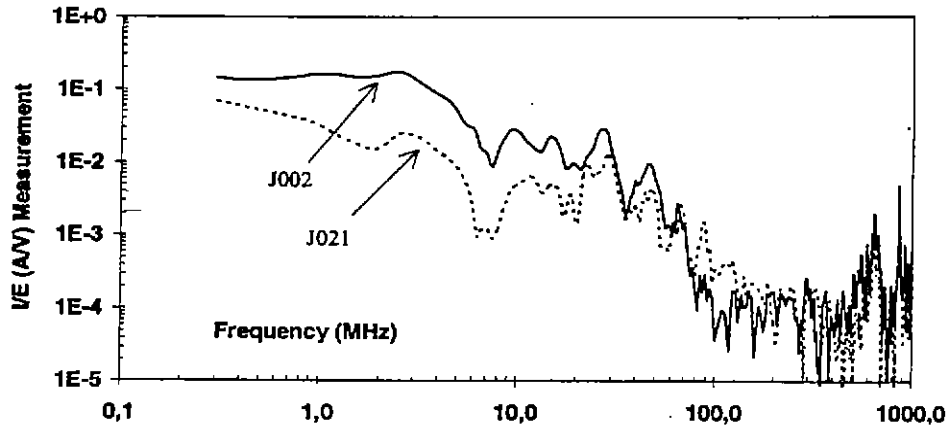


Fig. 5-11-a : Measured currents computed on J002 and J021 for an injection on LD6

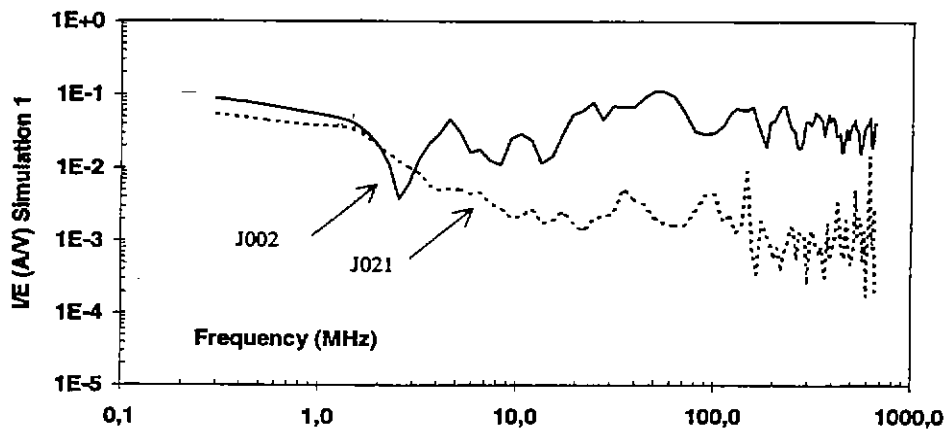


Fig. 5-11-b : Calculated currents on J002 and J021 for an injection on LD6 with a rough tube decomposition

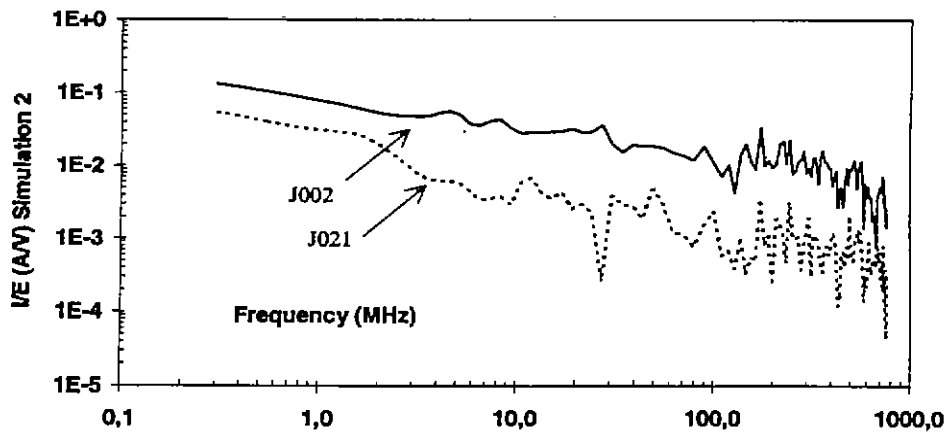


Fig. 5-11-c : Calculated currents on J002 and J021 for an injection on LD6 with a 10 cm tube decomposition

Fig. 5-11 : Comparison of currents measured and computed on J002 and J021 for an injection on LD6

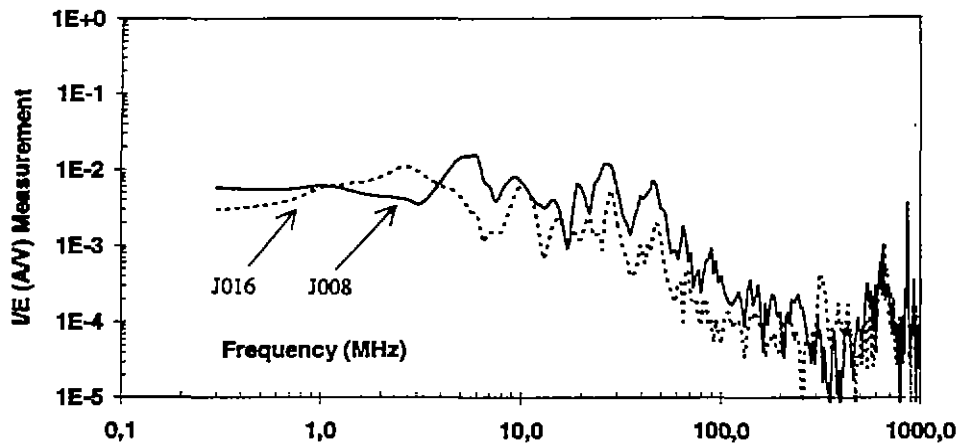


Fig. 5-12-a : Measured currents computed on J008 and J016 for an injection on LD6

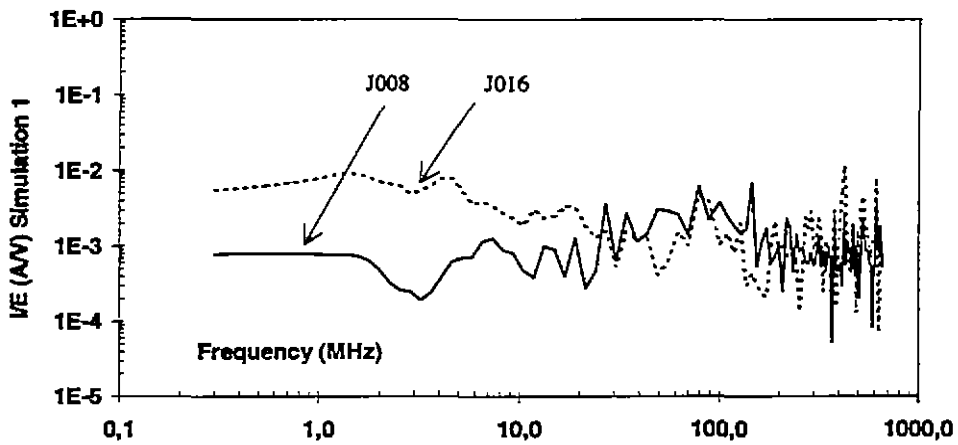


Fig. 5-12-b : Calculated currents on J008 and J016 for an injection on LD6 with a rough tube decomposition

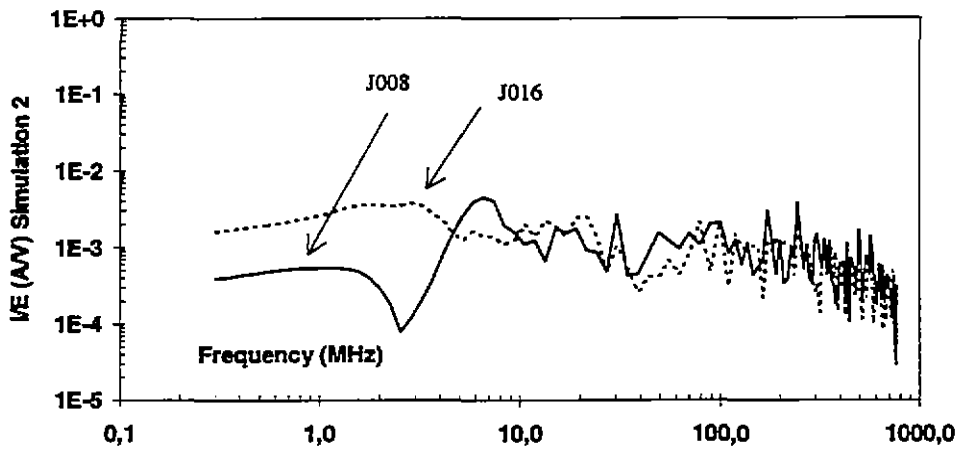


Fig. 5-12-c : Calculated currents on J008 and J016 for an injection on LD6 with a 10 cm tube decomposition

Fig. 5-12 : Comparison of currents measured and computed on J008 and J016 for an injection on LD6

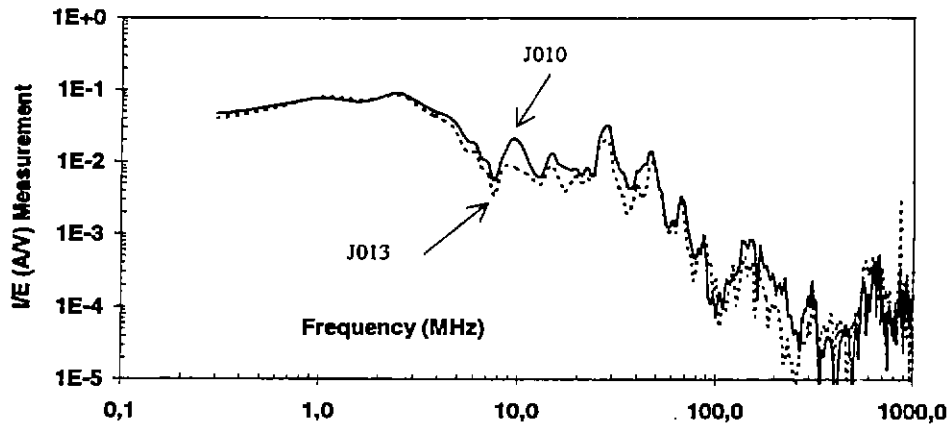


Fig. 5-13-a : Measured currents computed on J010 and J013 for an injection on LD6

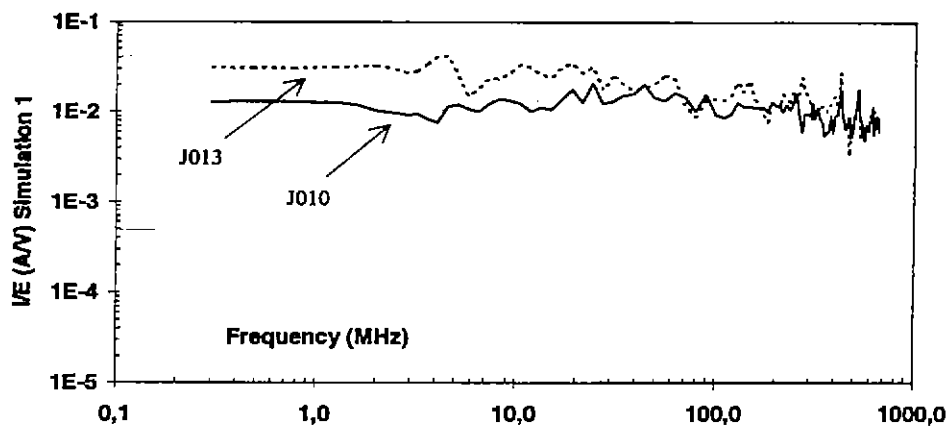


Fig. 5-13-b : Calculated currents on J010 and J013 for an injection on LD6 with a rough tube decomposition

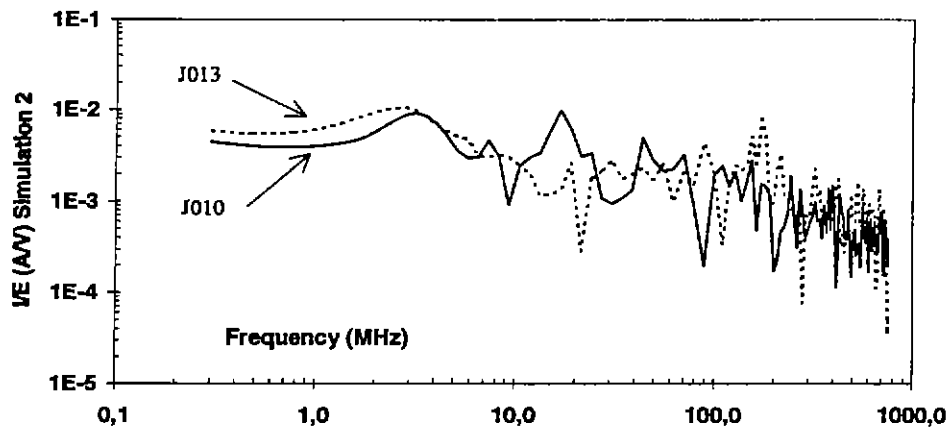


Fig. 5-13-c : Calculated currents on J010 and J013 for an injection on LD6 with a 10 cm tube decomposition

Fig. 5-13 : Comparison of currents measured and computed on J010 and J013 for an injection on LD6

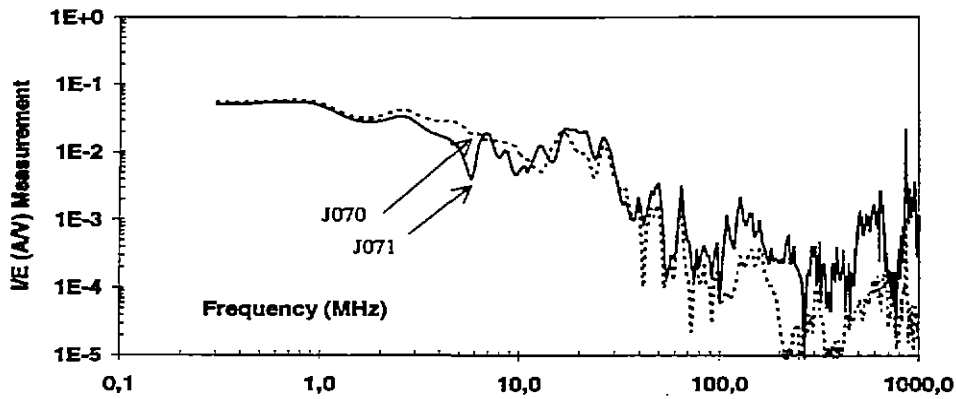


Fig. 5-14-a : Measured currents computed on J070 and J071 for an injection on LD6

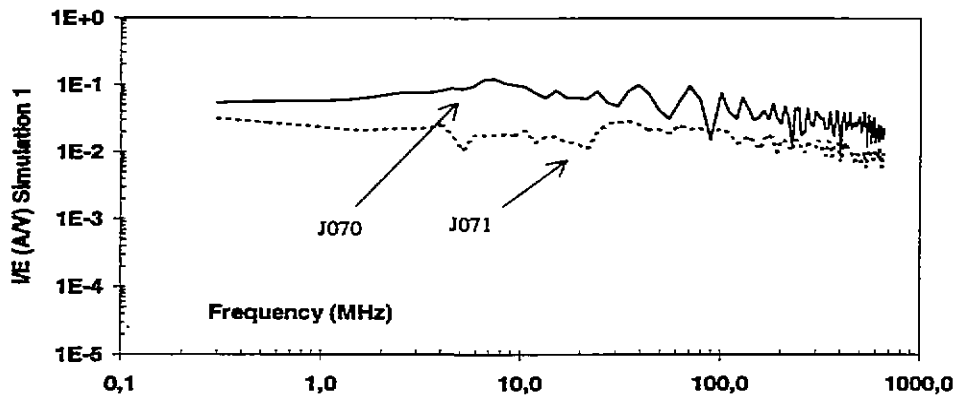


Fig. 5-14-b : Calculated currents on J070 and J071 for an injection on LD6 with a rough tube decomposition

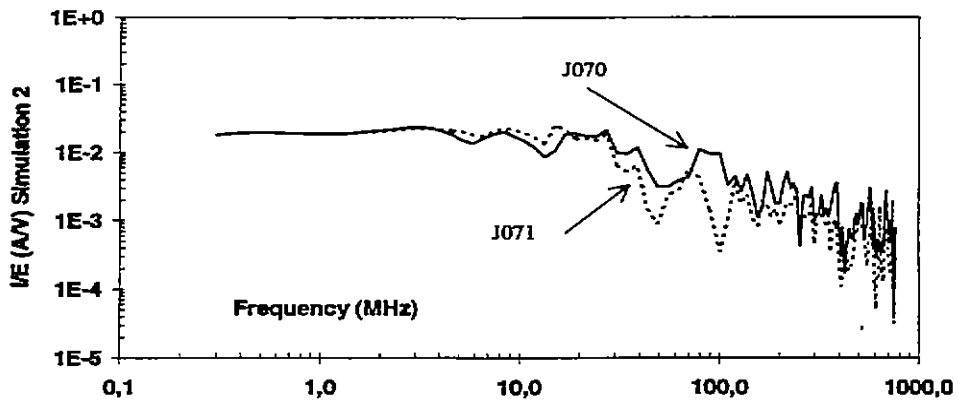


Fig. 5-14-c : Calculated currents on J070 and J071 for an injection on LD6 with a 10 cm tube decomposition

Fig. 5-14 : Comparison of currents measured and computed on J070 and J071 for an injection on LD6

5.3 Analysis of measurements under ELLIPTICUS

5.3.1 Introduction

The local current injection enabled us to understand the propagation of electromagnetic interference along the complex cable network under study. Moreover, the topological numerical modeling has been validated thanks to these current injections. The objective of our electromagnetic topology approach is to evaluate coupling phenomena along a cable network, running inside a complex structure which can be entirely excited by an electromagnetic environment. This is the reason why, the second phase of ETE III consisted in acquiring a data bank of the interference induced on the cable network by the electromagnetic fields generated by the ELLIPTICUS antenna in a wide frequency range.

In France, the external and internal electromagnetic fields in the EMPTAC have been computed using to a 3D code, based of finite difference time domain method. It consisted in meshing the entire aircraft with a 12 cm mesh. This 3D simulation were performed in order to be able to introduce afterwards the equivalent current and voltage generators resulting from an horizontal polarized plane wave (like under the ELLIPTICUS antenna) up to a few hundreds of MHz. In addition, 3D calculations with finite volume methods should be carried out in the next future.

Therefore, the objective of the ELLIPTICUS antenna experiment was restricted to the collection of the electromagnetic environment inside the aircraft, in order to compare it to the numerical 3D simulations and to analyze the coupling phenomena on the cable network. Once this 3D computations validated, the equivalent generators on the cable network will be introduced as "sources terms" in the topological modeling.

This last phase will be achieved in France. This paragraph is devoted mainly to the analysis of the electromagnetic fields and bulk currents measurements obtained under the ELLIPTICUS antenna in the frequency range 300 kHz - 1 GHz.

Unfortunately, the power at the input of the ELLIPTICUS antenna was too low and the EMPTAC has been built so that one can consider that the cable networks are shielded by their own shield or by the shield of the volume in which they are running. Therefore, in order to increase the coupling level and to carry out significant measurements, the door of the lower shielded volume had to be open.

5.3.2 Analysis of the electromagnetic environment inside the lower shielded volume

Electromagnetic fields measurements have been performed in various locations and configurations (door open or closed) inside the lower shielded volume. On figure 5-15, a typical tendency inside the lower shielded volume is represented.

The door of the lower shielded volume being open, electric fields have been measured :

- just close to the door (plain line),
- along the rear wall (dotted line).

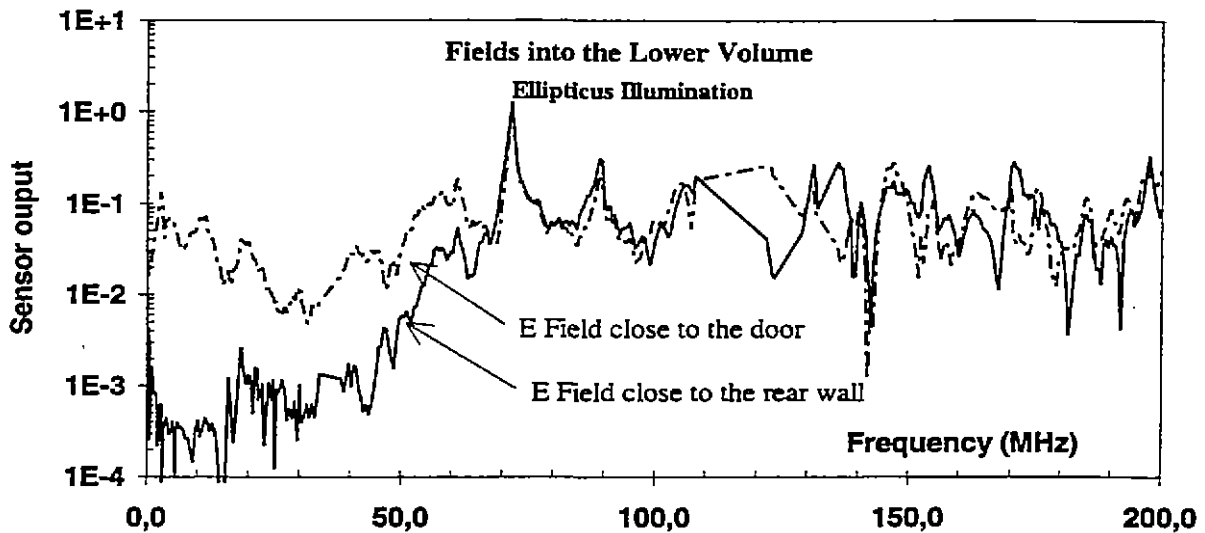


Fig. 5-15 : Electric field measurements inside the lower shielded volume

First of all, one can notice that the electric field measured near the door has quite the same level in the whole frequency range. This can be explained by the fact that this door open behaves as any aperture, that is to say as a high pass filter. The dimensions of this aperture being equal to a few wavelengths in that frequency range, the external interference between 300 kHz and 1 GHz can easily penetrate inside the lower shielded volume.

Moreover, from this overlay, one can notice two main ranges of frequency. In low frequency, below 50 MHz, the level of the electric field is much more important near the point of entry of the external electromagnetic interference than in other areas of the lower shielded volume. This can be explained by the fact that the electromagnetic fields can not propagate inside the cavity. In the upper frequency range, above 50 MHz, the cavity constituted by the lower shielded volume can be considered as overmodded. Therefore, the number of modes generated is important enough to give an homogeneous and isotropic electromagnetic field inside the lower shielded volume.

This conclusion is very interesting for the electromagnetic topology approach. Indeed, in this upper frequency range, the electromagnetic field inside a cavity is quite uniform, that is to say that the equivalent generators, "source terms", applied on the cable network should be therefore uniform along the cable network.

5.3.3 Analysis of bulk currents measurements

On figure 5-16, the bulk currents at LD7 input (inside the forward volume) have been measured, when the door of the lower shielded volume is open or closed.

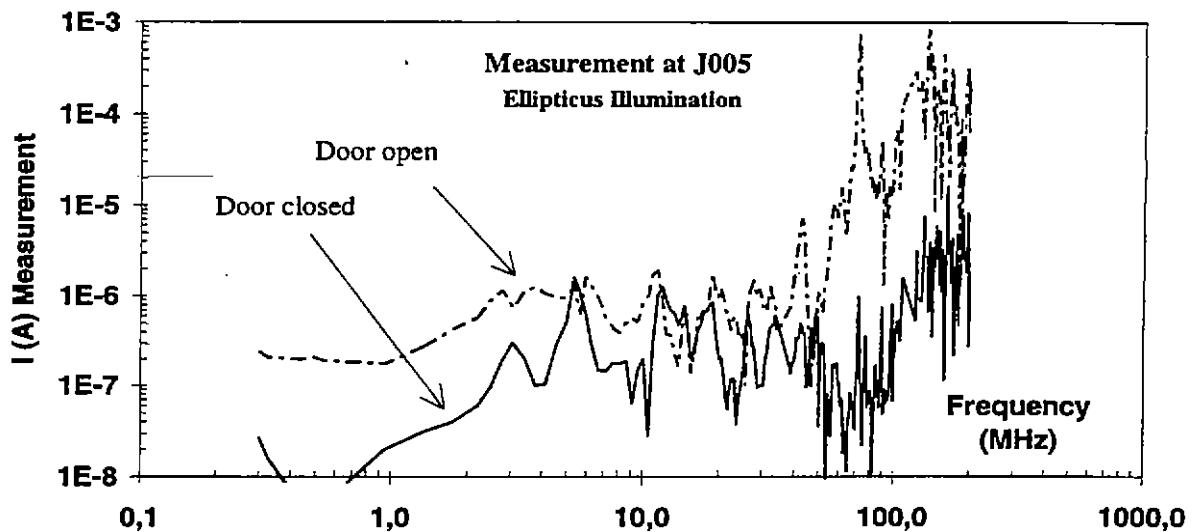


Fig. 5-16 : Bulk currents measured at LD7 input when the door is open or closed

Of course, in nearly the whole frequency range, the bulk current measured at the input of an equipment located inside the lower shielded volume is much more important when the door is open than when the door is closed.

But what is interesting on this graph is that in the medium frequency range, around a few tens of Mega-Hertz, both bulk currents have quite the same level. One can therefore assume that, in this frequency range, since the lower volume is very well shielded, the interference at LD7 input must come from the propagation of an interference induced by the penetration of the external field through other points of entry than the lower shielded volume. One can assume that penetration path was the cockpit.

These results are interesting for future computations and analysis of electromagnetic coupling phenomena inside such a cable network running inside the aircraft.

The previous conclusions concerning the electromagnetic paths inside the aircraft are confirmed by figure 5-17 on which are overlaid the bulk currents measured at J008 BIB input when the door of the lower shielded volume is open or closed. Indeed, once more, it is possible to distinguish the same three frequency ranges.

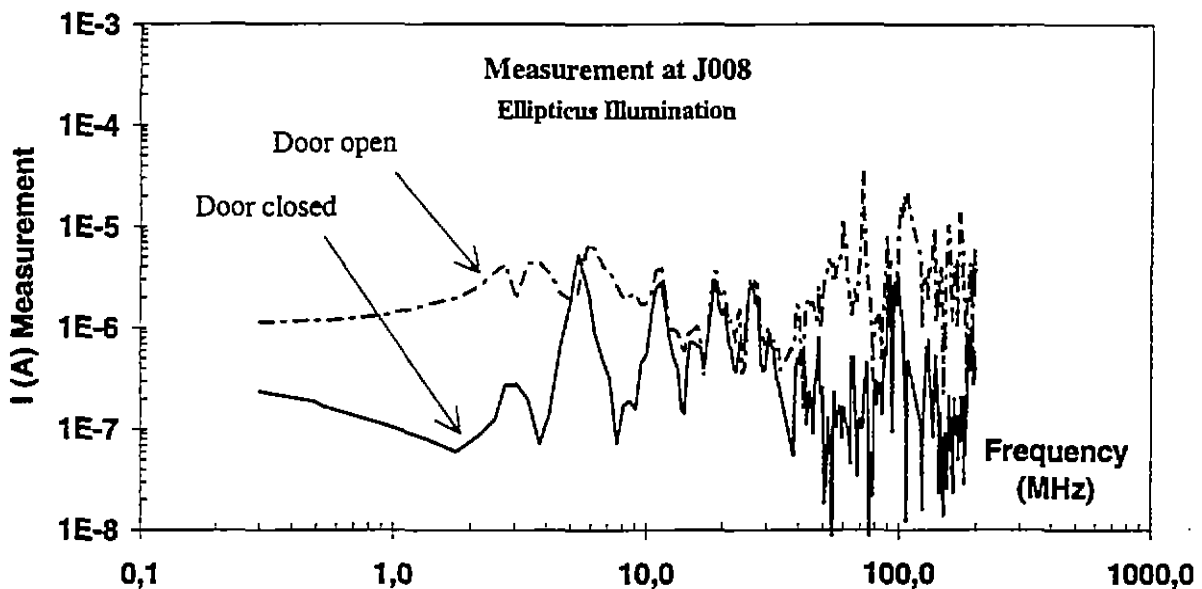


Fig. 5-17 : Bulk currents measured at the BIB input when the door is closed or open

5.4 Principles of 3D mapping of bulk currents

As developed in the introduction of this report, the objective of ETE III was to answer scientific questions concerning electromagnetic coupling in the EMPTAC in a wide frequency range, in the case of a local injection, current probe injection, and in the case of a global irradiation. To achieve this goal, measurements of bulk currents induced on the cable network running in the whole aircraft and the related numerical simulations, considering only propagation phenomena, were performed.

This chapter is devoted to the analysis of this data, from a numerical and experimental point of view. Let us recall that experimentation and computation with the CRIPTE code are performed in the frequency domain. Therefore, in order globally analyze electromagnetic coupling phenomena on the whole cable network, specific representations of the data have been developed, particularly a 3D visualization of bulk currents along the network for different frequencies.

A 3D-mapping visualization has been developed using Microsoft Excel, in order to observe how the current injected at one extremity of the whole cable network could propagate to the other extremities of the cable network located in other volumes. On such a 3D graph, the horizontal plane is associated to the spatial location of the various equipment boxes inside the aircraft, the boxes being placed in this plane as described on figure 5-18. The magnitude of the bulk current divided by the magnitude of the injected bulk current at these locations is reported along the Z axis at discrete frequencies.

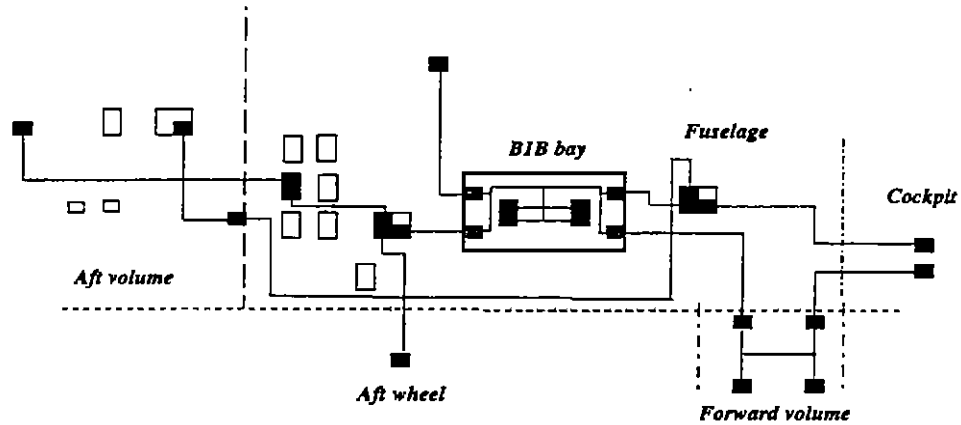


Fig. 5-18 : Plane visualization of the test points under study

An example of this 3D visualization is given on figures 5-19. On this graph, a current probe was placed on the bundle connected to LD7 box in the lower shielded volume. One can see the relative magnitude of the resulting bulk currents at the other equipment inputs 84 MHz. Therefore, at first sight, one could be able to define a criterion, depending on frequency, giving the distance from the injection point for which the attenuation of the interference is under a given threshold.

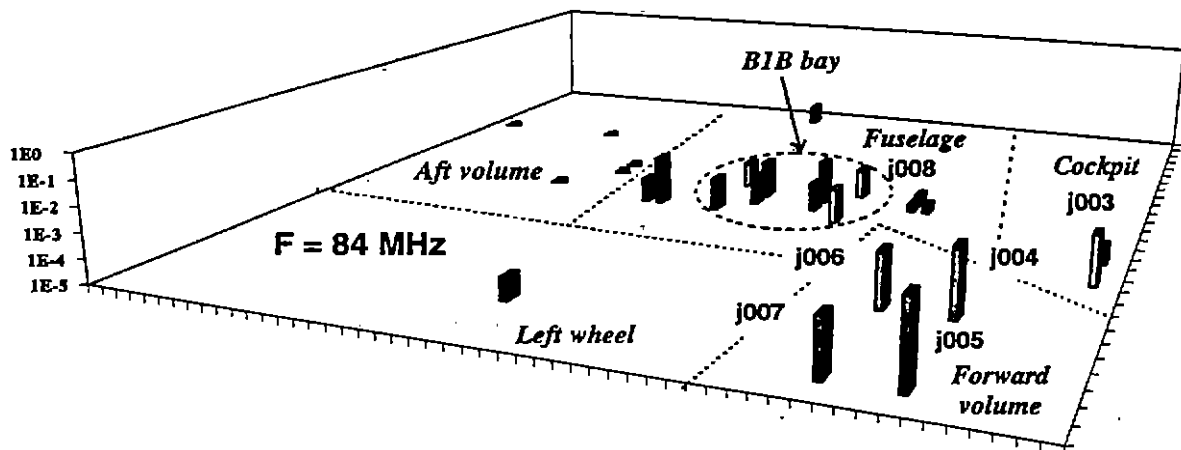


Fig. 5-19 : Example of 3D planar representation at 84 MHz

5.5 Application of 3D planar visualization

This kind of representation has been applied to the data collected during the experiment and enabled us to characterize the electromagnetic signals which could propagate on a cable network.

As an example, the figure 5-20 to 5-22 are related to a local bulk current injection on the LD7 box in the lower shielded volume at respectively 300 kHz, 50 MHz and 100 MHz. On these figures, the lines, which join the various boxes or connectors, represent the running in the whole aircraft of the cable network, stressed on LD7.

The analysis of these figures clearly puts to the fore several conclusions concerning the propagation of electromagnetic signals on a large cable network:

- in the whole frequency range, the magnitude of the signals measured on boxes connected to the stressed cable network are much more higher than on any other boxes. By comparing the magnitude, one could easily deduce the running of the wires inside the aircraft which had been excited by the local injection.

- Nevertheless, one can notice that the magnitude of the electromagnetic signal induced at one equipment is all the more attenuated that the measurement point, on the path of the excited wires or not, is far from the injection point (LD7). This attenuation also increases with frequency. One can conclude that in high frequency, the electromagnetic signal can not propagate or couple with others wires anymore. This is consistent with the CRIPTE code computations which showed that a realistic modeling of a cable network consists in splitting up this cable network into successive tubes of $\lambda/10$ length with various and random intrinsic geometry to reproduce the mismatching of wires inside a bundle and prevent the electromagnetic signal from propagating in high frequency.

These conclusions drawn from the analysis of these 3D plane representations can be applied to any other configurations of injection, as for an injection on the LD6 box.

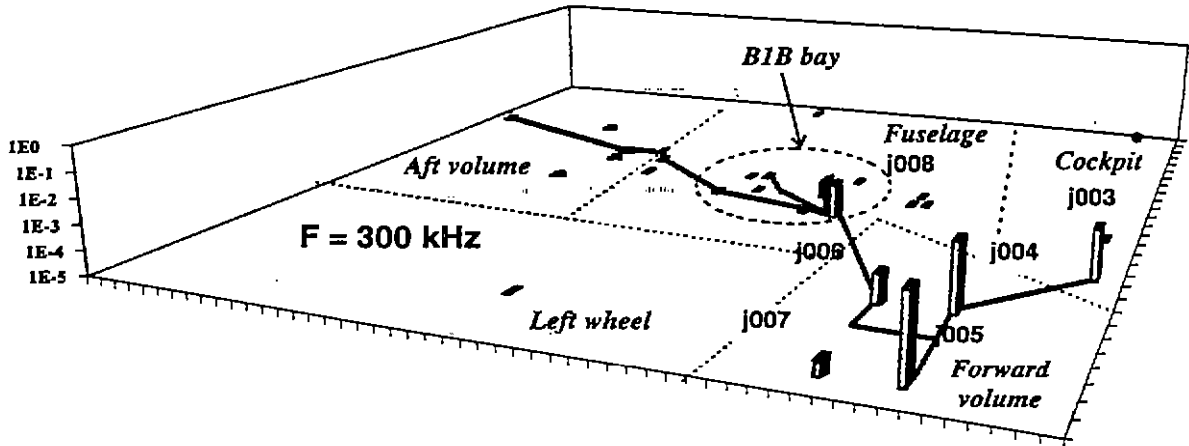


Fig. 5-20 : 3D representation of an injection at J005 (LD7 box) at 300 kHz

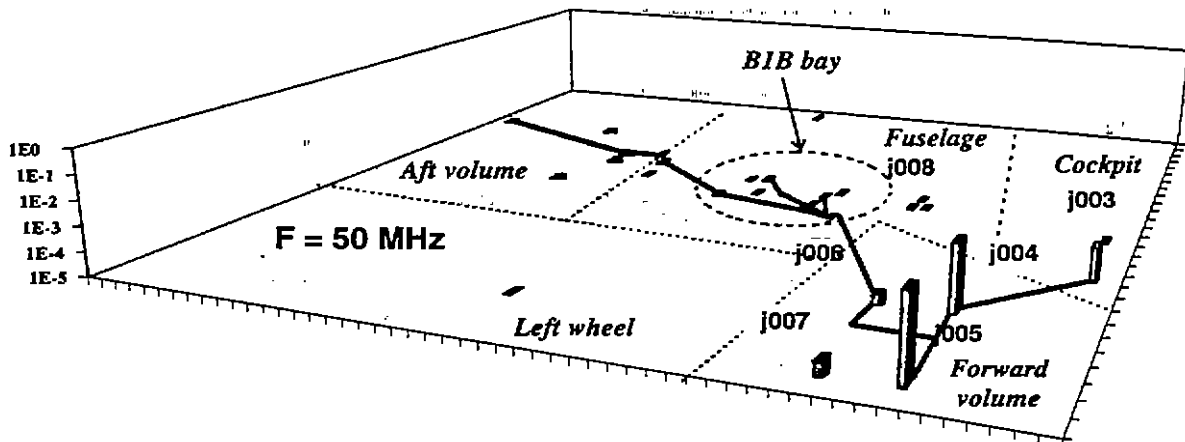


Fig. 5-21 : 3D representation of an injection at J005 (LD7 box) at 50 MHz

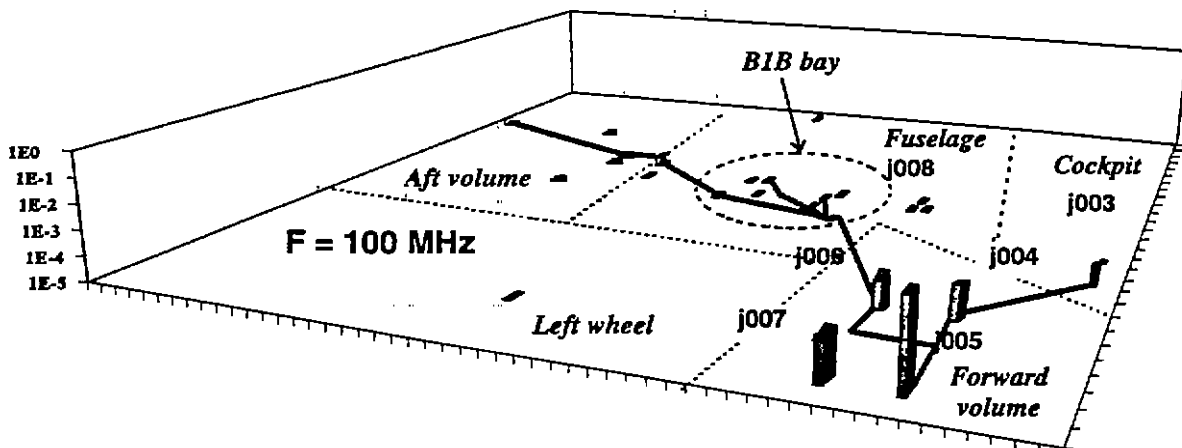


Fig. 5-22 : 3D representation of an injection at J005 (LD7 box) at 100 MHz

CONCLUSION

The ETE III experiment was the third experiment held on the EMPTAC aircraft in order to apply Electromagnetic Topology concepts. Compared to the two previous experiments, the objective of ETE III was to conduct both a numerical and an experimental approach, from 300 kHz to 1 GHz.

Dealing with the numerical approach one of the interesting results is that we showed that it was possible to take into account a large network. The network under study was a large part of the modified wiring of the EMPTAC airplane. All our computation work has been performed with low performance workstations. We have shown how the topological network decomposition could be useful to reduce the memory and computer time requirements.

For the first time in ETE experiments, we carried out full numerical simulations, that is to say that no measurement have been introduced in the models, as it was the case during previous experiments. This time, all bundles have been modeled thanks to a two dimension computer code. We took into account the unknown position of the wires inside the bundles thanks to a computer program generating randomly the geometry of the bundle sections.

Two kinds of measurements were performed :

- local current injections, and measurements of transfer functions in electrical boxes. Current measurements were very difficult to achieve, because of their low level. Both bulk current and wire current measurements have been carried out.
- current and field measurements with a global illumination under ELLIPTICUS.

Comparisons between measurements and computations could be achieved only for transfer function measurements. The ELLIPTICUS measurement will be processed in the future, in France, and compared to several 3D code calculations.

The transfer function measurements demonstrate the difficulty for a signal to propagate far from its injection points. A significant attenuation, generally beginning around 100 MHz, has been pointed out for all the measurements. Such an attenuation could not be always reproduced with the numerical code. Nevertheless, complementary numerical computations dealing with a fine modeling of the geometry of sections of a tube and the modeling of a connector make us think that such an attenuation could be taken into account. But the origin of this attenuation has still to be studied to give definitive conclusions.

Nevertheless, it was a satisfaction to verify that the CRIPTE code gave always good results in the low frequency range (up to 100 MHz). One must remember that all the parameters introduced into the code have been modeled and most of the numerical simulations plots depicted

in this report have been obtained at the first run, with no optimization of the models. Despite the care brought to the meshing of the network, it is not excluded that the modeling still contains mistakes. Back in France, systematically, verifications on the connections will be achieved on the network model.

The next future of the ETE experiments or similar experiments strongly depends on the conclusions of ETE III. The measurements will have to be processed and analyzed very carefully. More, additional measurements on piece of bundles will have to be carried out, specially up to 100 MHz. It is not excluded that a propagation model can still continue to be valid to take into account coupling on cables, for frequencies higher than 100 MHz. But in this case, one will have to determine what is the role played by the unknown position of wires inside the bundles and the filtering of the connectors.

The way to model the mismatching, consisting in the connection of numerous elementary wires, will have to be optimized. The implementation of the recently published NBLT formalism ([16]) would significantly help to this optimization.

The future of the ETE experiments should be now to perform full numerical simulations for global illuminations. This objective requires the use of 3D numerical codes. It must now be shown that fields can be calculated with such codes and then applied as equivalent generators on cable models similar to those achieved during ETE III. Such a procedure has already been demonstrated on small structures ([17]). The difficulty with a structure as large as an airplane will be the computational time and the memory requirement.

APPENDIX A : DESCRIPTION OF THE B1B VOLUME

A-1 Description of the geometry of the B1B volume

The B1B volume is a shielded box installed in the fuselage, close to the EMPTAC left wing. It contains 2 boxes (LD11 and LD12) and 4 connectors are located on its walls.

A complex wiring, made of elementary bundles (NBxxxx), links the various elements of the volume. The next figure is a schematic description of the B1B volume.

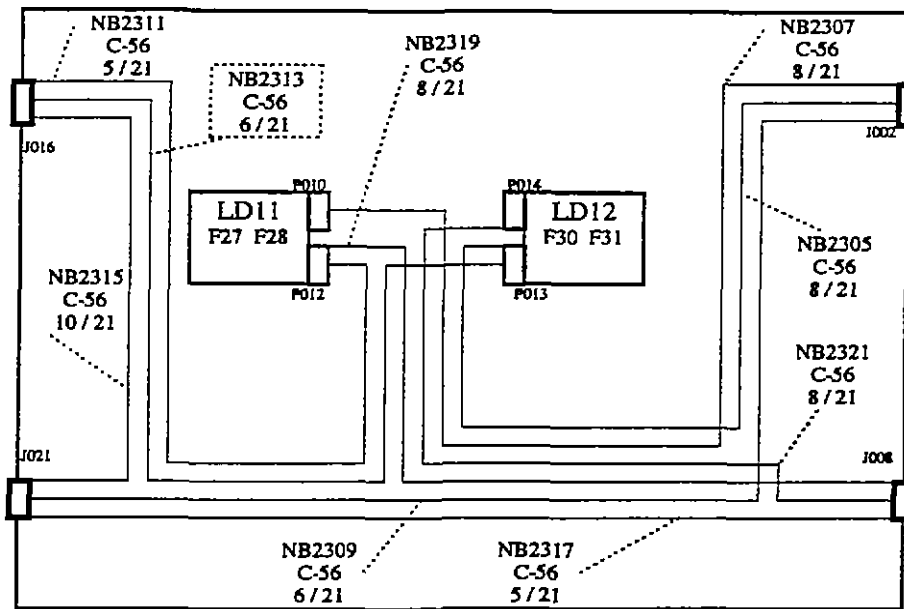
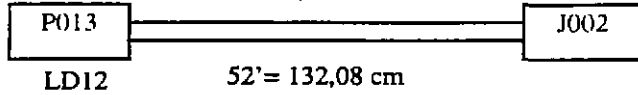


Fig A.1 : Schematic description of the B1B volume

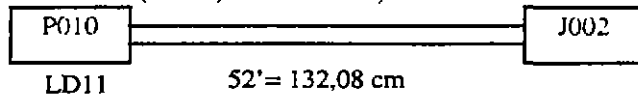
Each line represents an elementary bundle connecting components (box or connector). A description of the conductors constituting each bundle is following.

NB2305 (C-56; 9 / 12)



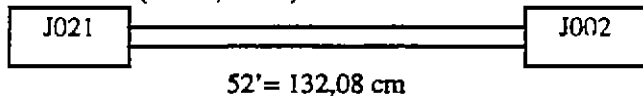
pin	wire number	n° CripTE	gauge	pin
g	Ground	1	22	g
k	2H01L1232	2	20	k
g1	shield bf1	3		g1
g2	shield bf2	4		g2
g3	shield bf3	5		g3
GG	2H01L1252	6	20	GG
t	2H01L1239R	1	20	t
u	2H01L1240B	2	20	u
v	2H01L1241R	3	20	v
w	2H01L1242B	4	20	w
x	2H01L1243R	5	20	x
y	2H01L1244B	6	20	y

NB2307 (C-56; 9 / 12=6+6)



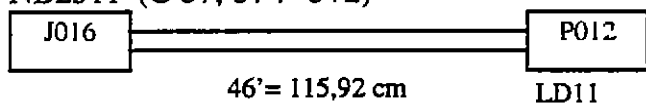
pin	wire number	n° CripTE	gauge	pin
g	Ground	1	22	g
z	2H01L1145	2	20	z
g1	shield bf1	3		g1
g2	shield bf2	4		g2
g3	shield bf3	5		g3
HH	2H01L1153	6	20	HH
AA	2H01L1146B	1	20	AA
BB	2H01L1147R	2	20	BB
CC	2H01L1148B	3	20	CC
DD	2H01L1149R	4	20	DD
EE	2H01L1150B	5	20	EE
FF	2H01L1151R	6	20	FF

NB2309 (C-56; 6 / 6)



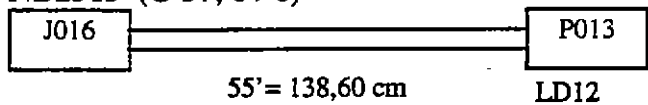
pin	wire number	n° Cripte	gauge	pin
m	2H01H0333	1	20	m
n	2H01H0334	2	20	n
p	2H01H0335	3	20	p
q	2H01H0336	4	20	q
r	2H01H0337	5	20	r
s	2H01H0338	6	20	s

NB2311 (C-57; 6 / 7=5+2)



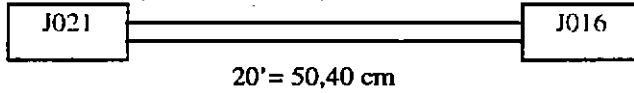
pin	wire number	n° Cripte	gauge	pin
g	ground	1	22	g
g1	shield bf1	2		g1
AA	2H04L1148A	3	20	AA
BB	2H04L1149B	4	20	BB
CC	2H04L1153C	5	20	CC
DD	2H04L1146B	1	20	DD
HH	2H04L1147R	2	20	HH

NB2313 (C-57; 6 / 6)



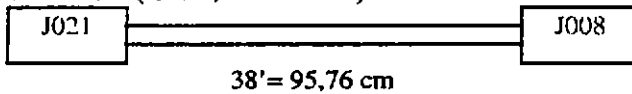
pin	wire number	n° Cripte	gauge	pin
m	2H04L1233	1	20	m
n	2H04L1234	2	20	n
p	2H04L1235	3	20	p
q	2H04L1236	4	20	q
r	2H04L1237	5	20	r
s	2H04L1238	6	20	s

NB2315 (C-57; 10 / 10)



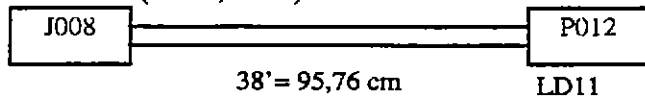
pin	wire number	n° Cripe	gauge	pin
t	2H03H0439	1	20	m
u	2H03H0440	2	20	n
v	2H03H0441	3	20	p
w	2H03H0442	4	20	q
x	2H03H0443	5	20	r
y	2H03H0444	6	20	s
z	2H03H0445	7	20	z
EE	2H03H0450	8	20	EE
FF	2H03H0451	9	20	FF
GG	2H03H0452	10	20	GG

NB2317 (C-57; 6 / 7=5+2)



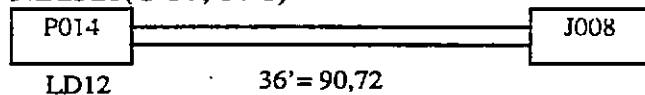
pin	wire number	n° Cripe	gauge	pin
g	ground	1	22	g
g1	shield bf1	2		g1
CC	2H02H0348A	3	20	CC
DD	2H02H0349B	4	20	DD
HH	2H02H0353C	5	20	HH
AA	2H02H0346B	1	20	AA
BB	2H02H0347R	2	20	BB

NB2319 (C-57; 8 / 8)



pin	wire number	n° Crite	gauge	pin
m	2H02L1133A	1	20	m
n	2H02L1134B	2	20	n
p	2H02L1135C	3	20	p
q	2H02L1136	4	20	q
r	2H02L1137B	5	20	r
s	2H02L1138C	6	20	s
t	2H02L1139	7	20	t
u	2H02L1140	8	20	u

NB2321(C-57; 8 / 8)



pin	wire number	n° Crite	gauge	pin
v	2H02L1241A	1	20	v
w	2H02L1242B	2	20	w
x	2H02L1243C	3	20	x
y	2H02L1244	4	20	y
z	2H02L1245	5	20	z
EE	2H02L1250A	6	20	EE
FF	2H02L1251B	7	20	FF
GG	2H02L1252C	8	20	GG

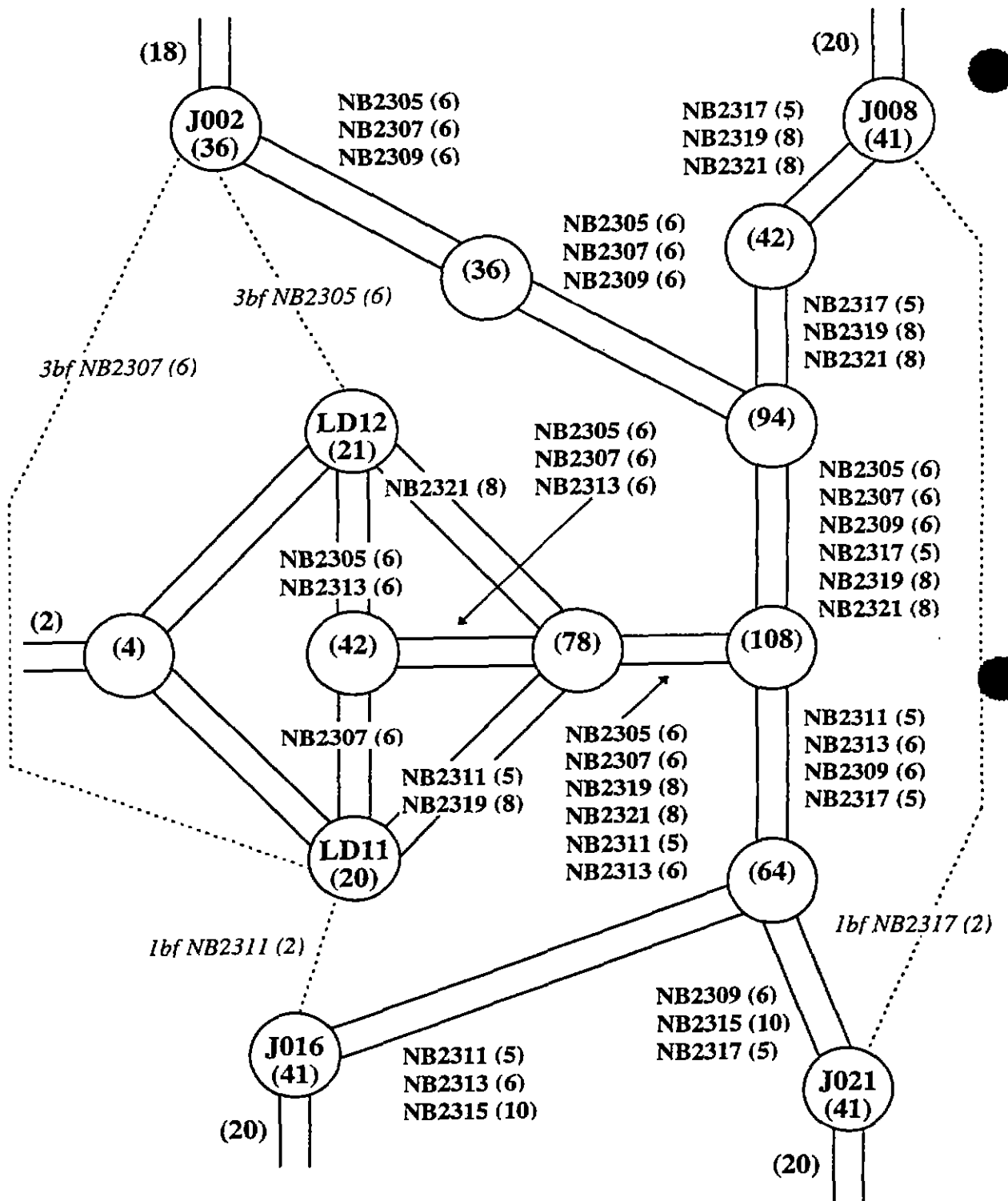


Fig A.2 : Final BIB volume CRIPTE modeling

A-2 Description of the connections on the LD11 and LD12 boxes

P010			Junction LD11a			
fil	port		port	P	pin	R(Ohm)
NB2307	1	1	1	P010	g	cc
	2	18	1	P010'	g1	cc
	3	2	2	P010'	g2	cc
	4	3	3	P010'	g3	cc
	5	4	4	P012	g	cc
	6	19	5	P012'	g1	cc
P012			6	P012	m	20,1
NB2311	1	5	7	P012	n	20,9
	2	6	8	P012	p	202
	3	15	9	P012	q	202,2
	4	16	10	P012	r	10,6
	5	17	11	P012	s	983
	6	7	12	P012	t	20,1
NB2319	7	8	13	P012	u	201,6
	8	9	14	P112	CC	544
	9	10	15	P112	DD	105,8
	10	11	16	P112	HH	102,7
	11	12	17	P110	z	994
	12	13	18	P110	HH	53,3
	13	14	19	P110	HH	53,3

P010			Junction LD11b			
fil	port		port	P	pin	R(Ohm)
NB2307	1	1	1	P010	AA	1032
	2	18	2	P010	BB	528
	3	2	3	P010	CC	101,9
	4	3	4	P010	DD	51,7
	5	4	5	P010	EE	10,7
	6	19	6	P010	FF	529
P012			7	P012	AA	10,2
NB2311	1	1	8	P012	BB	990
	2	2				
	3	3				
	4	4				
	5	5				
	6	6				
P010						
NB2319	7	7	cc	g		
	8	8	994	z		
			1032	AA		
			528	BB		
			101,9	CC		
			51,7	DD		
			10,7	EE		
			529	FF		
			53,3	HH		

Fig A.3 : Connections on the LD11 junction

P014		Junction LD12a						
fil	port	port	P	pin	R(Ohm)			
1	13	1	P013	g	cc			
2	14	2	P013'	g1	cc			
3	15	3	P013'	g2	cc			
4	16	4	P013'	g3	cc			
5	17	5	P013	k	1017			
6	18	6	P013'	m	529			
7	19	7	P013	n	19,8			
8	20	8	P013	p	52,1			
		9	P013	q	10,1			
		10	P013	r	1001			
		11	P013	s	52,1			
		12	P013	GG	99,5			
		13	P014	v	538			
		14	P014	w	52,7			
		15	P114	x	10,1			
		16	P114	y	20,4			
		17	P114	z	106,4			
		18	P114	EE	981			
		19	P114	FF	11,3			
		20	P114	GG	217,1			

P013			
fil	port		
1	1		
2	5		
NB2305	3		
	4		
	3		
	4		
	12		
	6		
	7		
	8		
NB2313	9		
	10		
	9		
	10		
	11		
	12		

P013		Junction LD12b			
fil	port	port	P	pin	R(Ohm)
	1	1	P013	t	10,4
NB2307	2	2	P013	u	19,6
	3	3	P013	v	201
	4	4	P013	w	524
	5	5	P013	x	104,5
	6	6	P013	y	213,7

P012				P013	
fil	port			cc	g
	1	1		1017	k
	2	2		529	m
	3	3		19,8	n
NB2305	4	4	P014	52,1	p
	5	5	538 v	10,1	q
	6	6	52,7 w	1001	r
			10,1 x	52,1	s
			20,4 y	10,4	t
			106,4 z	19,6	u
			981 EE	201,8	v
			11,3 FF	524	w
			217,1 HH	104,5	x
				213,7	y
				99,5	GG

Fig A.4 : Connections on the LD12 junction

APPENDIX B : CALCULATION OF THE ATTENUATION OF SIGNAL ALL ALONG AN OVER SHIELDED BUNDLE

Measurements and numerical computations often agree in low frequency. The two last experimental campaigns ETE-I and ETE-II have proved a transmission line network software, based on topological concepts, could give significant results up to 100 MHz. This campaign ETE-III enables us to compare measurements and numerical computations up to 1 GHz. At such a frequency, transmission lines theory is said to give bad results due to radiation. Comparisons between measurements and numerical calculations made by CRIPTE show a disagreement between an average frequency of 100 MHz and 1 GHz. Propagation phenomena taken into account in computation imply that numerical data follow the same level in magnitude over the whole frequency range. At the same time, measurements often decrease by 20 dB per decade. The difference between models and measurements is about 30 to 50 dB between 500 MHz and 1 GHz.

Some explanations about mismatching and losses in transmission have been given : they may explain why our models did not always give the attenuation we measured. However, most of our tubes were cut when obvious mismatching occurred. If we take into account mismatching of the wires, cutting a long cable in many tubes, we could check if this assumption is a good one or not.

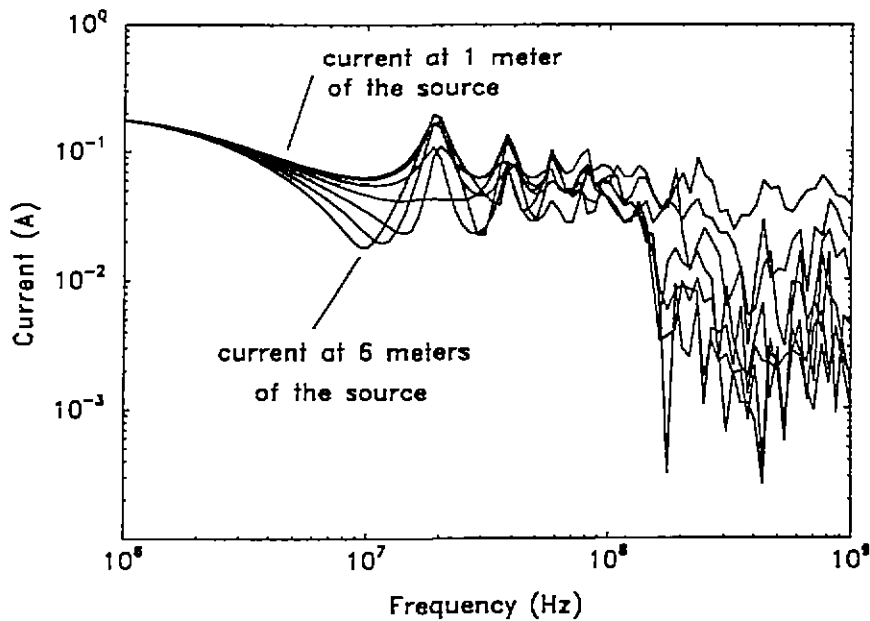


Fig B.1 : Calculation of currents all along a six meters long cable stressed at one extremity with a one volt generator on all the wires

Equivalent S-parameters of a cable of 6 meters, cut in 60 tubes, and a single cable of the same length, represented by only one tube, have been compared, showing that losses and mismatching could produce attenuation in high frequency. The phenomenon was noticed at 100 MHz. The decrease of the current level was proportional to the number of mismatching introduced in the network software. In order to confirm such a phenomenon, we plot the level of the current of this cable each meter. Numerical calculations totally confirm the fact that current level decrease with the distance of the source. The decrease of the current is clearly observed from 100 MHz.

APPENDIX C : DESCRIPTION OF TOPOLOGICAL NETWORKS

Liste des sous-reseaux:

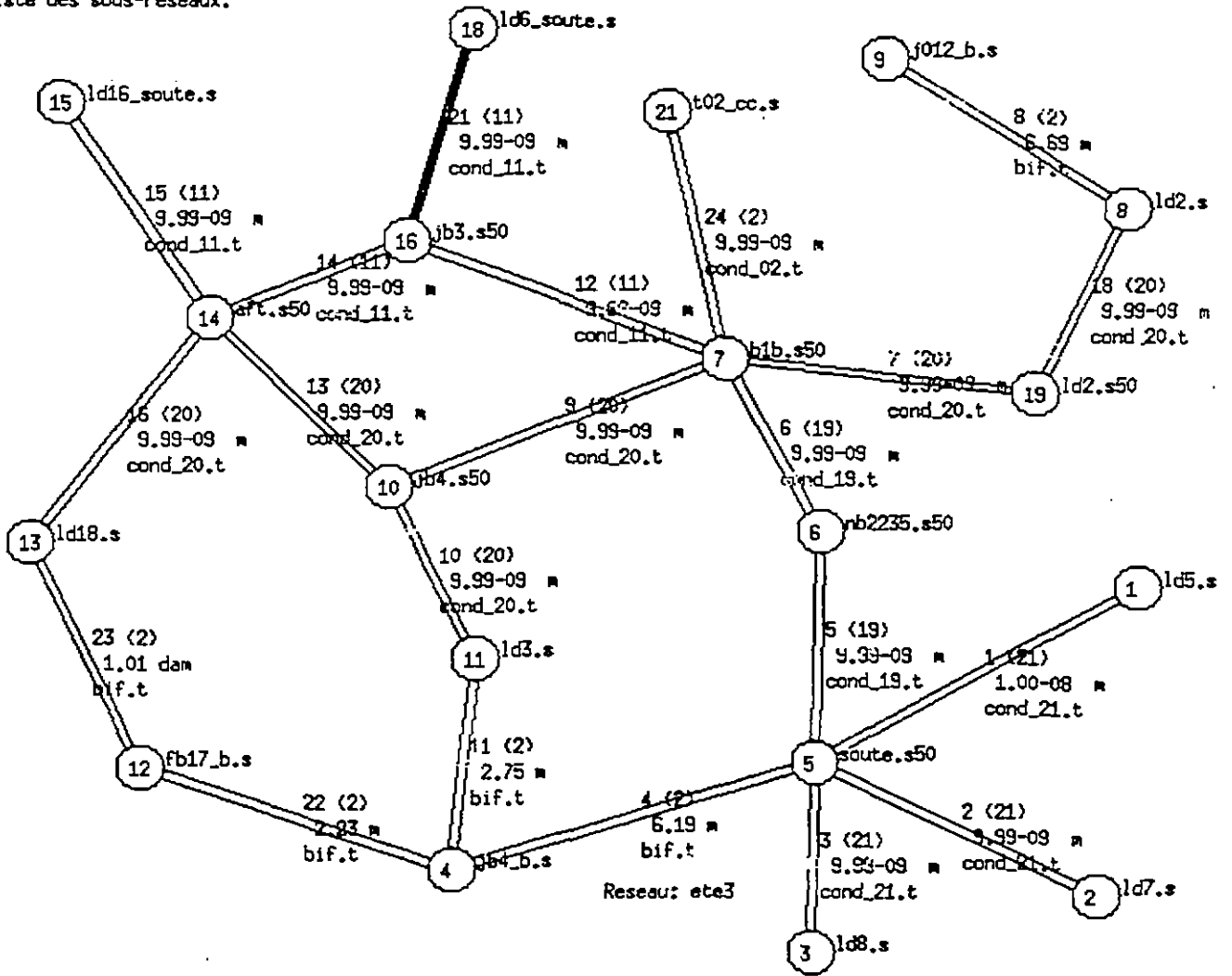


Fig C.1 : ETE III whole cable network topological network

Liste des sous-reseaux:

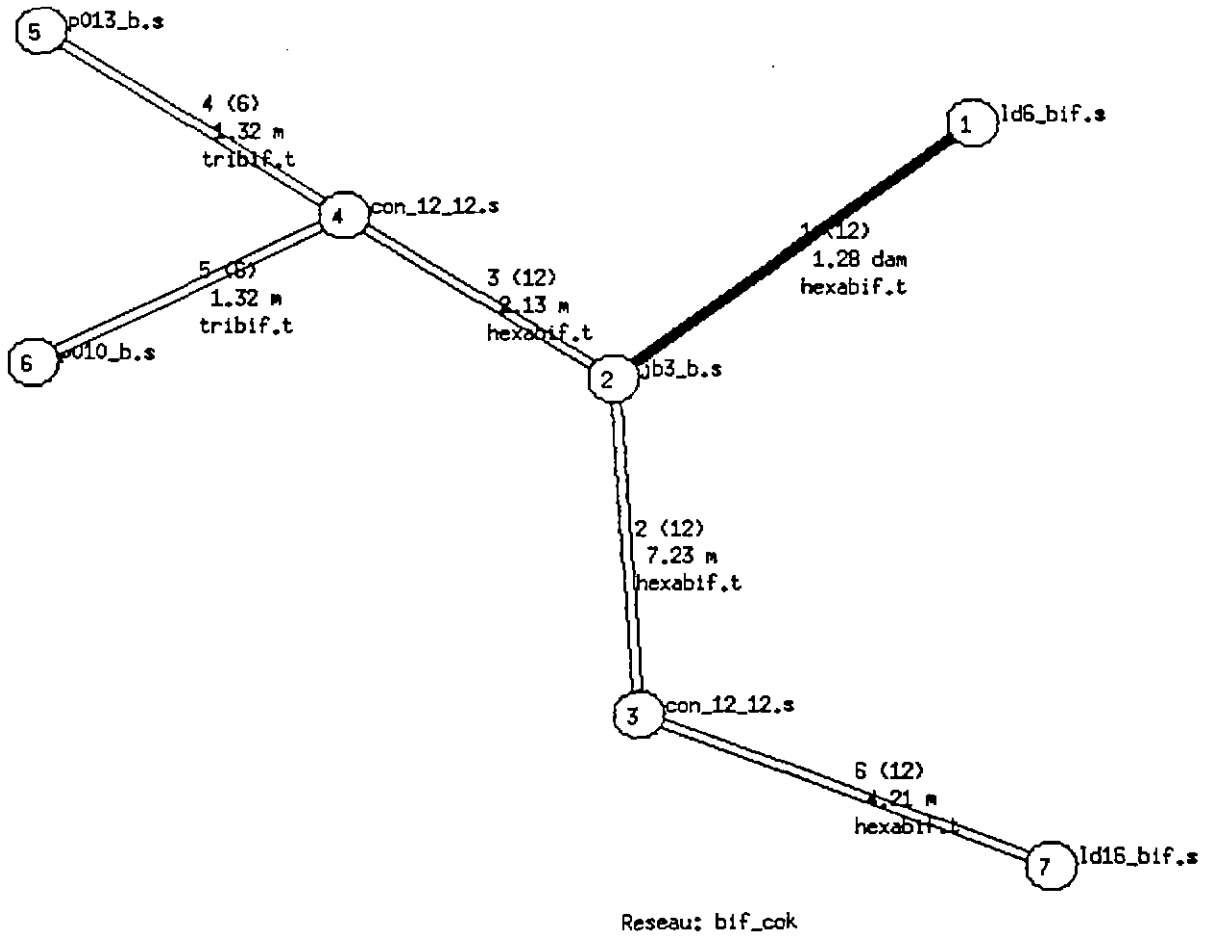


Fig C.2 : Shielded two wire cable topological model

Liste des sous-reseaux:

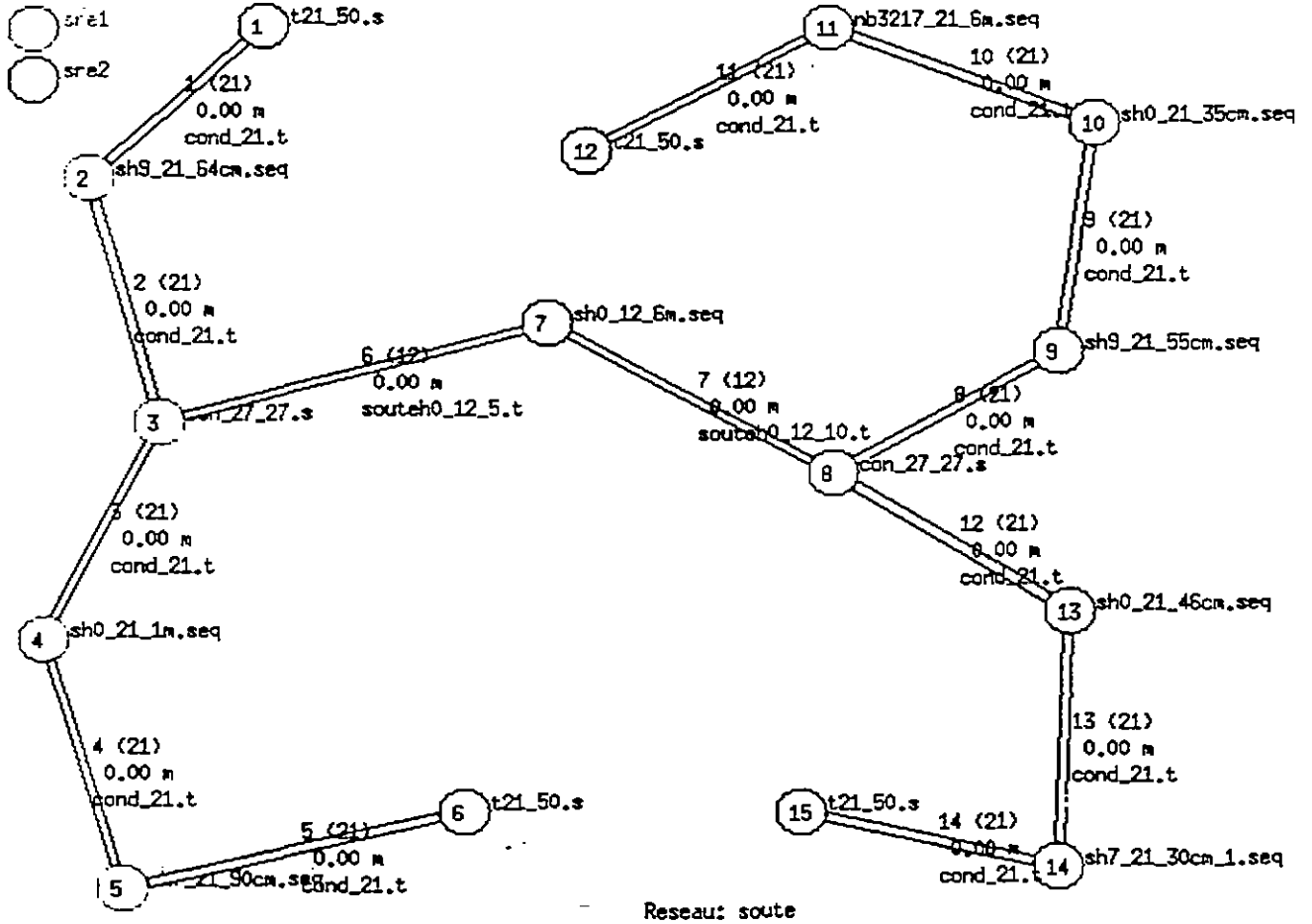


Fig C.3 : Lower shielded volume model

Liste des sous-reseaux:

○ nb2235_sre

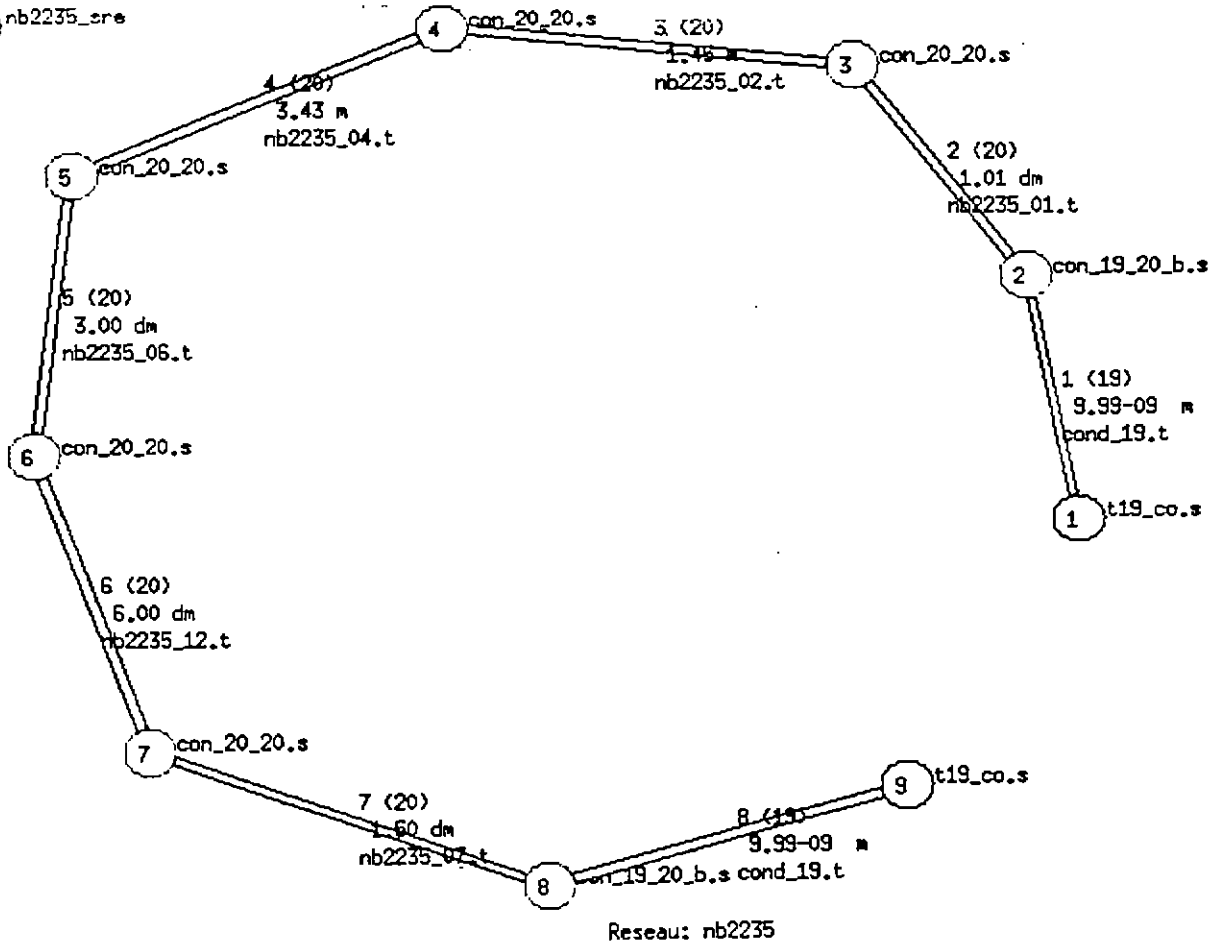
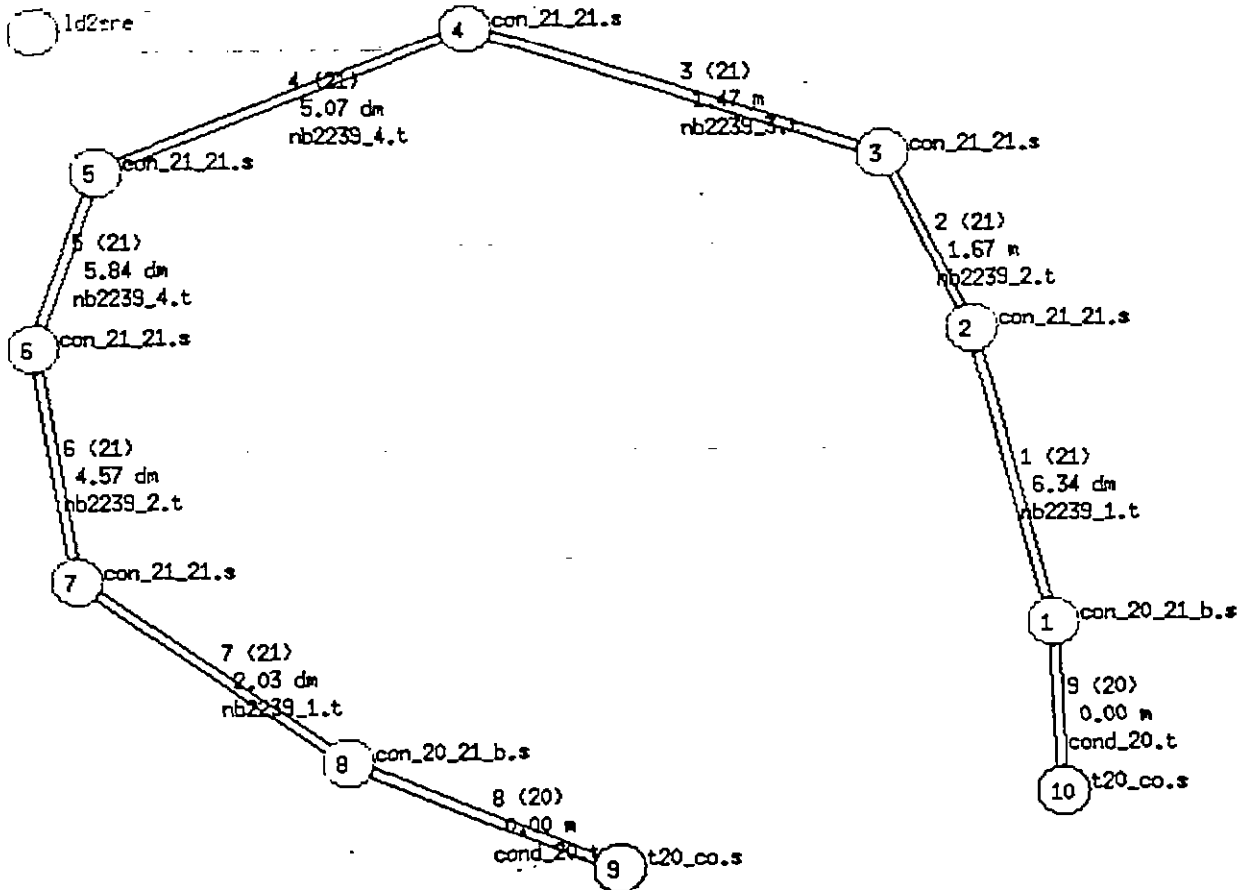


Fig C.4 : NB2235 (cable network between B1B and lower shielded volume) topological model

Liste des sous-reseaux:



Reseau: Id2

Fig C.5 : LD2 (cable network between the BIB volume and LD2 equipment box) topological model

Liste des sous-reseaux:

- jb41_sre
- jb42_sre

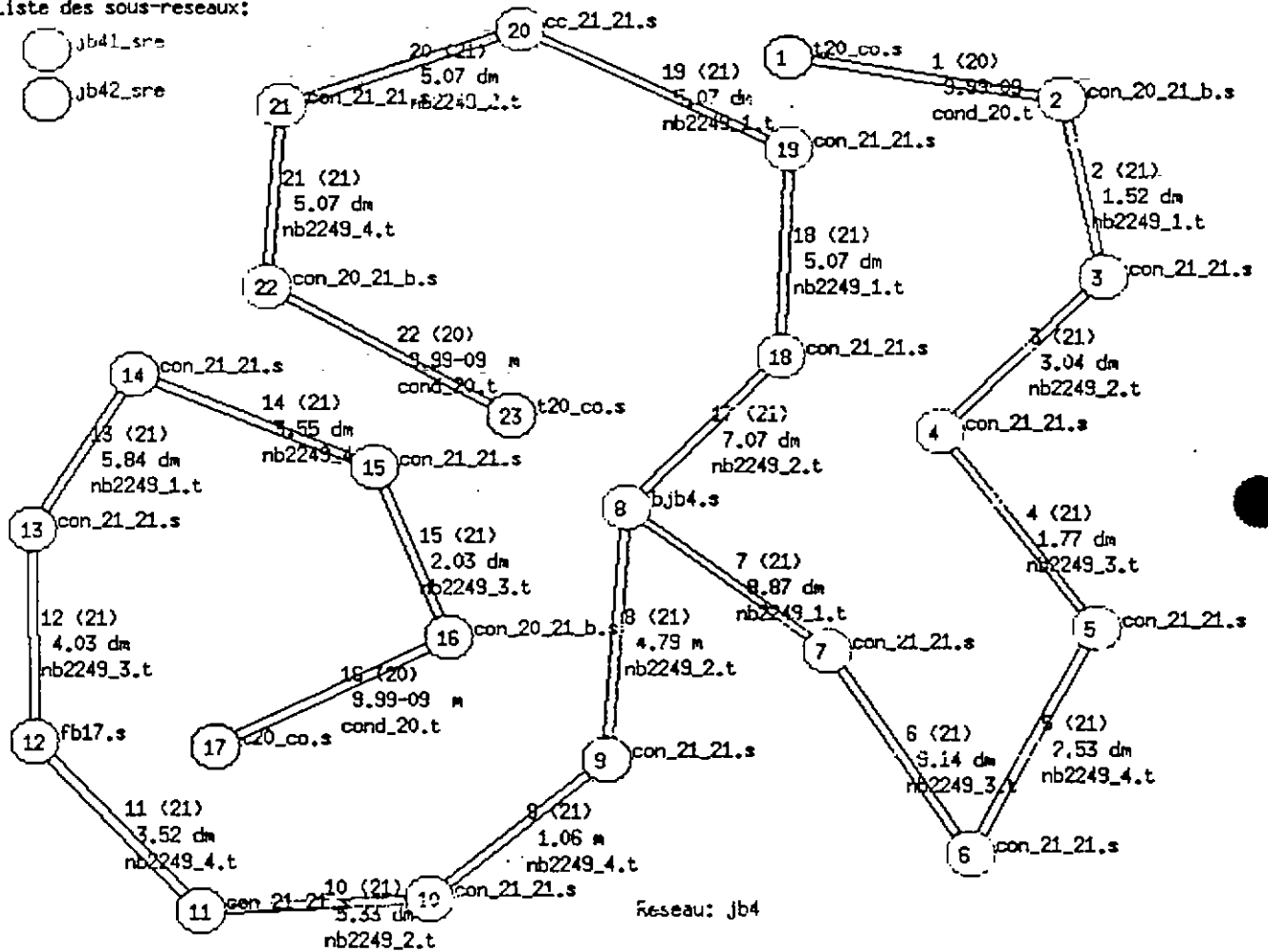
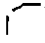
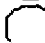


Fig C.6 : JB4 (cable network between the BIB and aft shielded volumes, gathering box JB4, FB17 and LD3) topological model

Liste des sous-réseaux:

-  jb3_sre1
-  jb3_sre2

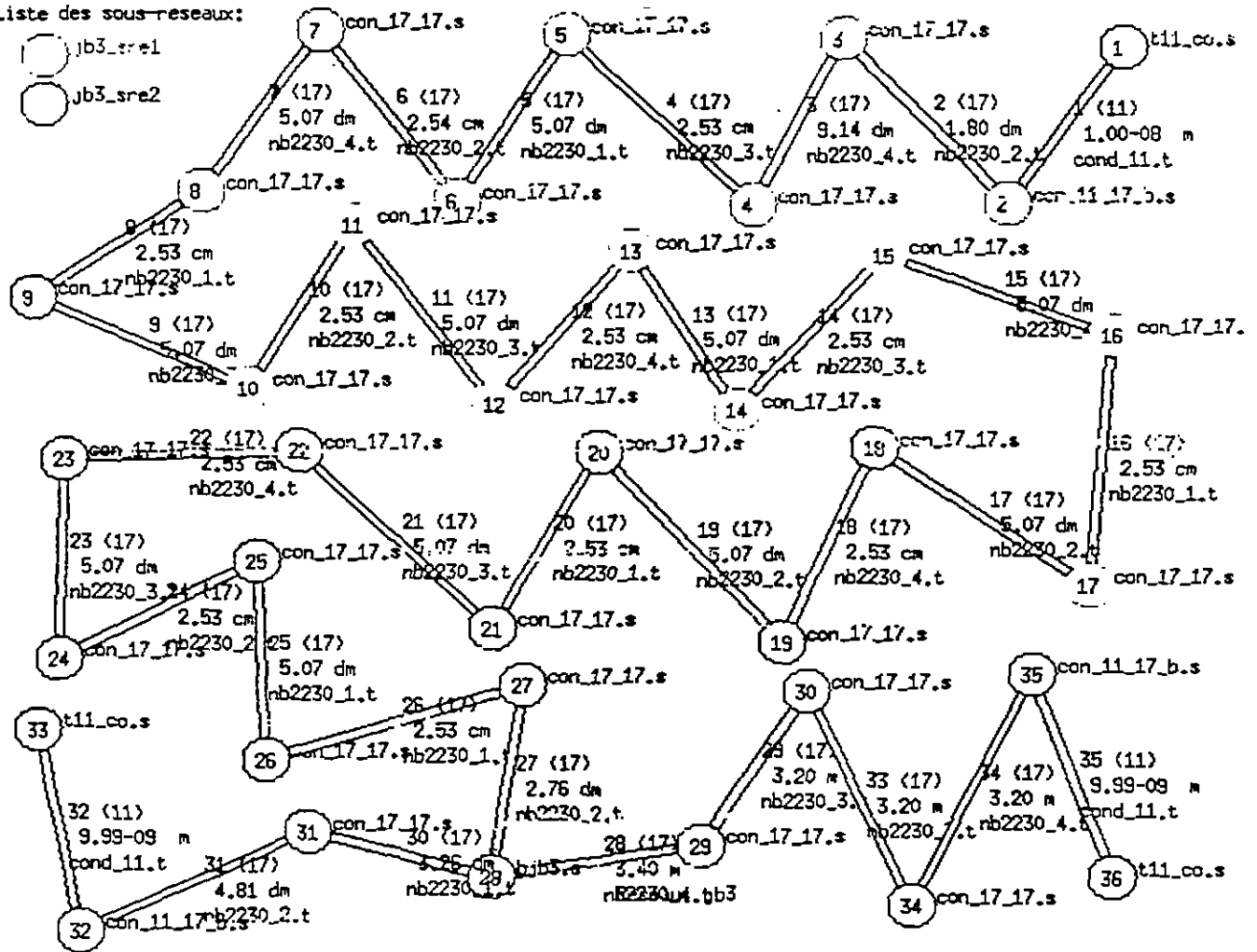


Fig C.7 : JB3 (cable network connected to JB3 and LD6 boxes between the cockpit, the BIB and the aft shielded volumes) topological model

Liste des sous-reseaux:

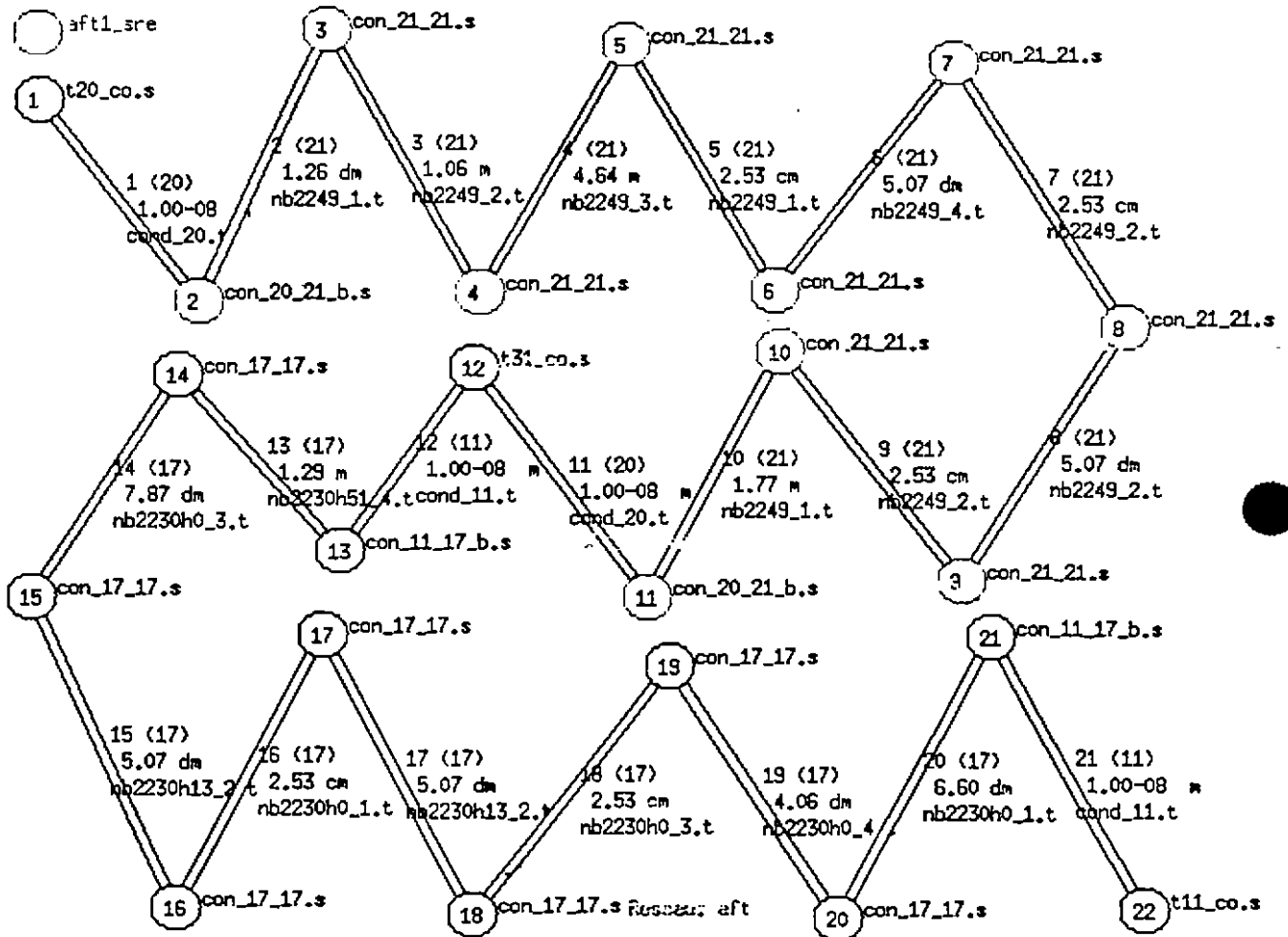


Fig C.8 : Aft shielded volume (cable network inside the aft shielded volume connected to LD16 and LD18 boxes) topological model



REFERENCES

- [1] C.E. Baum : "*The Theory of the Electromagnetic Interference Control*". Interaction Notes. Note 478, (December 1989) and, Modern Radio Science 1990, pp. 87-101, Oxford University Press.
- [2] J. P. Parmantier, G. Labaune, J. C. Alliot, P. Degauque : "*Electromagnetic Topology on Complex Systems: Topological Approach*". Interaction Notes, Note 488. May 1992.
- [3] J.P. Parmantier : "*Approche Topologique pour l'étude des couplages électromagnétiques*", Ph.D. report of Lille Flandres Artois University, December 1991. (in French - English translation available at ESA)
- [4] C.E. Baum, T. K. Liù, F.M. Tesche : "*On the Analysis of General Multiconductor Transmission-Line Networks*", Interaction Notes, Note 350, November 1978.
- [5] J.P. Parmantier, P. Degauque : "*Topology Based Modeling of Very Large Systems*". Modern radio Science 1996. Edited by J. Hamelin. Oxford University Press. pp. 151-177.
- [6] J.P. Parmantier, V. Gobin, F. Issac, I. Junqua, Y. Daudy, J.M. Lagarde : "*An Application of the Electromagnetic Topology Theory on the Test-bed Aircraft, EMPTAC*", Interaction Notes, Note 506, November 1993.
- [7] J. P. Parmantier, V. Gobin, F. Issac, I. Junqua, Y. Daudy, J.M. Lagarde : "*Analysis of E.M. Coupling on Large Structures Using E.M. Topological Concepts : Application to the EMPTAC Aircraft*". Proceedings of ICEAA95 symposium. Politecnico di Torino (Italy). 12-15 September 1995, pp. 81-84
- [8] Air Force Weapon Laboratory : "*Hardness Surveillance test Modification #2 : Volume II of II : Appendices. Sub-task Statement 02-06*". May 1987, Revision July 1987.
- [9] "*CRIPTE code users guide*", ESI/SEMCA, 1997.
- [10] J.P. Parmantier, M. Lemistre : "*Définition des paramètres pertinents permettant de caractériser des faisceaux de câbles constituant une liaison blindée*". ONERA's report, RTS n°8/6767 PY, March 1994. (In French).
- [11] J. P. Parmantier : "*Méthodes pour le traitement du couplage électromagnétique sur le câblage d'un système de grande dimension*". ONERA's report, RTS 12/6727 PY, February 1996. (In French).

[12] J. P. Parmantier, F. Issac : "*Améliorations dans le logiciel CRIPTE : - code LAPLACE, création de tubes, - calcul en des positions intermédiaires sur un tube*". ONERA's report, RTS 12/6767 PY, February 1997 (in French).

[13] J.P. Parmantier, S. Bertuol, X. Ferrières : "*Développements de modules de calcul dans le logiciel CRIPTE: - câble blindé, - onde plane, - RSIL*". ONERA's report, RTS n°16/6727 PY, January 1997. (In French)

[14] J. P. Parmantier, G. Labaune, J. C. Alliot, P. Degauque : "*Electromagnetic Topology: Junction Characterization Methods*". Interaction Notes, Note 489. May 1992.

[15] X. Ferrières, B. L. Michielsen : "*Résolution efficace des équations de lignes de transmission pour réseaux complexes*". Proceedings of the French EMC meeting. Toulouse, 2 - 4 March 1994.

[16] C.E. Baum : "*Generalization of the BLT equation*", Interaction Notes, Note 511, 11 April 1995

[17] L. Paletta, P. Dumas, J.P. Parmantier : "*Utilisation du champ électromagnétique tangentiel comme terme source dans les problèmes de Topologie Electromagnétique*", Proceedings of the French CEM meeting, Lille, 3-5 September 1996. (in French)